Titre: Title:	Subtle Changes in Hyperelastic Properties of Myocardium With Cardiotoxicity Remodeling From Cardiac Magnetic Resonance
Auteur: Author:	Marianna Gamba
Date:	2019
Type:	Mémoire ou thèse / Dissertation or Thesis
Référence: Citation:	Gamba, M. (2019). Subtle Changes in Hyperelastic Properties of Myocardium With Cardiotoxicity Remodeling From Cardiac Magnetic Resonance [Master's thesis, Polytechnique Montréal]. PolyPublie. https://publications.polymtl.ca/3846/

POLYTECHNIQUE MONTRÉAL

affiliée à l'Université de Montréal

Subtle changes in hyperelastic properties of myocardium with cardiotoxicity remodeling from cardiac magnetic resonance

MARIANNA GAMBA

Institut de génie biomédical

Mémoire présenté en vue de l'obtention du diplôme de *Maîtrise ès sciences appliquées*

Génie biomédical

Mai 2019

POLYTECHNIQUE MONTRÉAL

affiliée à l'Université de Montréal

Ce mémoire intitulé :

Subtle changes in hyperelastic properties of myocardium with cardiotoxicity remodeling from cardiac magnetic resonance

présenté par **Marianna GAMBA**

en vue de l'obtention du diplôme de *Maîtrise ès sciences appliquées*

a été dûment accepté par le jury d'examen constitué de :

Farida CHERIET, présidente
Delphine PÉRIÉ-CURNIER, membre et directrice de recherche
Caroline LAVERDIÈRE, membre externe

DEDICATION

To my friends and family

ACKNOWLEDGEMENTS

First and foremost, I would like to sincerely thank my advisor, Prof. Delphine Périé-Curnier, for the patient guidance and support she has provided me throughout the course of my graduate studies. I am also very grateful for the opportunity I have had to work on this project and gain insights into the issue of doxorubicin-associated cardiotoxicity.

Furthermore, I would like to express my gratitude to the rest of the thesis examination committee, Prof. Farida Cheriet and Dr. Caroline Laverdière, for their interest, consideration, and time devoted to reviewing this manuscript.

I certainly owe a great deal to the team of researchers of the PETALE project for providing me the experimental data as well as the opportunity to conduct this complementary analysis on survivors of childhood acute lymphoblastic leukemia. Thanks also go to Prof. Alistair Young and his team of programmers at the Auckland MRI Research Group, who has kindly made the Cardiac Imaging Modeling software available to us. Without this tool, we could not have achieved the objectives of the thesis. I wish to acknowledge those students of Polytechnique Montreal who contributed to the development of this work by providing some input data.

On a more personal note, I would like to express my deepest gratitude towards my parents and my siblings, who have constantly supported and encouraged me to do my best. Moreover, I take this opportunity to thank Maria Lacruz, Yasamin Majedi, Evelyne Lechevalier Hubertise, and Ana Segovia; this journey would not have been nearly as great without all the laughs and tears we shared together. Finally, a huge and sincere thanks to my lifetime friends, Rossella, Gloria, Alessandra, Federico, and Eleonora, who helped me keep things in perspective.

RESUME

La doxorubicine (DOX) est un puissant agent antinéoplasique fréquemment administré dans le traitement de nombreux cancers pédiatriques, notamment la leucémie lymphoblastique aiguë (LLA). La doxorubicine possède une efficacité démontrée dans le traitement du cancer, mais elle engendre également un large spectre d'effets cardiaques indésirables. Les changements structurels du myocarde s'accompagnent de modifications progressives de la géométrie de la paroi du myocarde du ventricule gauche (VG). La détérioration de la fonction myocardique peut progresser silencieusement pendant des années et se manifester sans avertissement ou même ne devenir apparente que longtemps après la fin du traitement. Des doses cumulatives plus élevées de DOX augmentent le risque d'effets nocifs associés au traitement. La faisabilité de la résonnance magnétique cardiaque (RMC) a été établie et plusieurs logiciels de modélisation géométrique 3D du cœur ont été développés pour évaluer la fraction d'éjection, l'épaisseur de la parois, et le volume télésystolique et le volume télédiastolique du VG. La modélisation par éléments finis (EF) de la mécanique du ventricule gauche et les stratégies inverses d'identification des paramètres des matériaux ont ensuite été introduites pour tenir compte du comportement mécanique passif du tissu myocardique.

Compte tenu de cela, nous avons entrepris une étude visant à analyser en détail les subtils changements asymptomatiques dans la géométrie et dans la fonction du ventricule gauche chez 84 survivants de la LLA infantile traités par chimiothérapie utilisant la doxorubicine (dose faible à modérée). Étant donné le grand potentiel de la modélisation numérique du cœur, cette évaluation a été réalisée à l'aide d'une approche basée sur un modèle EF qui intègre la forme et le mouvement spécifiques de la chambre ventriculaire directement à partir des données RMC.

84 survivants de la LLA, âgés de 23 ± 7 ans, ont été recrutés prospectivement et répartis en deux groupes distincts, nommés respectivement risque standard (SR, n = 19) et risque élevé en fonction du risque de récidive. En outre, les sujets du groupe associé à un risque élevé de récidive ont été subdivisés en deux sous-groupes selon qu'ils avaient reçu (HRdex, n = 36) ou non (HR, n = 45) la thérapie cardioprotectrice (dexrazoxane) dans le but de réduire le risque de lésions cardiaques à long terme. Par ailleurs, à des fins de comparaison, 10 volontaires en santé, d'âge similaire aux survivants (22 ± 4 ans) et n'ayant jamais été atteints de leucémie aiguë ou de cardiomyopathie, ont formé un groupe témoin.

Dans le cadre de l'étude de la cardiotoxicité tardive, tous les sujets ont subi une imagerie RMC, une échocardiographie transthoracique et des tests d'effort. À partir des données RMC acquises, un opérateur formé a extrait la forme et le mouvement spécifiques du ventricule gauche à l'aide d'un cadre de points de repère (CIM v8.1, University of Auckland, Nouvelle-Zélande). Les bordures intérieures et extérieures des parois du ventricule gauche ont été dessinées semi-automatiquement à partir de six points de guidage placés par l'opérateur, puis corrigés manuellement en cas d'erreurs d'alignement. À partir de ce tracé, on a calculé la fraction d'éjection, le volume de course, la masse myocardique, l'épaisseur de la paroi, le volume diastolique final et le volume systolique final pour chacun des participants de l'étude. Par la suite, la reproductibilité inter- et intra-observateurs des résultats de la segmentation a été quantifiée par des coefficients de corrélation intra-classe (ICC) sur quatre reconstructions de 15 survivants du cancer, chacune étant réalisée par quatre opérateurs formés, et sur trois reconstructions du même sujet, chacune étant effectuée par un seul opérateur. Pour un sous-ensemble de la population des survivants de la leucémie (n = 48), un modèle 3D conçu par éléments finis a été utilisé pour calculer la propriété hyperélastique (C_1) à partir d'une stratégie d'identification des paramètres inverses des matériaux basés sur la géométrie du VG lors de la diastase. Au départ, nous avons supposé des valeurs physiologiquement raisonnables de 0.75, 1.0 et 1.25 kPa comme contraintes de charge de pression pour tous les participants. Une fois les pressions ventriculaires spécifiques au sujet (au repos et à l'exercice maximal) connues, nous avons incorporé ces données dans le modèle et répété l'analyse aux éléments finis. Les valeurs résultantes de C_1 ont été notées et comparées entre les groupes pour chacun des cinq scénarios de charge. Les comparaisons statistiques ont été effectuées par analyse de variance à sens unique (ANOVA) sur les paramètres géométriques globaux et régionaux et par analyse de variance à mesures répétées bidirectionnelles sur les paramètres géométriques dépendants du temps. Enfin, une analyse de sensibilité a été effectuée pour évaluer la dépendance de la propriété hyperélastique de la diastase et de la pression.

Dans le cas de notre étude, la reproductibilité intra-observateur était bonne pour les paramètres géométriques régionaux (ICC, 0.60-0.74) et excellente pour les paramètres géométriques globaux (ICC, 0.75-1.00), alors que la reproductibilité inter-observateur était excellente pour les deux types de paramètres (ICC, 0.75-1.00). Aucune différence significative entre les quatre groupes n'a été observée relativement à la fraction d'éjection, au débit systolique, à la masse, au volume systolique final et au volume diastolique final. Quelques différences de volume épicardique ont été observées,

mais seulement entre la phase finale de la systole et la diastase ($p<0.01$) à l'intérieur des groupes HRdex et HV ou SR, et parmi les groupes HV et HR. Il est intéressant de noter que la propriété hyperélastique pour les pressions standard était légèrement plus faible dans le groupe HR comparativement au groupe HRdex ou SR et aussi relativement au groupe contrôle ($p<0.05$). En revanche, aucune différence appréciable n'a pu être détectée dans la propriété hyperélastique à des pressions intraventriculaires au repos ($p>0.5$) et à l'exercice maximal ($p>0.6$).

Il ressort clairement de cette analyse que les paramètres géométriques globaux et régionaux ne sont pas suffisamment sensibles pour détecter les changements subtils induits par la cardiotoxicité tardive de la doxorubicine dans la structure et la fonction du ventricule gauche. Toutefois, les paramètres globaux dépendants du temps constituent des preuves préliminaires que l'exposition à la doxorubicin a un effet plus néfaste sur la diastole précoce que sur la systole ou la diastole tardive. La propriété hyperélastique, plus faible dans le groupe HR, suggère un tissu myocardique plus enclin à la dilatation si une pression intra-ventriculaire plus élevée est appliquée, comparativement aux autres groupes d'étude. Cette constatation concorde avec ce qui a été observé chez les survivants à long terme ayant eu la leucémie adulte et traités par chimiothérapie à forte dose à base de doxorubicine. Il convient toutefois de noter que ces estimations ne peuvent tenir compte que des effets géométriques du remodelage du myocarde sur la mécanique ventriculaire passive, puisque la pression intra-ventriculaire gauche spécifique au sujet n'était pas incluse dans ces simulations. Des résultats similaires ont été obtenus lors de l'application de pressions intra-ventriculaires mesurées au repos et pendant l'exercice maximal.

En conclusion, cette étude démontre que la cardiotoxicité subclinique de la doxorubicine peut être évaluée par l'analyse du comportement mécanique du ventricule gauche sur des images RMC. Nos résultats doivent toutefois être confirmés par des analyses additionnelles avant d'en tirer une conclusion solide sur la signification pronostique, à long terme, des altérations de la raideur myocardique et de leur relation avec le statut de risque dans la cohorte de survivants étudiée ou dans une cohorte similaire. Il serait très pertinent, dans le cadre d'études ultérieures, d'inclure la simulation de la mécanique ventriculaire, avec la méthode des éléments finis, pendant la diastole précoce et la systole afin de mieux analyser les changements de rigidité dans les groupes. Dans le même but, il pourrait être utile d'augmenter la résolution temporelle des données d'imagerie chez les survivants de la leucémie et les sujets témoins.

Mots-clés : survivants de la leucémie lymphoblastique aiguë, cardiotoxicité induite par la doxorubicine, imagerie par résonance magnétique cardiaque, rigidité passive du myocarde, modélisation par éléments finis personnalisée, mécanique ventriculaire gauche.

ABSTRACT

Doxorubicin (DOX) is a potent chemotherapeutic agent routinely administered in the treatment of several pediatric malignancies, including acute lymphoblastic leukemia (ALL). Despite its efficacy to improve the outlook of cancer patients, doxorubicin is known to cause a wide spectrum of cardiac adverse effects. The structural changes in the myocardium are accompanied by progressive changes in LV myocardial wall geometry. The deterioration of myocardial function can progress silently for many years before the manifestation of clinical symptoms and become apparent even long time after completion of treatment. Higher cumulative doses of this agent increase the risk for late cardiac complications. The feasibility of CMR imaging has been established and a variety of software for 3D geometric modeling of the heart have been developed to assess wall thicknesses, ejection fraction, end-systolic and end-diastolic volumes. Finite element (FE) modelling and inverse material parameter identification strategies were then introduced to take into account the passive mechanical behavior of the myocardial tissue.

In light of the above, we undertook a study to assess the asymptomatic changes in LV structure and function in a group of long-term survivors of childhood ALL treated with low to moderate doses of doxorubicin therapy. Given the high potential of numerical cardiac modeling, this evaluation was conducted using a FE model-based approach that integrates the subject-specific shape and motion of the ventricular chamber directly from imaging data.

Eighty-four ALL survivors (23±7 years old) were prospectively enrolled and stratified into two different groups, designated as standard-risk (SR, n=19) and high-risk groups, according to their risk of tumor recurrence. Subjects treated for high-risk ALL were further divided into two groups depending upon whether they did (HRdex, n=36) or did not (HR, n=45) receive the protective therapy (dexrazoxane) in an attempt to reduce the likelihood of late cardiotoxicity. Furthermore, for purposes of comparison, 10 healthy volunteers (HV, 22±4 years), with no prior history of cancer or cardiac pathologies and similar in age to the survivors, were used as controls.

As a part of the investigation of late-onset cardiotoxicity, all subjects underwent CMR imaging, transthoracic echocardiography, and exercise stress testing. From the acquired CMR data, a trained operator extracted the subject-specific shape and motion of the LV using a guide-point framework (CIM v8.1, University of Auckland, New Zealand). The inner and outer borders of the LV walls were semi-automatically drawn from six guidepoints placed by the operator at end-systole and then

manually corrected for mis-registration errors. From this tracing, ejection fraction, stroke volume, myocardial mass, wall thickness, end-diastolic and end-systolic volumes were computed for each of the study participants. After that, inter- and intraobserver repeatability of the segmentation results were quantified by intra-class coefficients (ICC) on four reconstructions of 15 leukemia survivors, each by four trained operators, and on three reconstructions of the same subject, each by a single operator.

For a subset of the leukemia survivor population (n=48), a 3D finite element model was used to quantify the hyperelastic property (C_1) from inverse material parameters identification strategies based on the LV geometry at diastasis. This biomechanical parameter was initially calculated by assuming physiologically realistic values of 0.75, 1.0, and 1.25 kPa as pressure loading constraints for all participants. Once the subject-specific LV pressures (at rest and peak exercise) became available, we incorporated such data in the model and repeated the FE analysis. The resulting values of C_1 were reported and compared between groups for each of the five loading scenarios. Statistical comparisons were performed by one-way analysis of variance (ANOVA) on global and regional geometrical parameters, and two-way repeated-measures ANOVA on time-dependent geometrical parameters. Ultimately, a sensitivity analysis was conducted to evaluate the dependence of the hyperelastic property on the diastasis frame and the pressure load.

In our experience, inter-observer repeatability was good for regional geometrical parameters (ICC, 0.60-0.74) and excellent for global geometrical parameters (ICC, 0.75-1.00), while intra-observer repeatability was excellent for both regional and global parameters (ICC, 0.75-1.00). Groups had similar LV function values. No significant differences were observed among the four study groups in ejection fraction, stroke volume, mass, end-diastolic or end-systolic volumes. Some differences were detected in epicardial volume only between end-systole and diastasis phases ($p<0.01$) among the HRdex and HV or SR groups, and among the HV and HR groups. Interestingly, the hyperelastic property for standard pressures was slightly lower in the HR group when compared against the HRdex or SR group, and also when compared against the control group ($p<0.05$). In contrast, no appreciable difference could be noted in the hyperelastic property for intra-ventricular pressures at rest ($p>0.5$) and peak exercise ($p>0.6$).

From this analysis, it is clear that the global and regional geometrical parameters are not sufficiently sensitive to capture the subtle changes induced by late doxorubicin cardiotoxicity in LV structure

and function. Nevertheless, the time-dependent global parameters provided preliminary evidence that early diastole was more affected by doxorubicin exposure than systole or late diastole. The smaller hyperelastic property in the high-risk group suggested a myocardial tissue more prone to dilatation if increased intra-ventricular pressure is applied than in the other study groups. This finding is consistent with what has been observed in long-term survivors of adult leukemia treated with high-dose doxorubicin-based chemotherapy. It should be noted, however, that these estimates could account only for the geometrical effects of myocardial remodeling on the passive ventricular mechanics since the subject-specific LV cavity pressure was not included in these simulations. Similar results were obtained when applying intra-ventricular pressures at rest and peak exercise.

In conclusion, this study demonstrated that the subclinical cardiotoxicity of doxorubicin can be non-invasively assessed through the mechanical behavior analysis of the LV on CMR images. Additional investigations will be necessary to confirm our results and draw a firm conclusion about the long-term prognostic significance of alterations in myocardial stiffness and their relationship with ALL risk status in this or similar cohort of survivors. In future works, we hope to include the FE simulation of the left ventricular mechanics during systole and early diastole in order to better capture the changes in stiffness across groups. To the same purpose, it might be convenient to increase the temporal resolution of the image data in both leukemia survivors and control subjects.

Keywords: acute lymphoblastic leukemia survivors, doxorubicin-mediated cardiotoxicity, cardiac magnetic resonance imaging, passive myocardial stiffness, personalized FE modeling, in vivo left ventricular mechanics.

TABLE OF CONTENTS

LIST OF TABLES

LIST OF FIGURES

LIST OF SYMBOLS AND ABBREVIATIONS

3D	Three-dimensional
AHA	American Heart Association
ALL	Acute lymphoblastic leukemia
ANOVA	Analysis of variance
CIM	Cardiac Image Modeling
CMR	Cardiac magnetic resonance
DEX	Dexrazoxane
DFCI	Dana Faber Cancer Institute
DICOM	Digital Imaging and Communication in Medicine
DOX	Doxorubicin
DS	Diastasis
ED	End-diastole
EDV	End-diastolic volume
EF	Ejection fraction
ES	End-systole
ESV	End-systolic volume
FE	Finite element
GUI	Graphical user interface
HR	High-risk
HRdex	High-risk exposed to dexrazoxane
HV	Healthy volunteers
IRB	Institutional Review Board

LV	Left ventricle
LVM	Left ventricular mass
MRI	Magnetic resonance imaging
PETALE	Prévenir les Effets Tardifs de la Leucémie Lymphoblastique Aigüe chez l'Enfant
RMSE	Root mean square error
RV	Right ventricle
SD	Standard deviation
SR	Standard-risk group
SV	Stroke volume

CHAPTER 1 INTRODUCTION

1.1 Background

Acute lymphoblastic leukemia (ALL) is a malignant disease that arises from lymphocytes, a class of white blood cells, and is marked by the abnormal proliferation and accumulation of these cells in the bone marrow, blood and other tissues (Terwilliger et Abdul-Hay, 2017). In children and adolescents younger than 20 years, ALL is regarded as the most common tumor. In fact, 19% of the total cancer diagnoses and nearly 80% of the total leukemia cases in this age group are ALL (Rahman, Yusuf, et Ewer, 2007; Bhojwani, Yang, et Pui, 2015). The incidence of this neoplastic condition varies according to age at diagnosis, with the vast majority of cases occurring in the child's first decade of life and peak prevalence in subjects between 2 and 5 years of age (Belson, Kingsley, et Holmes, 2006). Today, children with a diagnosis of ALL have a favorable prognosis. Recent estimates indicate that about 95% of patients are still alive and cancer-free at 5 years after cessation of therapy, while more than 80% attain long-term remission (DeAngelo et al., 2015). This success was brought about by advances made in the management and treatment of the disease over the past five decades. In particular, the survival rates were influenced favorably by the introduction of the anthracycline doxorubicin and the asparaginase as chemotherapeutic agents, as well as by the treatment of the central nervous system (Yeoh et al., 2002; Hunger et Mullighan, 2015; Vrooman et Silverman, 2016). Personalized treatment regimens carefully tailored to the risk of tumor recurrence have been recently applied to reduce the intensity of therapy while optimizing its leukemic response (Yeoh et al., 2002; Vrooman et Silverman, 2016)

Although improving the survival outcomes, exposure to doxorubicin is linked with a broad range of cardiotoxicity which can seriously affect the quality and duration of life of ALL patients (Lipshultz, Cochran, Franco, et Miller, 2013). In a study… More than 50% of the ALL survivors has been reported to experience cardiac abnormalities arising from the treatment (Lipshultz et al., 2005). Morphological and functional changes in the myocardial tissue are accompanied by progressive alterations in the geometry of the left ventricle. This cardiotoxicity seems to manifest itself by a persistent and, often, progressive deterioration of the cardiac function, which may continue for years after the initial exposure to doxorubicin (Lipshultz et al., 2005). These harmful effects may become apparent months to years after completion of therapy. The manifestations of the spectrum of cardiac toxicity range from subtle abnormalities in LV structure and function to

more serious complications, such as cardiomyopathies and congestive heart failure (Wouters, Kremer, Miller, et Herman, 2005; Chang et Wang, 2018). Interestingly, cardiotoxicity is more likely to occur in ALL survivors who received high doses of doxorubicin throughout the course of treatment (Lipshultz et al., 2013). In particular, doses greater than 400-450 mg/m are associated with a more severe myocardial damage. Other factors, such as exposure to radiotherapy, younger age at diagnosis or female gender, increase the risk of developing late cardiovascular complications (Lipshultz et al., 2013).

In response to concerns about the cardiac health of ALL patients, a variety of protective strategies have been proposed to attenuate the toxicity of doxorubicin during and after therapy. Among them, the cardioprotective agent dexrazoxane has proven to be very effective in reducing the incidence of myocardial injury. However, at present, none of the available measures completely eliminates the potential for health complications, making the issue of DOX-induced cardiotoxicity even more concerning (McGowan, 2017).

Although a vast body of data has accumulated on DOX-induced cardiotoxicity in survivors of childhood ALL, relatively little is understood of the long-term effects of modern chemotherapy programs on cardiovascular health (Hashimoto et al., 1999; Hudson et al., 2007; Vandecruys et al., 2012). Specifically, limited information is available on the cardiac status of these individuals at 10 years or more after completion of therapy (Adams et Lipshultz, 2005). Such data are important to accelerate progress towards improving the prevention of myocardial injury to enhance the quality of long-term survival of patients (Gianni et al., 2008). It has been suggested that a better knowledge of this cardiotoxicity may help researchers and clinicians refine management strategies and develop more effective cardioprotective measures (Gianni et al., 2008; Lipshultz et al., 2013; Hudson, Link, et Simone, 2014). This calls for more research on the long-term effects of chemotherapy associated with modern treatment regimens.

Imaging techniques are routinely used in the assessment of cardiac function for detection and screening of doxorubicin-induced cardiotoxicity (Dodos, Halbsguth, Erdmann, et Hoppe, 2007). Echocardiography has been the preferred method for such an evaluation in daily clinical practice (Jurcut et al., 2008; Da Silveira et al., 2016). Clinicians typically analyze the alterations occurred in experimental measurements of the diastolic and systolic LV function with respect to baseline values. Ejection fraction, stroke volume, and shortening fraction are examples of these indices (Jurcut et al., 2008; Tham et al., 2013; Khouri, Klein, Velazquez, et Jones, 2015). Nevertheless,

this imaging modality has poor sensitivity, which makes the current echocardiographically-derived indices less suitable for detection and surveillance of subclinical myocardial toxicity (Briant et al., 2007; Jain, Russell, Schwartz, Panjrath, et Aronow, 2017). CMR imaging offers a valid alternative to echocardiography for assessing the cardiac health of long-term ALL survivors. In fact, investigations in CMR imaging have demonstrated it to be a highly accurate modality for use in evaluating ventricular performance (Dong and Chen, 2018). Software for 3D geometric remodeling of the heart allow the determination of LV volumes, ejection fraction and mass from MRI scans (Young, Cowan, Thrupp, Hedley, et Dell'Italia, 2000; Suinesiaputra et al., 2014). Due to the ability of CMR to provide clear definitions of the LV wall contours, ejection fraction estimates measured on CMR images result to be more reliable and reproducible than those obtained with the aid of other imaging modalities, including echocardiography (Fallah-Rad, 2011; Gusso et al., 2012; Loganathan, Bilgen, Al-Hafez, et Smirnova, 2005).

Another parameter that provides a non-invasive indication of global left ventricular function is myocardial tissue stiffness (Hsu, Bouchard, Dumont, et Wolf, 2005). Many investigators have examined muscle stiffness to gain some insight into the mechanisms underlying cardiomyopathies, heart failure, hypertension, and other cardiac disorders (Lee et al., 2013; Mojsejenko et al., 2015). These studies showed that changes in muscle are accompanied by alterations in tissue stiffness during filling, with potential consequences for the mechanical function of the myocardium (Gupta, Ratcliffe, Fallert, Edmunds, et Bogen, 1994; Wang et al. 2013). Their outcomes also suggest that this biomechanical parameter can yield useful information on the structural and functional LV changes following late-onset cardiotoxicity.

A non-invasive estimate of myocardial stiffness can be obtained through the use of magnetic resonance imaging in connection with 3D finite element models of the LV chamber (Mojsejenko et al., 2015). Numerical modeling of the heart provides a powerful tool to investigate how changes in the myocardial tissue at small scale affect the structure and function of the ventricle. This tool has been extensively used in research for estimating the in vivo mechanical properties of the LV myocardium in a non-invasive fashion. By incorporating the subject-specific imaging data into the FE modelling framework, this technique offers the potential to construct anatomically realistic model of the LV for a wide range of medical applications (Wang et al., 2015). In research setting, biomechanical models of the LV have been employed to elucidate the impact of various cardiac

pathologies and/or their treatments on cardiac functionality and myocardial mechanics (Sermesant, Delingette, et Ayache, 2006).

1.2 General and specific research objectives

Several studies have been carried out over the past years in an attempt to draw a comprehensive picture for doxorubicin-related cardiotoxicity in survivors of childhood ALL. Among them, a work of particular relevance for the current research is the PETALE project (Prévenir les Effets Tardifs de la Leucémie Lymphoblastique Aigüe chez l'Enfant). Initiated in 2010, this multidisciplinary study assessed 250 subjects who had previously undergone therapy with doxorubicin at the Sainte-Justine University Hospital Center in Montreal. This study was designed to characterize the delayed adverse effects of antileukemia treatment on various organs and systems, including the heart, in a young population of acute leukemia survivors. The current investigation develops from this study and was conducted on a subgroup of the PETALE cohort.

As part of the PETALE project, our study sought to assess the subclinical changes in LV structure and function in a group of long-term survivors of childhood ALL who received low-to-moderate doses of doxorubicin-based chemotherapy. Given the high potential of numerical cardiac modeling, this evaluation was conducted using a FE model-based approach that integrates subject-specific LV shape and motion directly from CMR scans.

In particular, the following specific objectives were addressed:

1. to extract from each patient's CMR images the geometric and function information required to build personalized biomechanical FE models of the LV and to calculate a set of relevant 3D geometrical parameters.
2. to examine the changes occurred in LV geometry and function after doxorubicin exposure (at both global and regional scales) by comparing the calculated geometrical parameters between cancer survivors and their matched healthy controls.
3. to simulate the mechanical events occurring during mid-diastole on the MRI-reconstructed FE models and to compute the hyperelastic property of the transversely-isotropic constitutive law used to describe the passive mechanical behavior of the myocardium.

4. to gain some insight into the long-term effects of DOX therapy on the passive LV mechanics by comparing the estimated hyperelastic property between cancer survivors and controls.

1.3 Research hypotheses

The current analysis was designed around a proper set of methodological assumptions and research hypotheses. In detail, we assumed that the administration of low-to-moderate cumulative doses of doxorubicin induced dose-dependent, subtle, and asymptomatic alterations in LV geometry and function in the study participants. As far as concern the hypotheses addressed by the study, we first speculated that the cardiac abnormalities can be detected and evaluated by means of LV myocardial mass, ejection fraction, and other selected 3D geometrical parameters. Furthermore, we tested the hypothesis that the hyperelastic property (as a measure of the in vivo myocardial stiffness) was able to unmask the subclinical myocardial injury caused by exposure to doxorubicin

1.4 Outline of the thesis

The present thesis is structured into six chapters and a bibliography as follows:

Chapter 1 provides the reader with a brief overview of the clinical context of the project, paying particular attention to the side effects of doxorubicin on the cardiovascular system and the methods for assessing this cardiotoxicity. The general and specific research objectives are also outlined in this section, along with the hypotheses underpinning the study.

Chapter 2 introduces the necessary background for a deep understanding of the issue documented. It details the anatomy and physiology of the heart and describes the main in vitro experiments to characterize the mechanical behavior of the heart muscle in relaxed and contracted conditions. Subsequently, it compares most pertinent examples of existing models of cardiac mechanics.

Chapter 3 describes the cardiac image analysis and modeling tools employed in the assessment of LV geometry and function on a subject-specific basis. This chapter also includes information about the study population, data acquisition protocols, and statistical methods applied in the data analysis.

Chapter 4 presents the results obtained by applying the methods outlined in survivors of childhood ALL. In particular, it reports estimates of 3D geometrical and mechanical properties of the LV are illustrated with the support of graphs and tables.

Chapter 5 analyzes and interprets the results in light of current knowledge about doxorubicin-induced long-term cardiotoxicity in ALL survivors. Furthermore, it discusses the limitations of the proposed methodology.

Chapter 6 concludes with a reiteration of the main findings of the study and their implications for the detection of late doxorubicin cardiotoxicity. Project implementations, as well as possible future directions for research on this topic, are also provided.

CHAPTER 2 FUNDAMENTALS

This chapter provides an overview of the basic cardiac anatomy and physiology. We also describe the mechanisms by which doxorubicin exerts its cytotoxic action and the features of this toxicity on the heart muscle. After that, we review the imaging techniques and the intervention strategies currently available to minimize the risk for early and late myocardial injury. In addition, we present the experimental techniques for the mechanical characterization of the myocardium. Numerical modeling of the heart is then introduced as a tool for estimating the passive mechanical properties of cardiac tissue and for evaluating cardiac dysfunction. We compare the most pertinent examples of existing models of cardiac mechanics and we conclude by making a point of the situation.

2.1 The heart

The heart, central organ of the cardiovascular system, is a complex structure that generates the adequate force for perfusing tissues throughout the body. In such a way, the heart provides cells all over the body and tissues with enough nutrients and oxygen (Volpe et Makaryus, 2019). In the following, the cardiac function, as well as its internal morphology, are shortly described.

2.1.1 Basic cardiac anatomy

The heart is a hollow muscular organ located in the center of the thoracic cavity, between the two lungs, in a luminal space known as mediastinum (Volpe et Makaryus, 2019). Grossly, the heart consists of four distinct chambers: the two posterosuperior ones are namely (left and right) atria and the two anteroinferior ones are namely (left and right) ventricles. A central wall (septum) separates the left atrium and ventricle from their right-sided counterparts. **Figure 2.1** illustrates the internal anatomy of the cardiac pump. In the human cardiocirculatory system, the heart and blood vessels are configured in two separate circuits in series, the pulmonary and circulatory circulations, that function at the same time to ensure the transports of nutrients and oxygen to all body tissue. Two valves connect each atrium to the corresponding ventricle. As well as allowing the communication between the chambers, the heart valves guarantee the unidirectionally of the blood flow and prevent any chance of backward flow. In particular, the atria communicate to the corresponding ventricles through the atrioventricular valves (mitral and tricuspid), whereas the ventricles communicate to the great arteries through the semilunar valves (aortic and pulmonary). Although atria and ventricles share a primary structural organization, their internal morphology

reveals distinctive anatomical features that are linked to the different function the two chambers deploy. Essentially, the atrium collects the blood entering the heart, while the ventricle pumps the blood into the circulations (Volpe et Makaryus, 2019).

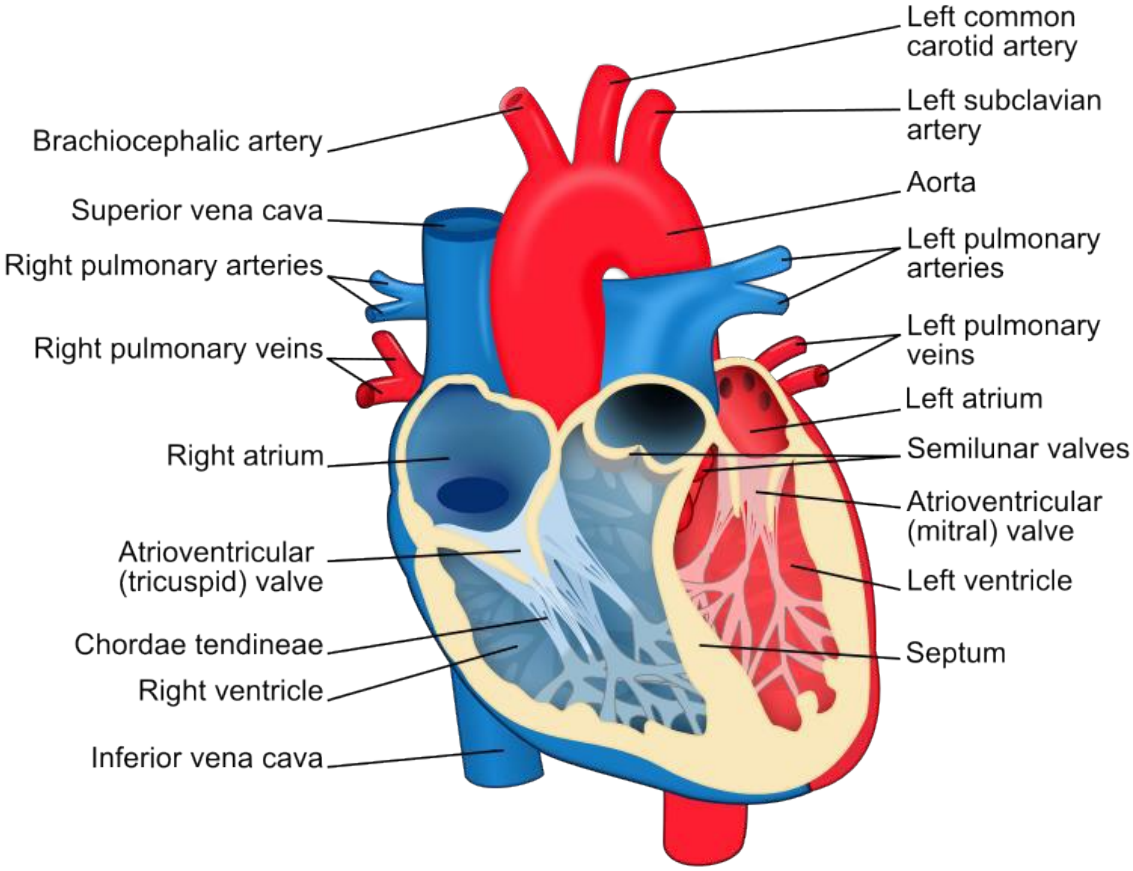

Figure 2.1. Anatomy of the inside of the heart, showing the four cavities and the roots of the great vessels, the other elements of the heart.

(Copyright 2010 by ZooFari. Reproduced with permission from Wikipedia Commons)

The cardiac wall is composed of three layers, each of which exerts a specific function. Moving from the external to the inner surface of the heart, it is possible to find epicardium, myocardium and endocardium. The myocardium is the cardiac muscle composed by myocytes which are behind the cardiac contraction. Endocardium and epicardium are, respectively, the inner and outer walls of the myocardium. It is interesting to note that the structure of the cardiac wall does not change along the length of the chambers but remains the same for the four chambers. Some differences are observed in the thickness of the cardiac wall among the chambers. The ventricles, which have to propel the blood through the systemic and pulmonary circulations facing higher pressures, exhibit

a more developed myocardium as compared with the atria. Additional differences were observed between the left and right ventricles. Specifically, the myocardium was shown to be thicker in the left ventricle, with wall thickness ranging from 6 to 16 mm (Petitjean et Dacher, 2011). The right ventricle (RV) presents a myocardial layer that is almost three to six times thinner than that of the left ventricle (Petitjean et Dacher, 2011). In fact, the right ventricle is responsible for pumping deoxygenated blood to the pulmonary circulation at lower physiological pressure.

2.1.2 The cardiac cycle

From a mechanical standpoint, the heart consists of two distinct pumps, operating in series, and whose function is to ensure blood transportation throughout the body by contracting alternatively with an average frequency of 75 beats/min (Baldissera, 2000). Indeed, atria and ventricles alternate between phases of contraction (systole), in which they propel the blood into the pulmonary and systemic circuits, and phases of relaxation (diastole), in which they are refilled with blood. The time interval between one diastole (or systole) and the beginning of the subsequent one is referred to as the cardiac cycle. In healthy individuals at rest, this sequence lasts 0.8 s. **Figure 2.2** (Wiggers diagram) illustrates the complete series of events occurring during a cycle in the left heart.

For purposes of discussion, the cycle of cardiac contraction can be decomposed into the following consecutive phases:

1. Ventricular isovolumetric contraction (preload): the contraction of the left ventricle causes an increase in intra-ventricular pressure, which results into the closure of the tricuspid and mitral valves and subsequently into an increase of atrial pressure. During isovolumetric contraction, the volume of the LV chamber remains constant. This phase terminates when the LV pressure attains 80 mmHg.
2. Ventricular ejection: when the LV pressure exceeds 80 mmHg (which is the aortic pressure), the aortic valve opens and the ventricle pumps blood into the aortic arch. The outflow is rapid up to a peak of 125 mmHg, followed by a slow outflow that stops at a pressure of 100 mmHg. The end of this phase coincides with the end of systole and the closure of the aortic valve.
3. Isovolumetric relaxation: the LV pressure drops to 0 mmHg, with 40% of the diastolic blood still in the chamber. The volume does not change during the isovolumetric relaxation.

4. Rapid diastolic ventricular filling: when the LV pressure decrease below the atrial pressure, the mitral valve opens allowing a quantity of blood to flow inside the ventricle.
5. Slow diastolic ventricular filling: this is the phase in which the LV pressure equals the atrial pressure, then following the systole, the mitral valve closes and the cardiac cycle resumes.

At the end of the ventricular systole, a new cycle begins: the ventricles begin the diastole and the semilunar valves close due to the high pressure in the aorta and pulmonary arteries. The atria are still in diastole, so overall the inner pressure is low throughout the entire heart.

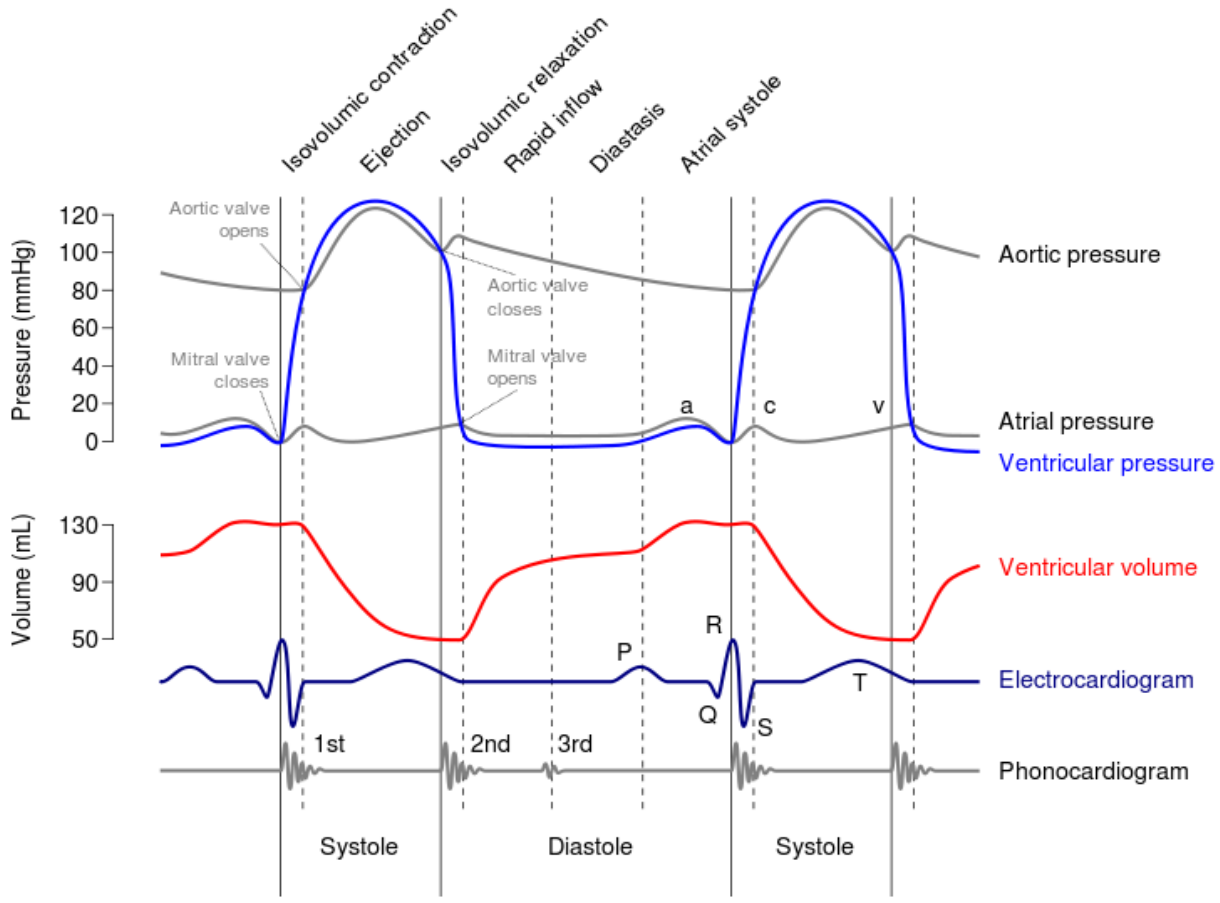

Figure 2.2. Shown is the temporal correlation between the left atrial and ventricular pressures (mm Hg), aortic pressure (mm Hg), left ventricular volume (mL), surface electrocardiogram (ECG), and phonocardiogram.

2.2 Cardiotoxicity of doxorubicin in the treatment of childhood ALL

Anthracyclines, such as doxorubicin, daunorubicin or epirubicin, are a class of anticancer agents that are routinely administered in the treatment of acute lymphoblastic leukemia (McGowan, 2017). Within this group, doxorubicin is the most commonly employed agent in virtue of its ability to significantly improve the prognosis of ALL patients (Vejpongsa et Yeh, 2014; Rahman et al., 2007). Survivors of ALL have been reported to experience a wide range of cardiovascular complications after doxorubicin exposure. Arrhythmias, pericarditis, myocarditis, left ventricular dysfunction, and heart failure are some examples of the toxic side-effects associated with chemotherapy (Lipshultz et al., 2013). According to recent estimates, more than 50% of these patients experience cardiovascular events within 6 years since the completion of treatment (Dong et Chen, 2018).

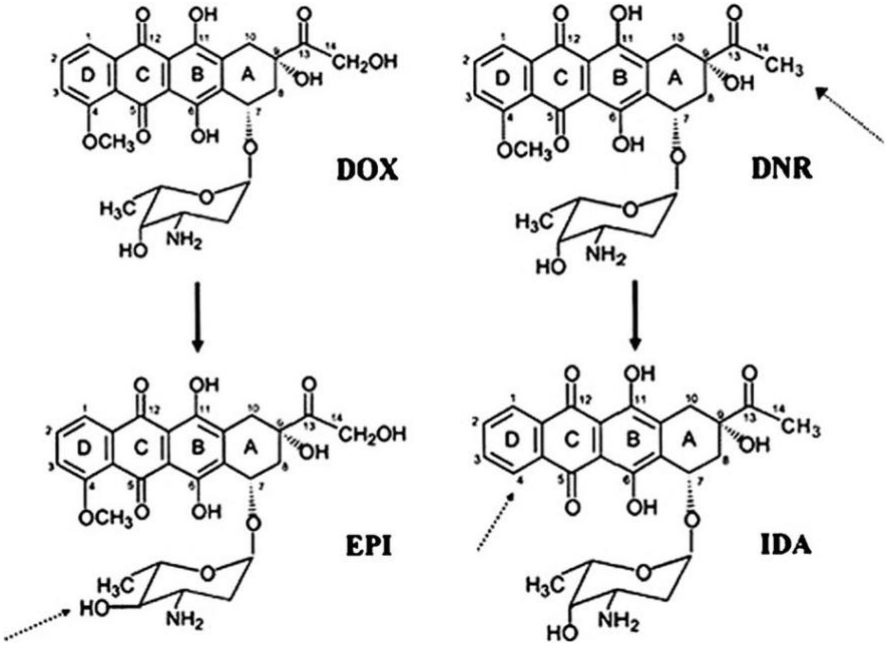

Figure 2.3. Chemical structure of the most commonly used anthracyclines. From top to bottom: doxorubicin (DOX), daunorubicin (DNR), epirubicin (EPI), and idarubicin (IDA).

(Reproduced with permission from: J. V., McGowan, R., Chung, A., Maulik, et al. *Anthracycline chemotherapy and cardiotoxicity*. Cardiovascular drugs and therapy. 2017; 31(1), 63-75. Copyright 2017 by McGowan et al.)

The harmful cardiac effects of doxorubicin can severely affect the extent and the quality of life of leukemia survivors (Dong et Cheng, 2018). This is true especially for survivors of childhood ALL who are more sensitive to these modifications (Lipshultz et al., 2013).
In the next four sub-sections, we describe the features of doxorubicin-mediated cardiotoxicity in greater detail as required for the current study.

2.2.1 Mechanisms of doxorubicin cytotoxic action

The mechanisms by which doxorubicin exerts its cytotoxic function have been extensively studied. Several molecular pathways have been proposed as modes of action but the exact global mechanism by which doxorubicin acts in cancer cells has not been fully elucidated to date (Yang, Teves, Kemp, et Henikoff, 2014).
The cytotoxic antileukemic action of this anthracycline has been primarily attributed to its ability of interfering with nucleic acid synthesis and, more specifically, with the catalytic function of the enzyme DNA topoisomerase IIα (Lynch, Guinee, et Holden, 1997; Lyu et al., 2007). This enzyme, which is a marker of proliferation expressed in proliferating cells and in neoplastic tissues, plays a critical role in several processes of the cell cycle, including DNA replication and RNA transcription It catalyze the unwinding of DNA: binds DNA supercoils, breaks both strands of one DNA duplex, passes the other duplex through the resulting gap, and reseals the break (Yang et al., 2014; Burden et Osheroff, 1998; Lyu et al., 2007). Under physiological conditions (i.e., in the absence of doxorubicin) the topoisomerase-DNA complex has reversible nature: the DNA breaks double-stranded cut generated in the process of DNA replication are resealed (Swift, Rephaeli, Nudelman, Phillips, & Cutts, 2006). In chemotherapy, the relegation of the cleaved DNA is prevented by the intercalation of doxorubicin. Doxorubicin traps the target and stabilizes the enzyme-DNA complex by cross-links the topoisomerase to tumor DNA molecules (Burden et Osheroff, 1998; Lyu et al., 2007; Chang et Wang, 2018). The formation of topoisomerase-doxorubicin-DNA complexes generates double-stranded cut in the genome of leukemia cells, which, if not repaired, ultimately trigger an apoptotic response (Swift et al., 2006; Lyu et al., 2007). Other molecular mechanisms that have been proposed to explain doxorubicin-induced cell death include inhibition of DNA and RNA synthesis, formation of formaldehyde-mediated doxorubicin-DNA adducts, ceramide overproduction, and generation of free radicals (Swift et al., 2006; Yang et al., 2014). It is important to stress that the enlisted mechanisms are not mutually exclusive (Swift et al., 2006). Furthermore,

it has been suggested that the generation of free radicals has an important role in the toxicity of doxorubicin within cardiomyocytes (Meiners, Shenoy, et Zordoky, 2018). Neoplastic cells require a higher uptake of iron compared to the myocytes. Doxorubicin is an iron chelator, binds the cellular iron and boosts the production of myocardial reactive oxygen species (ROS). These species damage the DNA which in turn can contributing to the generation of damage.

2.2.2 Histopathological features of doxorubicin cardiotoxicity

The nature of the histological cardiac injury caused by doxorubicin has been investigated in animal models and in humans primarily by biopsy of the ventricular myocardium (Aissiou, 2016). In such analyses, tissue specimens collected from the ventricular walls were processed and then attentively examined by the electron microscope in order to identify the lesions occurred at the cellular level.

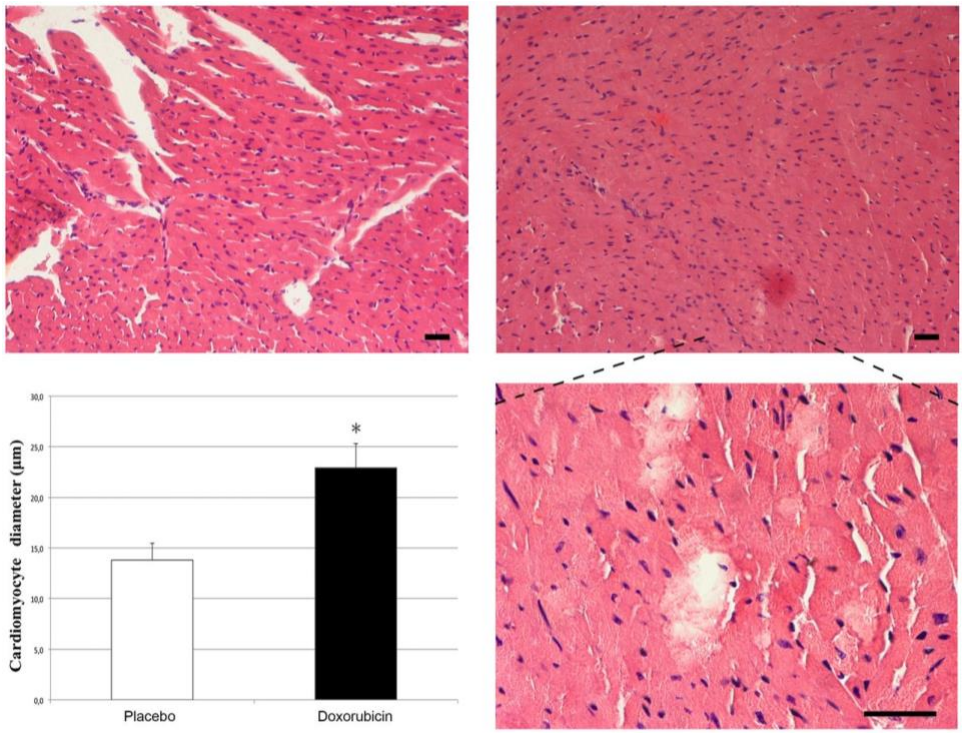

Figure 2.4. Myocardial sections collected from the doxorubicin-exposed and placebo groups at day 7 after injection: normal (**top left**); altered cardiac histology (**top right**).

(Reproduced with permission from: D., Rea et al. *Strain analysis in the assessment of a mouse model of cardiotoxicity due to chemotherapy: sample for preclinical research.* in vivo. 2016; 30(3), 279-290. Copyright 2016 by International Institute of Anticancer Research)

With this experimental technique, Rea et al. (2016) showed that myocardial injury manifests itself as vacuolization of the cytoplasm and an amplified apoptotic death of cardiomyocytes in the early days after doxorubicin exposure in mice (dose of 2.17 mg/kg for 7 consecutive days). Biopsy data acquired one-week post-injection revealed that treatment was also accompanied by an increase in the content of myocardial collagen and an enlargement of the remaining cardiomyocytes. Greater fibrosis was observed in myocardial samples from the treated animals when compared against the placebo group (**Figure 2.4**).

Similar results were found by Zhou et al. (2001) in a study to evaluate the effects of doxorubicin on the cardiovascular system of rats with 4 to 8 weeks of daily injections (2 mg/kg). Evidence of mitochondrial and myofibrillar damage and loss, and cellular edema were present in the treated animals. Furthermore, this study suggested that the degree of cytoplasmic vacuolization and, thus, the extent of cell injury relate to the duration of doxorubicin exposure. Mice with injections for 6 weeks exhibited myocytes with small cytoplasmic vacuoles, damage more diffuse after 8 weeks of injection. Histological examination also revealed that myocardial cell injury did not heal over time, but rather progressed for weeks after discontinuation of treatment. At 5 weeks after exposure to doxorubicin, damaged cardiomyocytes accounted for about 20% of the total number in rats with 6 weeks of injections. This percentage increased to 30% when the duration of exposure was 8 weeks. Similar histological alterations were documented by Lipshultz et al. (2012) in a group of pediatric ALL survivors (median cumulative dose of doxorubicin, 300 mg/m^2) when measuring biochemical biomarkers for myocardial injury. The blood levels of these biomarkers indicated that doxorubicin induced death of cardiac myocytes during treatment and for few months after the last exposure. Moreover, it was shown that the reduction in the number of functional cardiomyocytes caused an increase in the diameter of the remaining cells (as was seen in the doxorubicin-exposed mice) at 4 years after chemotherapy (Lipshultz et al., 2012). These myocytes were subjected to a greater workload which force them to compensate so as to maintain the normal heart structure (Sabbah et Goldstein, 1993; Lipshultz, Alvarez, et Scully, 2008).

2.2.3 Macroscopic features of doxorubicin-related cardiotoxicity

If sufficiently large, the loss of functional cardiac units results into a higher workload on the viable tissue, which in turn triggers a series of compensatory structural events (within the myocardium) aimed to preserve the normal ventricular structure (Sabbah et al., 1993; Adams et Lipshultz; 2005; Schunke, Coyle, Merrill, et Denhardt, 2013; Coviello, 2018). Throughout this process, the left ventricle undergoes progressive changes in geometry. Such alterations are referred to as ventricular chamber remodeling. The wall of the ventricle becomes progressively thinner, while the diameter increases, possibly leading to the dilation of the chamber. As a result of these changes in cavity size and shape, ventricular afterload and myocardial wall stress increase (Lipshultz et al., 1991; Wouters et al., 2005; Lipshultz et al., 2008). The loss of contractile tissue following doxorubicin therapy may also cause a reduction in myocardial contractility (Lipshultz et al., 1991; Giantris et al., 1998). This decreased contractility, together with an elevated afterload, in turn, can profoundly affect the global function of the LV, giving rise to give rise to compromised diastolic filling.

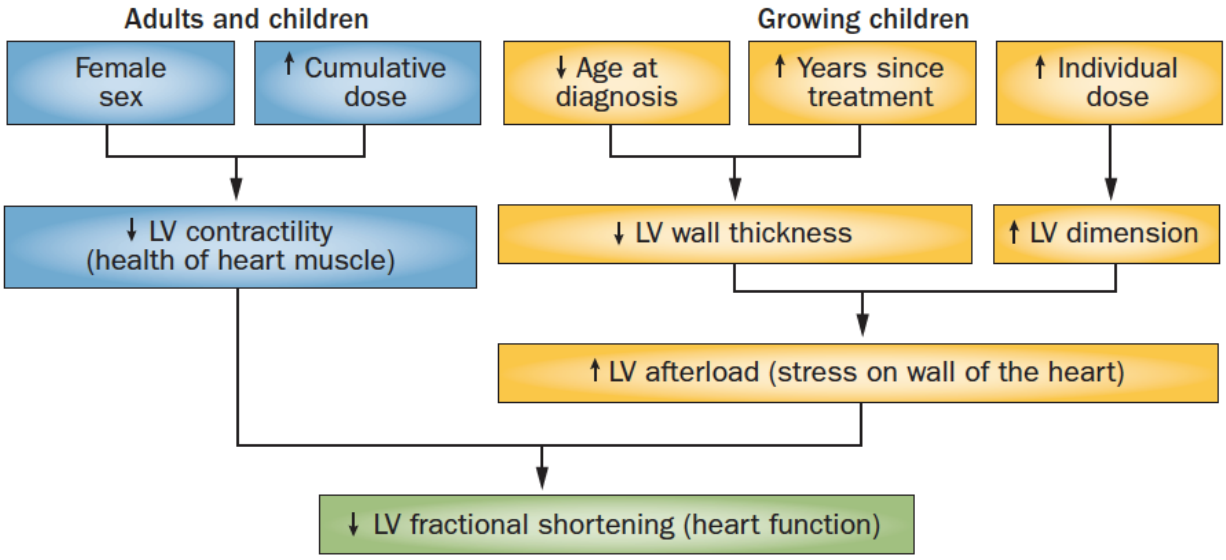

Figure 2.5. Risk factors for cardiac abnormalities after treatment with doxorubicin in long-term survivors of childhood and adult cancer.

(Reproduced with permission from: Lipshultz, S. E., Cochran, T. R., Franco, V. I., & Miller, T. L. *Treatment-related cardiotoxicity in survivors of childhood cancer.* Nature reviews Clinical oncology. 2013; 10(12), 697. Copyright 2013 by Macmillan Publishers Limited.)

LV chamber remodeling is progresses gradually over time and may turn into a pathologic process promoting the development of cardiomyopathy or congestive heart failure (Wouters et al., 2005). The deterioration of the ventricular function can continue for years and become apparent even 4 to 20 years after completion of treatment (Huang et al., 2010; Lipshultz et al., 2012; Vachhani et al., 2017). The manifestations of the spectrum of cardiotoxicity range from subtle alterations in the structure and function of LV to more severe complications, which are congestive heart failure and cardiomyopathy.

The degree and progression of doxorubicin-induced cardiotoxicity are associated with several well-established risk factors (Lipshultz et al., 2008). Clinical studies in childhood and adult leukemia survivors have demonstrated that the likelihood of developing late cardiovascular complications increases with the cumulative dose of doxorubicin administered during therapy (Meiners et al., 2018). In particular, doses of this agent greater than 450-550 mg/m^2 are linked with more serious complications. Higher rate of administration, female gender, very young and very old age at the time of therapy, and exposure to radiation have also been reported as risk factors for delayed cardiotoxicity (Bansal, Amdani, Lipshultz, et Lipshultz, 2017).

2.2.4 Prevention and reduction of doxorubicin-related cardiotoxicity

In response to concern about the cardiac health of cancer survivors, researchers and clinicians have implemented a variety of potential protective measures directed to prevent or minimize the harms of doxorubicin on the myocardial tissue (McGowan et al., 2017).

Given the close relationship between cumulative doxorubicin dose and risk for late cardiotoxicity, current preventive strategies primarily focus on limiting the total dose of doxorubicin delivered during treatment to 450-550 mg/m^2 so as to reduce the risk for short- and long-term cardiotoxicity without compromising the tumor-killing activity of doxorubicin (Dong et Chen, 2018). Lipshultz et al. (2012) have shown that the administration of doxorubicin doses above this threshold reduced significantly the incidence of heart failure. However, other authors observed that cardiotoxicity occurs even at lower doses, leading to conclude that no safe dose exists (Harake, Franco, Henkel, Miller, et Lipshultz, 2012; Silverman, 2014; Bassareo et al., 2016). This strategy does not guarantee that the cardiac injury will not occur and, therefore, needs to be complemented by other measures.

Clinicians have investigated the efficacy of different dosing schedules designed to lower the myocardial concentration of doxorubicin or its metabolites and, thereby, reduce the risk for cardiac

toxicity. In particular, continuous administration of doxorubicin was tested in both children and adults. The results of these studies were then compared with those obtained for the bolus injection. Continuous infusion had significant benefits in preventing cardiac functional deterioration over the bolus-infusion on a short-term basis in adult. No cardioprotective benefit was proven in children (Adams et Lipshultz, 2005). A study of the efficacy of continuous infusion in preventing cardiac functional deterioration reinforced this claim. No difference in LV structure and function was documented between the two schedules in children with high-risk ALL at 8 years after cessation of treatment (Lipshultz et al., 2012; Jain et al., 2017).

Another management strategy for toxicity involves the administration of structural analogues or alternative formulations of doxorubicin that are deemed to be less harmful to the cardiac tissue. Epirubicin, idarubicin, mitoxantrone, and liposomal doxorubicin are examples of such anticancer drugs (Giantris et al., 1998). Epirubicin and idarubicin induced fewer clinical and subclinical cardiac alterations compared with the same doses of doxorubicin, but they were also less potent as anticancer agents (Hande, 1998; Smith et al., 2010). Liposomal doxorubicin has yielded promising results in preliminary studies in survivors of adult ALL, reducing the incidence of cardiac complications significantly (Rahman et al., 2007). Studies of the efficacy and the late cardiac effects of this alternative formulation are underway in childhood ALL survivors (Silverman, 2014).

A deeper understanding of the mechanisms by which doxorubicin interacts with healthy and tumor cells has led to the development of a broad range of cardioprotective agents. Various beta-blockers, free-radical scavengers, antioxidants, and inhibitors of the renin-angiotensin-aldosterone system, have been considered as a means to reduce the incidence of doxorubicin-related myocardial injury during and after therapy (Wouters et al., 2005; Harake et al., 2012; McGowan et al., 2017). The cardioprotective efficacy of these agents and their side effects on heart have been evaluated in several clinical trials on survivors of adult and childhood cancers: some agents were able to provide some degree of protection, others failed in reducing cardiotoxicity (Vejpongsa et Yeh, 2014). At the current time, the only cardioprotectant approved for use in oncological practice is dexrazoxane (Sharalaya and Collier, 2018). Developed initially as an antitumor agent, this free-radical scavenger is recommended as part of the standard of care for adult patients assigned to receive large doses of doxorubicin, due to its ability to reduce the incidence of myocardial injury without compromising the chemotherapeutic value of doxorubicin (Hasinoff et Herman, 2007; Sepe, Ginsberg, et Balis, 2010; Harake, 2012). The protective activity of dexrazoxane has been primarily ascribed to its

affinity for intracellular iron, which is believed to be stronger than that showed by doxorubicin or the other anthracyclines. Once inside the myocyte, dexrazoxane binds free iron or sequestrates the metal complexed to the chemotherapeutic, thereby reducing the generation of iron-catalyzed ROS and lowering cellular damages associated to cardiac injury (Hasinoff et Herman, 2007; Bryant et al., 2007; Harake, 2012; Lipshultz, Franco, Miller, Colan, et Sallan, 2013).

2.2.5 Monitoring and Detection

Despite the proven efficacy in reducing the incidence of doxorubicin-related myocardial injury, none of the strategies currently available confer complete protection against the adverse effects of chemotherapy (Silverman, 2014). Taken together with the observation that cardiotoxicity may not manifest until weeks or years after the end of therapy, the lack of complete protection emphasizes the importance of screening and effective detection of toxicity (Jurcut et al., 2008; Dong et Chen, 2018). Monitoring the cardiac status of children who underwent treatment with doxorubicin is of great importance especially during the silent phase of left ventricular dysfunction. Intervention before the manifestation of clinical symptoms allows to prevent or inhibit the progression of tissue damage to a more advanced stage (Ali et al., 1994; Khouri, 2015; Coviello, 2018).

There are currently multiple invasive and non-invasive clinical techniques for follow-up and detection of doxorubicin-related cardiotoxicity. Traditionally, endomyocardial biopsy has been the preferred method for such an evaluation in virtue of its high sensitivity to structural changes in the myocardial tissue (Jain et al., 2000; Jain et al., 2017). In a study by Friedman et al. (1978) endomyocardial biopsy was able to detect the subclinical myocardial injury induced by a DOX dose of 180 mg/m^2. However, this procedure is invasive, with the risk of severe side effects (e.g. hematoma, damage to the tricuspid valve…), and thus not feasible for use in daily clinical practice (Rahman et al., 2007; Jurcut et al., 2008; Tham et al., 2013).

Echocardiography is the current imaging modality of choice for evaluating the structural and functional cardiac abnormalities associated with chemotherapy in a non-invasive fashion (Jurcut et al., 2008; Da Silveira et al., 2016). Various parameters of systolic (LV ejection fraction, shortening fraction, and systolic wall thickening) and diastolic function (mitral inflow pattern E/A ratio, isovolumic relaxation time, and pulmonary venous flow pattern) are measured in ALL survivors (Jurcut et al., 2008). The alterations in the experimental measurements of these clinical indices with respect to baseline values are then analyzed by the clinicians (Khouri et al., 2015). Advantages

of the echocardiography include the non-invasiveness of the measurements, the absence of ionizing radiation, the high portability and the easy availability of the acquisition apparatus (Rahman et al., 2007). Nevertheless, this imaging modality has poor sensitivity in detecting structural and functional cardiac changes during the silent phase, which makes the echocardiographically-derived indices less suitable to evaluate subclinical myocardial toxicity (Briant et al., 2007; Levis, Binkley et Shapiro, 2017; Jain et al., 2017).

Another imaging modality to assess the cardiotoxic impact of doxorubicin in cancer survivors is cardiac magnetic resonance (Lunning et al., 2015). CMR is a more sensitive test for monitoring cardiotoxicity than echocardiography (Fallah-Rad, 2011). The feasibility of CMR for cardiac toxicity evaluation has been recently established. Software for 3D geometric modeling of the cardiac chambers allow determination of LV volumes, ejection fraction, wall thicknesses and mass from CMR scans (Levis et al., 2017; Jain et al., 2017). These estimates were proven to be more reliable, precise and accurate compared to echocardiographically-derived indices due to the ability of CMR to provide clear definitions of the LV wall contours (Loganathan et al., 2005; Fallah-Rad, 2011; Gusso et al., 2012). Nonetheless, the routine use of CMR imaging is restricted by its limited availability, the patient tolerance to the examination, as well as the high costs associated with this procedure (Jurcut et al., 2008).

2.3 Analysis of the mechanical properties of the passive LV myocardium

In the context of cardiac dysfunction, ventricular function has been evaluated using the mechanical properties of the resting myocardium. These parameters are valid indicators of global and regional cardiac performance, as the mechanical functioning of the left ventricle is strongly influenced by the mechanics of the myocardium (Wang et al., 2013; Kichula et al., 2014, Wang et al., 2015). The architecture of the myocardium at the small scale and the 3D morphology of the ventricle determine the mechanical properties of the tissue, which in turn are responsible for the mechanical function of the ventricle (Costa, Holmes, et McCulloch, 2001; Sirry et al., 2016). It therefore follows that pathophysiological changes within the myocardium can adversely affect the mechanical properties of the intact tissue. This may result in alterations in the shape and size of the ventricular chamber, which can eventually give rise to compromised diastolic filling (Harris et al., 2002; Zhang et al., 2018). Given these facts, the evaluation of the myocardial tissue properties offers the potential to investigate the mechanisms underlying cardiovascular pathologies and their treatment (Bensamoun

et al., 2006; Hsu et al., 2007; Dorsey et al., 2015). Also, this approach may yield valuable insights into doxorubicin-attributable adverse effects on the hearts of cancer patients.

2.3.1 Mechanical characterization of passive myocardium

The passive material properties of the cardiac muscle have been commonly characterized by means of mechanical testing (Holger, 2006). Such experiments are performed on samples of tissue excised from the ventricular walls and cut out to desired shape and dimensions. Once the specimens have been prepared and mounted on the testing apparatus, one or more loads of appropriate intensity are applied to the tissue along specific axes (see **Figure 2.6**) and following a pre-established protocol (Sommer et al., 2015; Sirry et al. 2016). It is noteworthy that the choice of the test parameters (e.g., frequency and loading rate) and the direction of the specimen cut is related to the information that the investigators aim to obtain (Weiss et Gardiner, 2001). Depending on the goal, a variety of experimental tests can be carried out on the isolated myocardium.

- **Uniaxial mechanical tests**: this test is the most commonly performed on isolated myocardium (Holger, 2006). In uniaxial testing, the specimen is cut along the direction of the myocardial fibers (which is the predominant loading axis in vivo) and is subjected to a compression or tension along the very same direction. It is therefore clear that this class of tests is inadequate to fully characterize the 3D mechanics of the cardiac muscle, which exhibits an anisotropic behavior (Gupta, 1993; Costa et al., 2001; Sirry et al., 2016). The myocardium exhibits an anisotropic behavior, while uniaxial testing provides information on the material response only along the fiber direction (Holger, 2006; Gaemi, 2008). The structure and organization of the muscle fibers and extracellular matrix components are behind this complex behavior (Sirry et al., 2016). Gaemi et al. have conducted this test on isolated papillary muscle and trabeculae.
- **Biaxial mechanical tests**: this testing technique is among the most common tests performed on isolated myocardial tissue, together with the uniaxial experiment. Compared with the latter, biaxial test provides a more complete characterization of the mechanical response of the tissue. Biaxial testing allows to determine the properties of myocardium in the two primary loading axes. The specimen, which usually is rectangular-shaped, is oriented parallel and transverse to the fiber direction and the load is applied in two in-plane orthogonal directions (Hu, 2015). Sirry et al. (2016) have performed biaxial loading experiments in rat model. They tested

specimens derived from an infarcted myocardium with the intent to elucidate the effects of this disease on the mechanics of the rat myocardium.

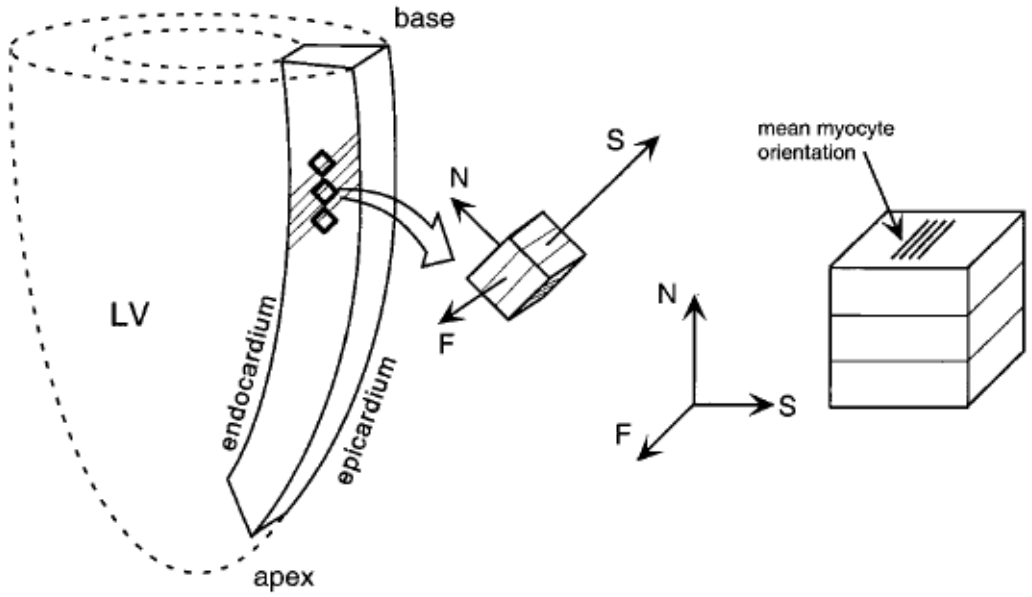

Figure 2.6. Diagram showing the main directions along which the load is applied to the tissue sample during the mechanical tests: the fiber axis (**F**) which is the direction of the muscle fibers; the sheet axis (**S**) which is the direction transverse to the fiber axis; the normal axis (**N**) which is perpendicular to the specimen (Holger, 2006).

(Reproduced with permission from: S., Dokos, B. H., Smaill, A. A., Young, et I. J., LeGrice. *Shear properties of passive ventricular myocardium*. American Journal of Physiology-Heart and Circulatory Physiology. 2002; 283(6), H2650-H2659. Copyright 2002 by the American Physiological Society.)

- **Triaxial mechanical tests**: Triaxial tissue testing is performed by pulling the myocardial sample into three directions simultaneously. In addition to the loading directions of the biaxial tests, compression or tensile loading is applied in the third orthogonal direction of the specimen. Despite its ability to capture the 3D mechanics, the use of triaxial tissue testing is limited for technical reasons (Halperin et al., 1987). The samples are typically a thin membrane: the small dimensions of the membrane make difficult to handle them (Holger, 2006).

- **Multiaxial simple shear experiments**: are used to gain insight into the shear properties of the excised passive myocardium (Dokos, Smaill, Young, et LeGrice, 2002). This test provides an additional means to gain an increased understanding of the anisotropic behavior of the cardiac tissue.

2.3.2 Modeling ventricular myocardium

Experimental tests on the isolated cardiac muscle have highlighted some important features of the mechanical response of the tissue. By performing a series of biaxial experiments, Yin et al. (1987) demonstrated that the myocardial tissue exhibits an anisotropic mechanical behavior. Nevertheless, these techniques do not allow the complete characterization of the 3D mechanics of the intact heart or its component chambers (Wang et al., 2009; Wang et al., 2015). As we explained above, the behavior of the cardiac muscle is imparted by the microstructural organization of the myocardial tissue and the 3D structure of the cardiac wall (Costs et al., 2001). The contribution of the latter element is not taken into account in the mechanical tests on isolated tissues, thus limiting the description of the properties of the intact ventricular muscle (Guccione, McCulloch, et Waldman, 1991). Furthermore, we must keep in mind that the vascularity of the myocardium changes greatly after death (Périé, Dahdah, Foudis, et Curnier, 2013). This contributes to the uncertainty about how well the information from tissue samples are translated to the intact muscle. Consequently, isolated tissue testing needs to be complemented by other strategies to fully characterize the 3D mechanics of the left ventricle.

A complementary approach to quantify the material properties of the intact myocardium is offered by mathematical modeling of the ventricular mechanics (Sermesant et al., 2006; Costa et al., 2001; Wang, Nielsen, et Nash, 2015). Numerical modeling of the heart is a powerful tool and its use for estimating myocardial properties has attracted interest for a broad spectrum of medical applications. Finite element models of the left ventricle have been applied to identify and investigate the mechanisms underlying heart failure, cardiomyopathies, myocardial infarction, and other cardiac disease processes (Sermesant et al., 2006; Lapointe, 2016). In research setting, models have also been used to evaluate the efficacy of various therapeutic approaches, such as surgical ventricular remodeling and biomaterial injection therapy, in limiting the adverse LV remodeling and restoring normal cardiac geometry and function (Guccione et al., 2003; Lee et al., 2013; Kichula et al., 2014). This approach provides information about the 3D mechanics of treated and

diseased hearts that may facilitate the development of more efficacious treatment strategies or the optimization of the therapy (Wang et al., 2015; Sack, Davies, Guccione, et Franz, 2016). Moreover, by simulating the treatment effects on myocardial mechanics and cardiac functionality before the intervention, patient-specific mathematical modeling can potentially assist health care providers with treatment planning and clinical decision (Sack et al., 2016).

2.3.2.1 Previous FE model studies

The development of a realistic mathematical model of the left ventricular mechanics requires the integration of structural and functional information from different sources (Wang et al., 2009; Sack et al., 2016).

- **Cardiac geometry**. A description of the shape and structure of the LV chamber is due. The vast majority of models documented in the literature were created from in vivo measurements of the cardiac structures. For a more realistic model, authors derived the in vivo geometry and structure of the LV chamber directly from computed tomography, echocardiographic, or CMR imaging data of the subject under examination via a segmentation process (Lapointe, 2016). This task was performed with the aid of software for 3D geometric modeling, which are able to extract the heart morphology and to transform the segmented image data into an anatomically accurate model of the ventricle. The incorporation of in vivo data enables prediction of cardiac function on a subject-specific basis.
- **Constitutive laws**. After obtaining a geometrical description of the LV chamber, we need to integrate the constitutive relations that describe the mechanical response of the cardiac muscle to the intra-ventricular pressure (relationship between stress and strain of the myocardium) (Costa et al., 2001).
- **Boundary conditions**. Lastly, physiologically-consistent loading and displacement boundary conditions are imposed on the model in order to simulate the deformation of the LV throughout the cardiac cycle (Costa et al., 2001). Specifically, the boundary conditions are the pressures developed in the LV cavity during systole and diastole. Obtaining this information is possible through imaging experiments in vivo or through hemodynamic models of the heart in silico (Lumens et Delhaas, 2012; Wang et al., 2015).

A few examples of finite element models of the left ventricle are reported in the following.

Guccione et al. (2003) formulated a FE model of a globally dilated LV to evaluate the impact of a remodeling device for the treatment of cardiomyopathy and heart failure on myocardial mechanics and cardiac functionality. In this investigation, the geometry of the LV chamber was based on experimental measurements reported in the literature. More specifically, the LV chamber was modeled as a thick-walled axisymmetric truncated ellipsoid with the following dimensions: endocardial volumes of 213 mL, epicardial volume of 333 mL, and ratio of diameter to length of 0.732. Data on fiber orientation (from canine heart model) was also incorporated into the LV model, with the intent to more closely match the in vivo behavior of the cardiac muscle. The myofiber angle varied linearly across the ventricular wall, ranging from -60° at the epicardium to 60° at the endocardium. To create the FE mesh for simulation, the reconstructed 3D geometry was discretized into 384 smaller elements, which included 8 longitudinal elements, 12 circumferential elements, and 4 transmural elements. The passive and active mechanical properties of the muscle tissue were described by transversely isotropic, hyperelastic constitutive relations and were then computed to evaluate the efficacy of the remodeling device. The FE model of Guccione does not allow the subject-specific estimation of the myocardial mechanical properties since the ventricular dimensions were derived from experimental data and were only representative of the patient population. Information about the realistic shape of the heart are necessary to assess subject-specific efficacy of the device.

The model of Young (2000), developed by a team of researchers at the University of Auckland (New Zealand), was used to conduct a preliminary study on the mechanisms behind the heart failure (Wang et al., 2009). Unlike the previous FE model, the current one was customized to image data of the subjects under examination. To be more precise, the in vivo geometry of the LV at mid-diastole was obtained directly from the CMR scans of the study participants using a guide-point framework (Cardiac Imaging Modeling v8.1, University of Auckland, New Zealand). Both inner and outer borders of the LV chamber were employed for the segmentation and 3D reconstruction. Subsequently, the geometrical model of the LV was meshed with 16 elements. Each element was defined using (cubic) Hermit interpolation in the circumferential and longitudinal directions and linear interpolation in the transmural direction (4 longitudinal elements, 4 circumferential elements, and one transmural elements) (Wang et al., 2009). This analysis accounts for myofiber orientation from a canine heart model. Myocardium was modeled as a hyperelastic material with the Guccione transversely-isotropic hyperelastic constitutive law (Guccione et al., 1991). The model was also

able to estimate the in vivo diastolic and systolic material properties of the infarct tissue. Passive stiffness and contractility of myocardial tissue in these laws were identified via an inverse modeling approach by comparing the predicted and the experimentally recorded myocardial deformations.

Using a FE model of the left ventricle, Wenk and colleagues (2011) evaluated the efficacy of intra-myocardial biomaterial injection in inhibiting the adverse cardiac remodeling triggered by heart failure. To replicate the in vivo geometry at early diastole, the model was developed from the 2D echocardiographic data of two ovine hearts (from a treated and an untreated animals), which were imaged two months after infarction. Thirty-two circumferential elements, 18 longitudinal elements and 3 transmural elements (total of 1728) composed the FE mesh for the LV mechanics simulation. In the study, the Guccione transversely-isotropic hyperelastic constitutive law was also employed to represent the mechanical behavior of the myocardial tissue in relaxed condition. By matching the LV cavity pressure measured in vivo with that predicted by the FE model, the stiffness parameter of the Guccione law was estimated for both untreated and treated infarct regions. The FE-simulated results were then compared and analyzed to assess the impact of biomaterial injection therapy on ventricular mechanics.

More recently, Lee and associates (2013) described a personalized biomechanical model of the LV that allows to investigate the effects of surgical ventricular restoration, a therapy for heart failure, on cardiac performance. Subject-specific information on the ventricular geometry at early diastole were integrated into the model directly from the CMR scans of 12 patients diagnosed with heart failure. To be more specific, the model was reconstructed on the segmented contours of the inner and outer borders of the LV chamber. In addition, the myofiber distribution was incorporated in the FE model with the intent to more closely match the in vivo behavior of the cardiac muscle. The orientation of the myocardial fibers varied linearly across the ventricular wall, ranging from -60° at the epicardium to 60° at the endocardium. The FE discretization for numerical simulation was obtained by projecting a mesh between the two reconstructed surfaces. Lee et al. made use of the transversely-isotropic hyperelastic constitutive law by Guccione to model the mechanical response of the passive and active myocardium (Guccione et al., 1991). The passive stiffness parameter was the result of a calibration to match the in vivo measured and the simulated LV cavity volumes of the FE model. The efficacy of surgical ventricular restoration in limiting the ventricular chamber remodeling was assessed by analyzing the passive and active mechanical properties of the treated myocardium.

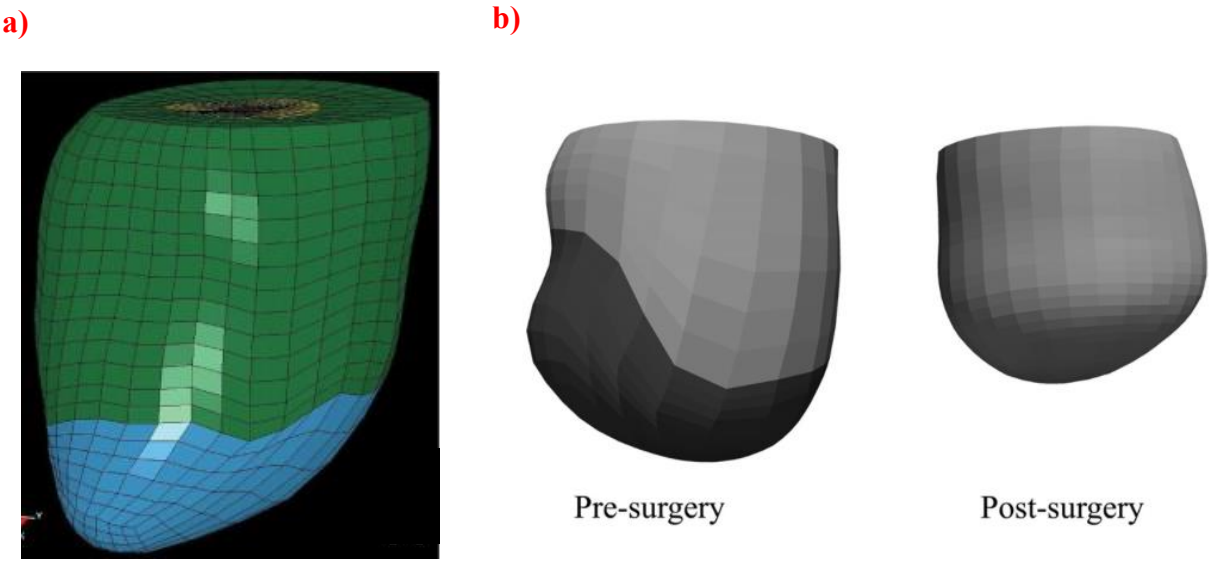

Figure 2.7. Computational models of the left ventricle showing the boundaries of the FE mesh: model of Wenk et al. (2011) (**a**); model of Lee et al. (2013) (**b**).

(Reproduced with permission. L. C., Lee et al. *Analysis of patient-specific surgical ventricular restoration: importance of an ellipsoidal left ventricular geometry for diastolic and systolic function*. Journal of applied physiology. 2013; 115(1), 136-144. Copyright 2013 by the American Physiological Society.

J. F., Wenk et al. *A novel method for quantifying the in-vivo mechanical effect of material injected into a myocardial infarction*. The Annals of thoracic surgery. 2011; 92(3), 935-941. Copyright 2011 by The Society of Thoracic Surgeons.)

2.3.3 Passive stiffness of the left ventricular myocardium

Among the mechanical properties underlying the behavior of the resting myocardium, stiffness has attracted particular interest as a means of assessing cardiac dysfunction. The passive stiffness of the myocardial muscle is an indicator of global LV performance and, more precisely, a determinant of diastolic function (Hsu et al., 2007; Sommer, 2015; Miller, Kolipaka, Nash, et Young, 2017). Myocardial stiffness has been defined as the resistance of the tissue to stretching by the pressure developed in the LV cavity during the cardiac cycle (Mirsky, 1984). It is thus dependent upon the intra-ventricular pressure. LV myocardial stiffness varies throughout the heart cycle together with

the ventricular pressure, attaining higher values during systolic contraction (Wassenaar et al., 2016; Kolipaka, Araoz, McGee, Manduca, et Ehman, 2010).

2.3.3.1 Prognostic value of altered passive myocardial stiffness

Extensive literature exists about the prognostic significance of passive myocardial stiffness in the context of cardiac dysfunction. Many investigators have examined this myocardial stiffness with the intent to gain a greater understanding of the ventricular remodeling process that takes place in a variety of cardiac pathologies and therapeutic approaches (Kolipaka et al., 2009; Mojsejenko et al., 2015; Mazumder et al., 2017). These studies showed that the changes in ventricular structure and function were accompanied by an altered tissue stiffness during filling (Gupta et al., 1994). Much of the research in this area have relied on cardiovascular imaging for non-invasive evaluation of muscle stiffness. Obtaining this information was possible through cardiac magnetic resonance elastography imaging or acoustic radiation force impulse (Hsu et al., 2005; Kolipaka et al., 2010; Ohtani et al., 2012; Li et al., 2017). As an alternative, echocardiographic parameters, such as the diastolic wall strain index, were used as measures of myocardial stiffness (Da Silveira et al., 2016). Only a limited number of studies have quantified this biomechanical parameter by using medical imaging data in connection with 3D computational models of the LV. Among them, two works warrant particular mention as they explain our interest in the assessment of passive tissue stiffness in cancer survivors. Their outcomes suggest that myocardial stiffness may yield valuable insights into the ventricular chamber remodeling related to doxorubicin therapy.

Using the FE LV model described in paragraph 2.3.3.1, Wang et al. (2013) estimated the in vivo muscle stiffness during diastasis for a mixed cohort of normal subjects and asymptomatic patients with a heart failure diagnosis (range of age, 45 to 84 years) (Fonseca et al., 2011). **Table 2.1** reports the results of this investigation in terms of hyperelastic property (C_1), which served as a surrogate of myocardial stiffness. As can be seen, the mean values of C_1 were 1.8 kPa, 5.9 kPa, and 6.0 kPa for normal, hypertrophic, and heart failure subjects, respectively. The comparison demonstrated that the stiffness parameter was significantly higher in the diseased subjects compared with their referent controls ($p<0.05$). The LV remodeling process triggered by heart failure results in altered myocardial stiffness. Pathophysiological changes in LV performance due to heart failure were associated with changes in myocardial stiffness during mid-diastolic filling.

Table 2.1. In vivo estimates of passive myocardial stiffness (mean ± standard deviation) for the three groups of study participants. Asterisks denote difference with respect to the healthy group at $p<0.05$ significance level.

Study group	**C1** (kPa)
Normal	1.8 ± 0.6
Hyperthrophy	6.0 ± 1.3*
Non-ischaemic heart failure	5.9 ± 1.7*

In a recent study, Li and colleagues (2017) assessed 94 long-term survivors of acute lymphoblastic and myeloid leukemias (age at the time of investigation, 22.2 ± 5.5 years) who had been previously treated with moderate doses of doxorubicin therapy. All subjects were asymptomatic and exhibited a normal ejection fraction (lower than 50%). Echocardiographically-derived measurements of LV structure and function were employed for this assessment. Diastolic wall stress (DWS) index was used as a measure of passive myocardial stiffness: leukemia survivors exhibited a lower DWS and, thus, a higher myocardial stiffness compared with the control subjects ($p<0.001$). Furthermore, in accordance with previous observations, Li et al. documented an association between myocardial stiffness and cumulative dose of doxorubicin administered to the patient. These findings led the authors to conclude that passive myocardial stiffness was impaired by doxorubicin toxicity.

2.4 Key points

We now briefly reiterate a few concepts which are deemed to be particularly relevant to the full understanding of the rest of this work.

- Doxorubicin, which is widely used to treat acute lymphoblastic leukemia, can cause a wide range of acute and chronic adverse reactions on the heart. This cardiotoxicity may trigger a maladaptive remodeling of the left ventricular geometry, which may importantly affect global cardiac function. The risk of cardiotoxicity is higher in ALL survivors who underwent high-dose chemotherapy with doxorubicin.

- A variety of intervention strategies have been implemented in an attempt to confer protection against the side effects of doxorubicin during and after treatment. Among them, the protective agent dexrazoxane has proven particularly effective in reducing the incidence of myocardial injury in cancer patients. However, thus far, none of the current measures completely eliminates the risk for long-term cardiac complications, making the issue of doxorubicin toxicity more concerning.
- CMR imaging has recently emerged as an alternative to echocardiography for evaluating the structural and functional cardiac abnormalities associated with chemotherapy due to superior accuracy and repeatability. Although echocardiography is the imaging modality of choice for detection and screening of cardiotoxicity in routine patient care, there is evidence that the current echocardiographic indices are not sensitive enough to identify subtle (silent) alterations in LV structure and function.
- The effects of various cardiac diseases on cardiac functionality and myocardial mechanics have received increasing attention for finite element modeling. The use of numerical models of the LV mechanics as a tool for estimating myocardial tissue properties has the potential to provide information regarding the mechanics of the intact myocardium that would be not feasible to measure experimentally.
- The importance of myocardial stiffness as a determinant of global ventricular function has been established in earlier studies in treated and diseased hearts. Changes in LV function have been associated with alterations in muscle tissue stiffness during diastolic filling. The outcomes of these investigations also suggest that passive myocardial stiffness can yield valuable insights into the structural and functional LV changes triggered by exposure to doxorubicin.

CHAPTER 3 MATERIALS AND METHODS

In the present chapter, we provide relevant information about the study population and the data acquisition protocols for clinical assessment of the participants. We outline the basic steps of the procedure for generating a subject-specific finite element model of the ventricular geometry from the acquired medical data. Subsequently, we introduce the FE modeling framework developed by the University of Auckland and detail the mechanical analyses performed on the reconstructed 3D models using this framework. Ultimately, we describe the statistical methods employed for data analysis.

3.1 Study population

The population for this study included 84 long-term survivors of childhood ALL who underwent doxorubicin-based chemotherapy at Sainte-Justine University Hospital Center in Montreal between January 1989 and July 2005 (Delvin et al., 2018). These subjects were cancer-free at the time of our analysis and had attained a minimum of 9 years of complete remission. They were drawn from the PETALE study, a larger project intended to gain new insights into the late adverse effects of the antileukemic treatment in a selected subgroup of the Quebec Childhood ALL cohort (Healy et al., 2010; Marcoux et al., 2017). The enrollment of survivors from the cohort was conducted after obtaining appropriate approval from the Institutional Review Board of Sainte-Justine Hospital, and after subjects and/or their parents signed an informed consent authorizing the use and analysis of personal medical records.

Once recruited, the participants were sorted into two groups according to their risk of tumor relapse: standard-risk (SR) and high-risk groups. To be specific, risk stratification was performed using a prognostic index incorporating several demographic and clinical features, such as the patient's age at diagnosis of cancer, the severity of illness, and cumulative dose of doxorubicin (Aissiou, 2016). Moreover, for the present analysis, the subjects treated for high-risk ALL were further divided into two groups depending on whether they did (HRdex) or did not (HR) receive the cardioprotective therapy (dexrazoxane) in an attempt to mitigate cardiotoxicity during and after chemotherapy. In brief, of the 84 long-term ALL survivors, 18 were classified as SR, 30 as HR, and 36 as HRdex. In **Table 3.1** we report relevant demographics and treatment-related characteristics for the entire cohort and by study group.

Table 3.1. Select demographic and clinical characteristics of the study population are reported as means with standard deviation. Data were abstracted from the medical records of the participants.

	Total ALL childhood survivors (n=84)		
	SR	**HR**	**HRdex**
Subjects per group	18	30	36
Female gender	9	13	19
Height (cm)	1.65 ± 0.10	1.66 ± 0.09	1.65 ± 0.11
Weight (kg)	67.28 ± 15.96	72.22 ± 16.22	64.81 ± 14.72
Age at diagnosis (years)	4 ± 2.33	8 ± 5.89	10 ± 5.06
Age at the time of analysis (years)	21 ± 6.45	27 ± 6.77	21 ± 5.35
Length of treatment (years)	2.12 ± 0.17	2.07 ± 0.26	2.18 ± 0.15
Years since exposure	14.52 ± 6.89	8.54 ± 3.32	17.12 ± 4.03
Mean cumulative dose of doxoruicin (mg/m2)	82.64	284.57	287.32
Mean cumulative dose of dexrazoxane (mg/m2)	-	-	2801.06
Cranial RT (subjects)	7	28	29
Median cumulative RT dose (Gy)	18.00	18.00	18.00

As this table illustrates, the survivor population consisted of 41 females and 43 males, whose ages ranged from a few months to 19 years at the time of diagnosis (mean±sd, 8±5.0 years) and from 11 to 36 years at the time of the clinical assessment (23±7 years). In particular, the standard-risk and dexrazoxane-exposed groups were similar in terms of age (21 years), and significantly younger as compared with the high-risk group (one-way ANOVA, $p<0.05$).

These subjects were treated for a median of 2.17 years according to one of five consecutive Dana Faber Cancer Institute ALL Consortium protocols (87-01, 91-01, 95-01, 00-01, and 05-01). While some small variations have been made over the years, all protocols included the administration of doxorubicin as a chemotherapeutic agent. For clinical reasons, the patients with standard-risk ALL received low cumulative doses of doxorubicin, whereas those judged to be at higher-risk of ALL recurrence received moderate doses (Marcoux et al., 2017). At the end of chemotherapy, the mean cumulative doses of doxorubicin amounted to 82.64 mg/m^2 body surface area, 284.57 mg/m^2, and 287.32 mg/m^2 for the SR, HR and HRdex groups, respectively. The mean cumulative dose of dexrazoxane delivered to the HRdex group amounted to 2801.06 mg/m^2. Other chemotherapeutic agents, such as cytarabine, vincristine, and prednisone, were administered to complement the anticancer action of doxorubicin. In addition, more than half of the cohort required cranial radiation therapy (RT; median cumulative radiation dose, 18 Gy) as part of their treatment. None of the participants underwent hematopoietic stem cells or bone marrow transplantation at any time during the treatment course. Further details about the dosing regimens, schedules, and treatment plan have been reported in the works by Silverman et al. (2010) and by Marcoux et al. (2017).

The group of survivors called for research was screened for metabolic disorders, bone morbidities, and delayed neurologic, cardiovascular, and musculoskeletal sequelae by a multidisciplinary team of experts. As indicated in **Table 3.1**, the data collection was carried out at nearby hospitals after 14.52 ± 6.89 years since the completion of chemotherapy for the SR group, after 8.54 ± 3.32 years for the HR group, and after 17.12 ± 4.03 years for the HRdex group. For the entire cohort, the median follow-up was 13.22 ± 5.97 years.

In order to establish a baseline for comparison, a proper control group was included in the study cohort. Ten healthy volunteers (HV; mean age at the time of examination ± sd, 22±4 years), with no history of cancer or cardiomyopathy and similar in terms of age to the childhood ALL survivors, were enrolled from an in-house study. Four subjects were of female sex, while 6 were males.

3.2 Clinical measurements

Investigation of late-onset cardiotoxicity due to doxorubicin-based chemotherapy included CMR imaging (for n=89 ALL survivors), transthoracic echocardiography (for n=89), and exercise stress testing (for n=34). The details of the protocols used for data collection are described as follows.

3.2.1 Cardiac magnetic resonance imaging

The acute leukemia survivors underwent CMR imaging at Montreal Heart Institute in Montreal. CMR data for the leukemia survivors were acquired with a standard ECG-gated cine sequence (Steady-State Free Precession) on a clinical 3T MRI system (Skyra, Siemens Healthcare, Erlangen, Germany) and an 18-channel phased array body matrix coil (Aissiou, 2016). The imaging protocol parameters used for acquisition include: slice thickness 8 mm, repetition time 34.6 ms, effective echo time 1.2 ms, flip angle 38°, iPAT factor 3, matrix 208x210 and in-plane pixel size 1.25x1.25 mm. About 14 slices were acquired in short-axis view, whereas a total of 3 to 4 slices were acquired at every heartbeat in long axis 2-chamber and 4-chamber views. For each slice, 25 phases of the cardiac cycle were obtained during multiple breath-holds. The total acquisition time per study was on the order of 15 minutes.

In the healthy volunteers, normal heart function was assessed at the Centre for Advanced MRI in Auckland according to a different acquisition protocol than the childhood ALL survivors. The scans were acquired with a Siemens 3 Tesla scanner (Skyra, Siemens Medical Systems, Erlangen, Germany). The following imaging parameters were employed for acquisition: slice thickness 6mm, repetition time 26.32ms, effective echo time 1.45 ms, flip angle 38°, iPAT factor 3, matrix 208x210, and in-plane pixel size 1.25x1.25 mm. About 5 slices were acquired at every heartbeat in long axis 2-chamber and 4-chamber views. The same number of slices was taken in the short- and long-axes. For each slice, a median number of 33 cine phases was acquired during multiple breath-holds (range, 32 to 36).

3.2.2 Exercise stress testing

As part of the cardiovascular screening procedure, an incremental exercise stress test was carried out on a subgroup of 39 leukemia survivors. The control group did not undergo this examination. The test was performed on a bicycle ergometer at Sainte-Justine University Hospital Center with the assistance of an impedance cardiograph device (PhysioFlow, Manatec Biomedical, Macheren,

France). A set of electrodes was placed on each subject's chest according to the protocol and then calibrated. The testing protocol comprised of several steps: a rest period, standing up and then sitting position, followed by the stress period itself with several levels (increment of load of 25W) (25W, 50W, 75W, 100W, 125W), and an active recovery period (Guillemont, 2016).
Outcomes of the exercise stress test included systemic vascular resistance, systolic and diastolic arteries blood pressures, heart rate, and cardiac output. This personalized data was later employed as input for simulation of the left ventricular cavity pressure in the CircAdapt model (section 3.3.3).

3.3 Image segmentation and finite element model generation

The first step towards assessing the long-term cardiac effects of doxorubicin on in vivo ventricular geometry and function was the segmentation and 3D reconstruction of the left ventricle from the acquired image data. In the present work, this was achieved by using Cardiac Imaging Modeller (CIM) v8.1, a semi-automated image analysis software developed by the Auckland MRI Research Group (Auckland, New Zealand) for the accurate characterization of ventricular shape and motion. The cardiac studies were processed individually by an operator who was instructed on how to read MR scans as well as how to employ the software before beginning the analysis. As a means to consolidate the collected information, the operator practiced the segmentation repeatedly on the data sets of the first 15 survivors, initially under the trainer's supervision and subsequently alone. To realistically represent the shape of the subjects' ventricle and permit proper comparisons among analyses, the operator performed the segmentation in compliance with the guidelines delineated by the software developers and some MRI technicians (Lin, Cowan, et Young, 2006). Below, we give a brief overview of the main steps for creating a 3D finite element model of the LV in CIM.

Step 1: Load the subject's image data and create a cardiac case in CIM database.
A typical analysis session in CIM v8.1 begins by loading the image data (stored in DICOM - Digital Imaging and Communications in Medicine - format) for the individual subject into the software database. Both the long-axis and short-axis MR images are uploaded and employed for myocardial delineation in order to provide a complete 3D representation of the left ventricular geometry.

Step 2: Identify the apex, base, RV insertions and baseline points on the images.
Once the subject's images are available for viewing and analysis in CIM, the user proceeds to initialize the segmentation process manually. Six guide points are positioned on the endocardium and epicardium of images at the end-systolic phase in the following time order: apex point (one per

frame), basal point (one per frame), LV centroid points (two per frame), RV insertion points (two per frame), and base plane points (two per frame). Four of these points are placed onto specific short-axis slices, whereas the other two are placed onto any of the long-axis slices (**Figure 3.1**). In so doing, the user provides to the software essential information about the center of the LV apex and base, the location of the intersections of the endocardial RV free wall with the interventricular septum, the location and angulation of the mitral valve plane. This information permits to gradually adapt the initial generic model to the shape of the subject' ventricle. Afterward, the guide points are tracked along the cycle from one imaging frame to another one via a non-rigid registration (Lam, 2012). The LV surface contours are automatically computed from the tracked points. **Error! Reference source not found.** illustrates the epicardial and endocardial borders delineation for a typical CMR data set.

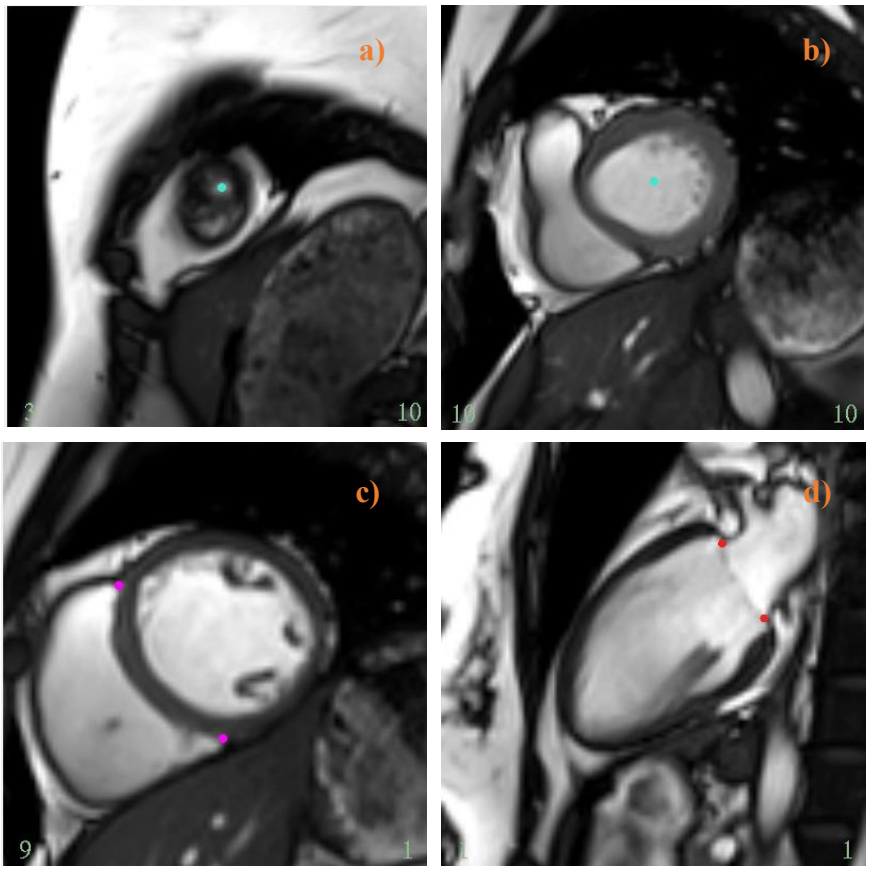

Figure 3.1. Shows the locations of apex point (**a**), basal point (**b**), RV insertion points (**c**), and base plane points (**d**) at end-systolic frames on a series of CMR images.

Step 3: Correct tracking errors and major breath-hold mis-registrations.

The last stage of the segmentation workflow is devoted to improving the accuracy of the model fit to the subject's data and to manually correcting the major breath-hold mis-registrations. In essence, the analyst attentively screens each slice of the cardiac cycle, verifying whether the CIM-generated tracing finely tracks the inner and outer borders of the LV walls from apex-to-base. When this match is not satisfyingly achieved, the analyst intervenes by dragging the contours to a new, more suitable position and/or inserting new guide points (up to a maximum of five per slice) to improve the overlap. In response to these adjustments, the model updates and deforms in real-time to better match the image data. During this process, the user applies his knowledge of the cardiac structures to evaluate the accuracy of the segmentation and ensure that the papillary muscles and ventricular trabeculations are not included in the segmented ventricle. Particular attention has to be paid to the model fit to the end-diastolic and end-systolic frames. Finally, the analysis session comes to an end when a satisfactory level of accuracy is attained in the contours fitting.

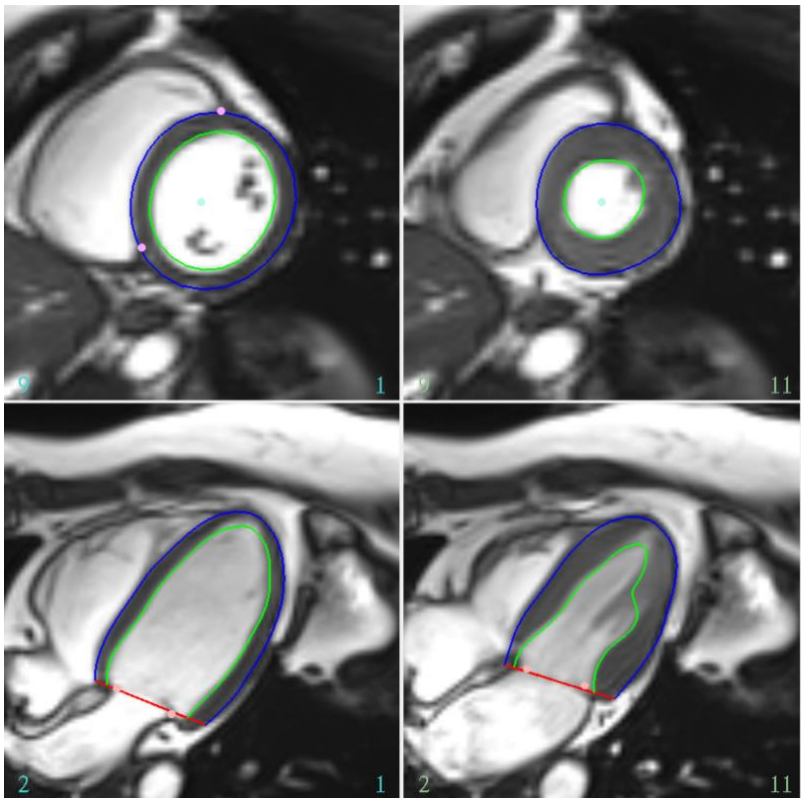

Figure 3.2. An example of short-axis (**top**) and long-axis (**bottom**) MRI images of a heart with the left ventricular endocardial and epicardial borders denoted, respectively, by green and blues lines.

Upon completion of the analyses, we were able to visualize the subject-specific models constructed on the segmented LV surface contours. **Figure 3.3** reports an example for one of the 89 leukemia survivors. As can be seen, the resulting models move and deform in 3D providing sophisticated information about the shape and motion of the LV inner and outer walls along the imaged portion of the heart cycle. The geometric data extracted in this fashion were then utilized for the mechanics simulations detailed in the subsequent sections.

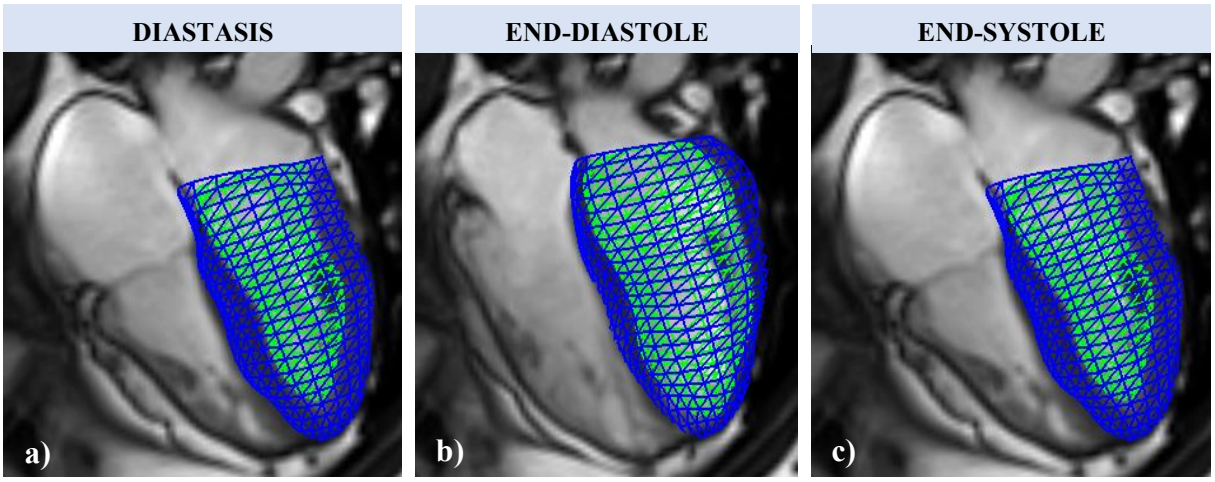

Figure 3.3. Shows a representative CIM's 16-element 3D model of the LV (4-chamber long-axis view) reconstructed at three different phases of the heart cycle: diastasis (**a**), end-diastole (**b**), and end-systole (**c**). In green and blue wireframes are the 3D endocardial and the 3D epicardial surface. Observe how the model convincingly reproduces the apex-to-base shortening experienced by the LV during the systolic phase.

In our experience, the average time required to conduct a left ventricular analysis in CIM v8.1 was on the order of 20 minutes. In particular, manual editing of the computed LV contours turned out to be the most time-consuming task in the segmentation procedure, taking more than 10 minutes to accomplish. It should be pointed out, however, that the examination time can vary widely depending on the size of the data set, numbers of slices or frames in the study, quality of the images, user experience, and severity of mis-registrations and tracking errors.

3.3.1 Global analysis of LV geometry and function

From the subject-specific FE models of the ventricle, CIM software provided automatic calculation of a series of 3D global geometrical parameters: epicardial and endocardial volumes, end-diastolic

volume (EDV), end-systolic volume (ESV), ejection fraction (EF), stroke volume (SV), myocardial mass (LVM), and wall thickness (WT). A brief description of each parameter can be found in **Table 3.2**. As determinants of cardiac performance, these parameters were measured to assess the effects of doxorubicin-induced myocardial remodeling on LV geometry and function (at the global and regional levels) in a non-invasive fashion.

Table 3.2. A summary of the cardiac indices employed for LV structure and function analysis at a global scale (Young et al., 2000; Peng et al., 2016).

Global measurements of LV function and structure		
INDEX	CALCULATION METHOD	DESCRIPTION
Endocardial volume (**LVVendo**, [mL])	slice summation	The volume measured on the endocardium
Epicardial volume (**LVVepi**, [mL])	slice summation	The volume measured on the epicardium
End-diastolic volume (**EDV**, [mL])	frame with max LVVendo	The amount of blood in the left ventricle at end-diastole
End-systolic volume (**ESV**, [mL])	frame with min LVVendo	The amount of blood in the left venticle at end-systole
Stroke volume (**SV**, [mL])	(EDV - ESV)	The amount of blood ejected from the ventricle at each beat
Ejection fraction (**EF**, [%])	(EDV - ESV) / EDV * 100%	The amount of blood pumped out of the heart at each beat
Left ventricular mass (**LVM**, [%])	(LVVepi - LVVendo) * 1.05	mass of the myocardium
Wall thickness (**WT**, [mm])	slice summation	thickness of the myocardium

LV wall thickness, epicardial and endocardial volumes were simulated along the cardiac cycle via slice summation. These parameters were first computed for each frame and then averaged over the cycle so as to produce the global value (Young, Cowan, Schoenberg, et Wintersperger, 2008). With reference to **Table 3.2**, end-diastolic volume was estimated on the cardiac frame with the largest LV cavity volume, while end-systolic volume was measured on the frame with the smallest cavity volume. Stroke volume was calculated as the difference between end-diastolic and end-systolic volumes. Estimates of ejection fraction were derived from the ratio between stroke volume and

end-diastolic volume. LV mass was obtained by subtracting the endocardial from the epicardial volumes at each slice and by multiplying this difference by the density of myocardial tissue (1.05 g/mL). The papillary muscles were taken into account in the calculation of LV mass but excluded in the calculation of the indexed volumes (Young et al., 2000).

3.3.2 Regional analysis of LV geometry and function

For the assessment of in vivo ventricular geometry and function on a regional basis, each geometric model of the LV was automatically partitioned into 16 anatomical regions (of particular interest to the clinicians) according to the 16-segment scheme issued by the American Heart Association. A detailed description of this segmentation model can be found in the work of Cerqueira et al. (2002). Briefly, in the direction perpendicular to the long-axis imaging plane, the LV was sectioned into three equal sectors designated as basal, mid-cavity, and apical. Basal and midventricular short-axis slices were, then, further divided into six regions of uniform arc lengths, whereas the apical short-axis slice was partitioned into four regions of uniform arc lengths. The recommended nomenclature of these 16 regions and their relative locations within the ventricular wall are shown on the bull's eye diagram of **Figure 3.4**.

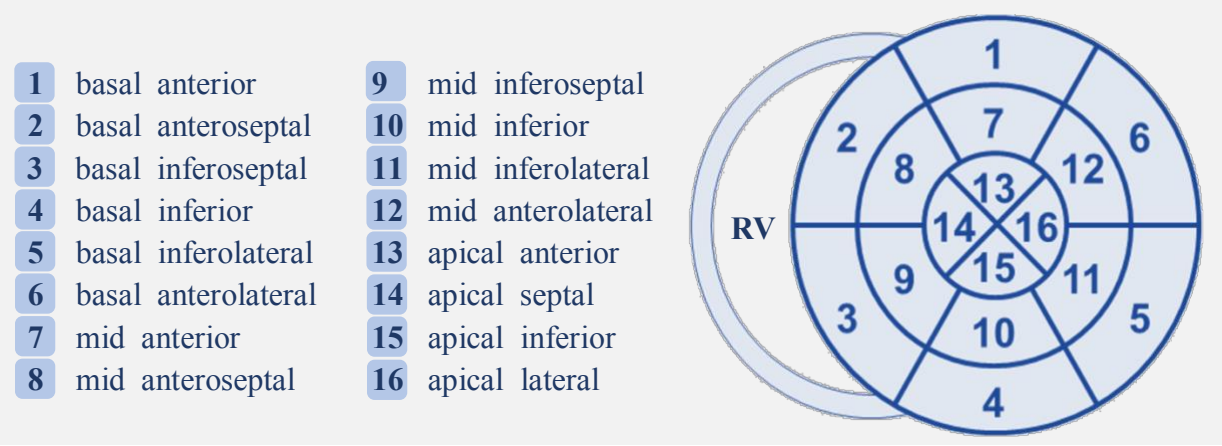

Figure 3.4. Standard representation of the 16-segment model of the American Heart Association. In the short-axis view, the left ventricle is depicted as a series of three concentric rings: the basal segments are in the outer ring, the midventricular segments are in the middle ring, and the apical segments are in the inner ring. RV stands for right ventricle. Diagram modified from Lang et al. (2015).

After the segmentation, LV mass, wall thickness, and all the indexed volumes were re-computed throughout the heart cycle for each of the 16 myocardial sectors, rather than for the single imaging slice. To be specific, regional mass, wall thickness, ED and ES volumes were estimated with a true surface integration algorithm (Alistair et al., 2013). Regional ejection fraction and stroke volume were determined from the corresponding regional ED and ES volumes, as was done for the global analysis of LV function and geometry.

3.4 Finite element analysis

After obtaining description of the geometry of the LV, we need to integrate the constitutive law that describes the behavior of the myocardium in the model. We simulated the mechanical events occurring during the mid-portion of diastole (diastasis) using the computational mechanical analysis framework formulated by the Auckland MRI Research Group (Wang et al., 2009). In this framework, the mechanical behavior of the passive myocardium was represented by a nearly incompressible, transversely isotopic, hyperelastic constitutive law, which is defined as (Guccione et al., 1991):

$$W = C_1 e^Q \quad \text{where} \quad Q = C_2 E_{ff}^2 + C_3(E_{rr}^2 + E_{cc}^2 + 2E_{cr}^2) + 2C_4(E_{fc}E_{cf} + E_{fr}E_{rf}) \qquad (3.1)$$

In this function (**Eq.3.1**), the term E_{ij} represents the six independent components of the Lagrangian Green's strain tensor (E_{ff}, longitudinal; E_{rr}, radial; E_{cc}, circumferential; E_{cr}, circumferential-radial shear; E_{cf}, circumferential-longitudinal shear; E_{fr}, longitudinal-radial shear); C_1 is the global stiffness of the myocardium, C_2 and C_3 are the stiffness along fiber and transverse directions, and C_4 is the shear stiffness (Vetter et McCulloch, 2000; Wang et al., 2013).

In order to investigate the effects of doxorubicin-induced geometric remodeling on the passive LV mechanics, we conducted a subject-specific estimation of the global myocardial stiffness for a subset of the study population. The mechanical stiffness of myocardium can be described by the hyperelastic property C_1. The value of the global stiffness parameter C_1 is determined by applying an inverse materials parameters identification strategy. Given the subject-specific ventricular geometry at diastasis, the information about the ventricle motion from CIM, and the hemodynamic pressures acting on the inner surface of the ventricle during diastole, the stiffness was derived.

3.4.1 Input parameters of the ventricular mechanics model

The use of the ventricular mechanics model described above as a tool for estimating myocardial stiffness required the prior identification of a set of four input parameters, one for each subject under investigation. These parameters included the frame numbers corresponding to end-diastole, end-systole, and diastasis, and the total number of cine phases acquired for the given CMR scan. In this analysis, the end-diastolic and end-systolic frames were automatically identified by the CIM software on the basis of the mitral valve movement and LV volumetric results. More specifically, in each CMR series, the ED was set at the image frame with the largest LV cavity volume, and the ES was defined as the image frame with the smallest LV cavity volume. The ED frame was always the first frame in the image series, and the ES was located around frame 10 in both healthy and patient studies. This subject-specific information was gathered from the data files generated by the CIM software at the end of each segmentation. Such reports also provided us the total number of frames acquired per cardiac study, which was 25 for the ALL survivors and 32 to 36 (median, 33) for the controls. Indeed, as discussed in section 3.2.1, the latter were imaged following a different acquisition protocol than the ALL survivors, which resulted in a higher number of cardiac phases. As regards the diastasis, the corresponding frames were determined through visual inspection of each sequence of CMR images. Knowing that the mitral valve leaflets are in their closed position at end-diastasis (Nishimura, Housmans, Hatle, et Tajik, 1989), we attentively examined the valve motion from the long-axis images depicting the passive filling of the LV and set the diastasis at the frame wherein the valve was shut. To make this clearer, in **Figure 3.5** we report an illustrative example. From this figure, it can be seen that the diastasis was located at the frame in which the valve leaflets shifted between open and closed positions.

Table 3.3 lists the personalized values of the input parameters for some of the study participants. It is noteworthy that the diastasis ranges from frame 16 to frame 21 across the CMR scans used for 3D reconstruction.

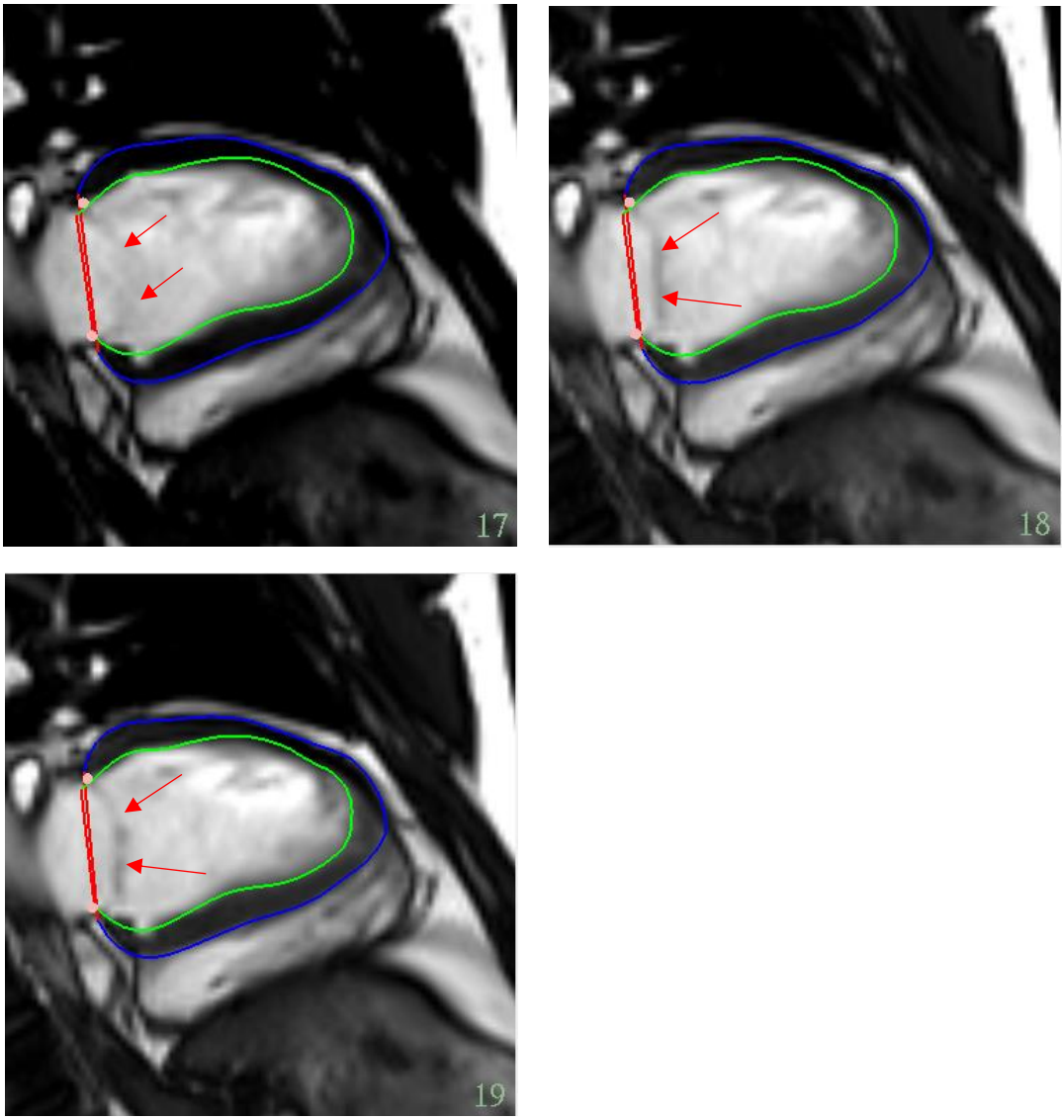

Figure 3.5. The three consecutive CMR frames (4-chamber long-axis view) display the movement of the mitral valve throughout the imaged portion of the cardiac cycle: the valve, initially open to permit the slow filling of the left ventricle (frame 17), switches in its closed position (frame 18), then moves again towards reopening to allow the refilling of the ventricle in atrial systole (frame 19). Frame 18 of the image series was therefore selected as diastasis. The red line identifies the position of the mitral valve, the red arrows point toward the leaflets of the valve (viewed in cross-section).

Table 3.3. Shown are the input parameters used for the mechanics simulations on a subset of ALL survivors (P, n=18) and healthy volunteer (HV, n=3) studies. The numbers featuring in the subjects' identifiers are random and were assigned during the image loading process to avoid biases in the segmentation.

		MRI frame numbers			
Cardiac study	**Group**	**Diastasis**	**End-diastole**	**End-systole**	**Frames per dataset**
PETALE_P002	HRdex	18	1	11	25
PETALE_P008	HRdex	16	1	9	25
PETALE_P034	HRdex	18	1	10	25
PETALE_P038	SR	17	1	10	25
PETALE_P046	SR	17	1	11	25
PETALE_P047	SR	18	1	11	25
PETALE_P049	HRdex	16	1	10	25
PETALE_P052	HR	18	1	11	25
PETALE_P073	SR	18	1	10	25
PETALE_P077	HRdex	18	1	9	25
PETALE_P084	HR	16	1	10	25
PETALE_P088	HR	17	1	9	25
PETALE_P097	SR	17	1	10	25
PETALE_P113	HR	18	1	10	25
PETALE_P129	HRdex	18	1	9	25
PETALE_P147	SR	18	1	11	25
PETALE_P186	HRdex	17	1	10	25
PETALE_P207	HR	20	1	10	25
PETALE_HV01	HV	19	1	12	32
PETALE_HV02	HV	21	1	12	33
PETALE_HV03	HV	20	1	11	33
…	…				

3.4.2 Passive mechanics simulation for standard diastasis pressures

Using the mechanical analysis framework introduced earlier, we simulated the passive phase of the mid-diastolic LV filling and computed the myocardial stiffness (C_1) for a subset of the study cohort. To be precise, 6 healthy and 48 survivor cases were considered for this analysis: 20 belonged to the HRdex group, 12 to the SR group, and 16 to the HR group. Given that the personalized data on intra-ventricular pressure was not available at this stage of our analysis, we decided to load each FE model with three physiologically consistent pressure loading constraints: 0.75 kPa, 1 kPa, and 1.25 kPa. This was done in order to achieve a realistic prediction of the hyperelastic property. The listed values (rounded numbers for the sake of simplicity) were arbitrarily chosen based on the experimental data reported by Nash et al. in a work of 1998, showing that the typical LV cavity pressure at end-diastole is on the order of 1.0 kPa in a clinically healthy subject. Remark that, due to the model architecture, pressure data must be included in the framework in units of kPa.

In this framework, the solution of the stress-strain problem was performed iteratively by applying the pressure loading in incremental steps of 0.1 kPa to the internal surface of the model (Wang et al., 2013). The loading scheme was chosen because it guarantees numerical stability in the convergence of the nonlinear equations governing the simulation. An optimization procedure led to the solution: the output of the model was the value minimizing best the estimate of stiffness C_1. Each analysis required an average of 10 minutes to run on a high-performance computing platform located at the Auckland Bioengineering Institute (University of Auckland). The remote connection to this high-performance computer was achieved using PuTTY v0.7 (https://www.putty.org), an open-source software that allowed to display, import and export data to and from another computer. In summary, we completed three suites of FE simulations per model, for a total of 138 stiffness estimates (3 states of loading multiplied by 46 subjects). For each applied pressure load, stiffness estimates and root-mean-square-error (RMSE) computed by the optimization routine were reported and, subsequently, compared across the four study groups. At the end of the simulations, we were able to visualize the LV models and the corresponding stress maps with the assistance of CMGUI software package (www.cmiss.org/cmgui, University of Auckland).

3.4.3 Estimation of in vivo myocardial stiffness

The application of individualized pressure boundary constraints to the FE model is fundamental for the accurate prediction of the in vivo myocardial stiffness. This information can be obtained by inserting a catheter equipped with manometer sensors into the ventricular chamber. With the aid of cardiovascular imaging, pressure recordings can be acquired simultaneously with the shape and wall motion of the heart (Wang et al., 2009). However, this data is not easily accessible in the clinical setting. The direct assessment is invasive and, therefore, is not recommended in clinically healthy subjects (Wang et al., 2013).

In the current study, this limitation was circumvented by coupling the FE model of the LV to the closed-loop lumped parameter model CircAdapt (CARIM school for Cardiovascular Disease, University of Maastricht, Maastricht, The Netherlands). The constitutive laws of this model are discussed in the work of Lumens et al. (2009). CircAdapt describes the cardiac pump as a structure of three thick walls mechanically coupled and allows to simulate its hemodynamic (Lapointe, 2016). For prediction of LV cavity pressure, the hemodynamic parameters (i.e., mean systemic arterial blood pressure, cardiac rate, and cardiac output) derived from the incremental exercise tests were used for inputs into the model. With this tool, we were able to obtain reasonably realistic boundary constraints.

CircAdapt provides the simulated LV pressure as a string of 25 values describing its evolution throughout the imaged portion of the cardiac cycle. To obtain physiologically realistic values of muscle stiffness, the hemodynamic data from CircAdapt needed to be temporally synchronized with the correspondent CMR sequence. To provide a good match, we first identified the pressure corresponding to the diastasis frame, which was the lowest value in the array. Next, we assigned the selected value to the diastasis image frame, as it featured in the heart cycle in CIM, and shifted the pressure array with respect to this reference. The CMR sequence began with the end-diastole in CIM and so did the pressure array. Accordingly, the first value of the shifted array was taken to be the end-diastolic pressure. Before proceeding with the calculation of myocardial stiffness, the pressure data were plotted over the cardiac cycle for each study participant and then visually analyzed with the intent to validate our choice of diastasis and ED pressures. As an example, **Figure 3.6** illustrates the simulated LV cavity pressures at rest and peak exercise for one of the ALL survivors, before and after the temporal synchronization. As for the pressure measured at peak exercise, the pressure-time graphs served as a reference to identify the diastasis frame and, once

the hemodynamic and CMR imaging data were temporally synchronized, the value of ED pressure. By incorporating the subject-specific LV cavity pressure in the mechanical analysis framework, we estimated the hyperelastic property (as a measure of the in vivo myocardial stiffness at diastasis) for a subset of ALL survivors at rest and during exercise. Ten subjects were classified as standard-risk, 15 as high-risk, and 14 as dexrazoxane-exposed.

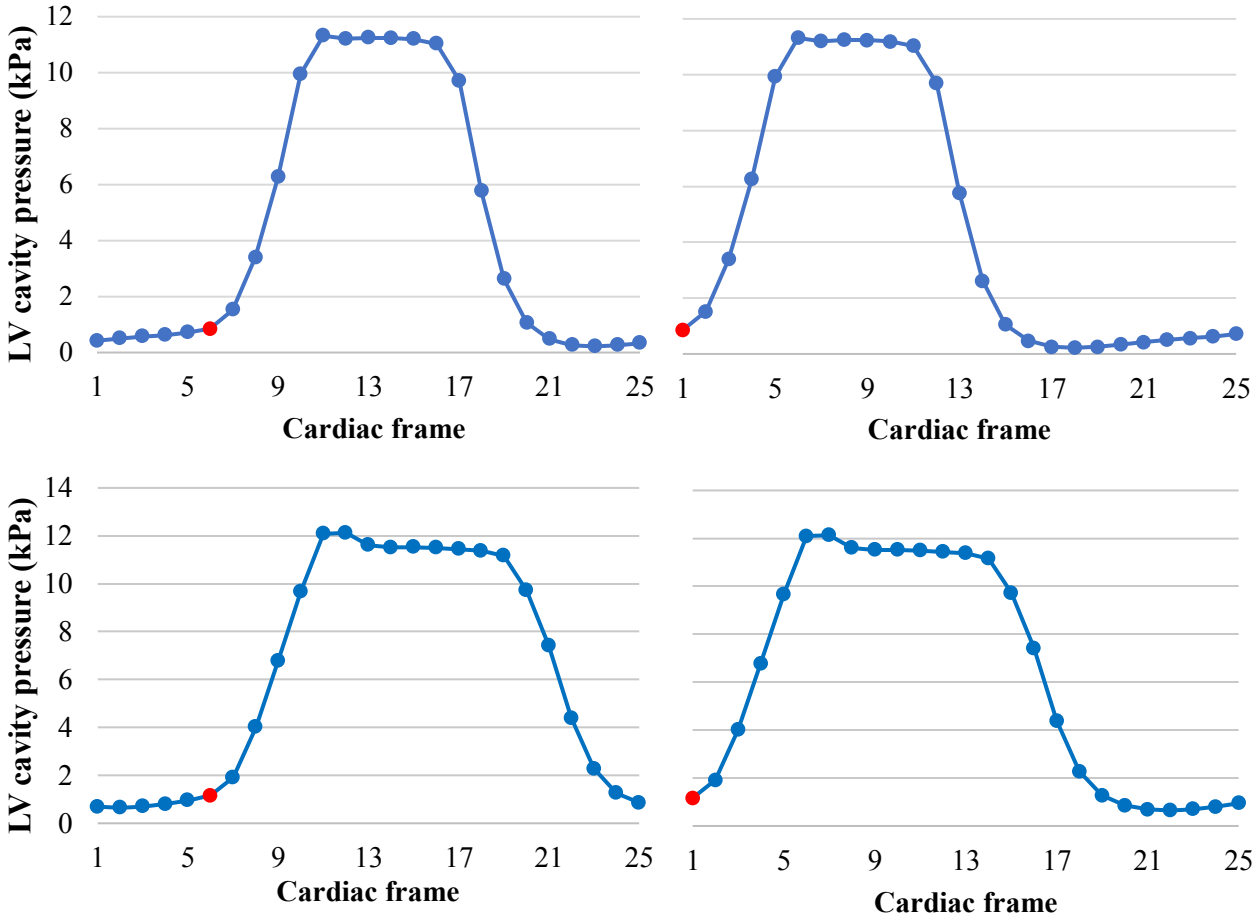

Figure 3.6. The evolution of the intra-ventricular pressure simulated at rest (*top*) and peak exercise (*bottom*) as a function of time for a typical case, before (**left**) and after the temporal synchronization (**right**). The red dot identifies the end-diastolic frame, which is the beginning of the cardiac cycle in the segmentation software CIM.

3.5 Repeatability analysis

In the present study, subject-specific LV geometry was extracted from cine CMR images using a semi-automated framework that relies on user interaction to obtain an accurate delineation of the

myocardium. As detailed in paragraph 3.3, the operator subjectively assesses the accuracy of the segmentation and, if deemed necessary, takes actions to improve the match between the software-computed tracing and the inner and outer boundaries of the LV. Segmentation results are, thus, inevitably susceptible to intra- and interobserver variabilities, that may introduce notable errors in the estimates of LV volume and mass parameters even when the guidelines are carefully followed. In light of the above, we decided to carry out a repeatability analysis to test the level of agreement between the segmentation results obtained by different operators or by the same operator on several image analysis sessions. For the assessment of the interobserver repeatability, the MRI scans of 15 arbitrary selected survivors were processed by four trained analysts, all of whom were blinded to the subject-related information (demographics and group) and others' results. To be more precise, the first operator was a highly experienced MRI technician from the University of Auckland; the second one was a professor who received full training about the segmentation tool from the expert himself and, in turn, trained the latter two operators (both master students).

For intraobserver repeatability analysis, a single trained operator, blinded to his previous outcomes, segmented a randomly chosen CMR scan on three different occasions. At this point, we quantified intra- and interobserver repeatability using the intraclass correlation coefficient (ICC) and repeated measures ANOVA hypothesis test. For each parameter, a Friedman's two-way ANOVA by ranks was carried out on the segmentation results obtained by the four analysts and, separately, on those obtained by the single analyst. Next, we used the mean square variance terms from the ANOVA tests (computed in Statistica v13.2) to calculate the ICCs according to **Eq.3.2**:

$$\mathrm{ICC} = \frac{\mathrm{MS_{Row}} - \mathrm{MS_E}}{\mathrm{MS_{Row}} + \mathrm{df_{col}}\mathrm{MS_E} + (\mathrm{df_{col}}+1)(\mathrm{MS_{col}} - \mathrm{MS_E})/(\mathrm{df_{Row}}+1)} \tag{3.2}$$

where $\mathrm{MS_{Row}}$, $\mathrm{MS_E}$, and $\mathrm{df_{col}}$ represent the between-subjects variance, within-subjects variance and error variance, respectively.

Following this procedure (described by McGibbon in the work of 2003), we assessed the similarity between repeated estimates of LV mass, ejection fraction, stroke volume, ED and ES volumes, and wall thickness. Additionally, we were able to evaluate the degree of agreement between multiple measures of regional myocardial mass, epicardial and endocardial volumes, maximum, minimum, and average wall thickness. At each apical, mid, and basal region of the LV model (section 3.3.2),

the ICC calculation was repeated six times resulting in 96 local coefficients (6 indices multiplied by 16 segments).

To judge the repeatability, we adopted the categorization proposed by Fleiss (1986) and reported by Collins and De Luca (1993): values of ICC less than 0.4 were associated to a poor repeatability, values in the range of 0.4 to 0.75 indicated a good-to-fair repeatability, and values greater than 0.75 corresponded to an excellent repeatability.

3.6 Sensitivity analysis of the model parameters

To complement the previous analysis, we evaluated the sensitivity of the hyperelastic property C_1 to two inputs of the ventricular mechanics model: diastasis frame and pressure loading constraint. The rationale for this was to gain insight into the qualitative behavior of the model applied here and determine the effects of changing the diastasis frame or LV pressure on the model prediction. To conduct such an examination, we arbitrarily selected 6 ALL survivors from those enrolled in the study ran two sets of FE simulations for each subject. We simulated the ventricular mechanics by varying one model parameter at a time across a defined range of values while leaving all others constant. Accordingly, in the first series, the diastasis was varied from frame 15 to frame 21 (by steps of one) whereas the pressure load was kept fixed at the physiological value of 1.0 kPa. It is worthy of note that the range of sensitivity investigation for the diastasis was derived from the subject-specific data described in paragraph 3.4.1, which show that the diastasis lies between frame 15 and frame 21 in the 25-frame cardiac studies.

Table 3.4. List of the frames corresponding to the diastasis for each of the subjects analyzed here.

Study name	Real diastasis
PETALE_P003	18
PETALE_P004	18
PETALE_P012	18
PETALE_P039	18
PETALE_P079	16
PETALE_P081	19

In the second run of simulations, the diastasis was held constant as the passive pressure load was progressively increased from 0.5 kPa to 1.5 kPa with a linear increment of 0.25 kPa. The assumed pressure values (rounded numbers for simplicity) were randomly chosen in the neighborhood of 1.0 kPa, which represents the typical diastolic pressure in a healthy subject (Nash, 1998). As for the diastasis, the frame numbers used to examine the sensitivity of the stiffness to changes in the pressure loading are the same as those previously employed for the analysis of the LV mechanical behavior (see section 3.4.2). These values are reported in **Table 3.4**.

Once the simulations have been completed, the subject-specific FE model results were represented using scatter plots (as suggested by Frey and Patil, 2002) in order to give a rapid visualization of the input/output relationships for the analyzed LV cases.

3.7 Statistical analysis of data

To aid the interpretation, the data obtained by applying the mechanical modeling framework by Wang et al. (2009) were analyzed as follows.

3.7.1 Statistical methods

We began our data analysis by computing summary statistics (group mean and standard deviation) for global myocardial mass, ejection fraction, stroke volume, ED and ES volumes, wall thickness, epicardial and endocardial volumes, and LV myocardial stiffness. Given that the total number of frames acquired per cardiac study was higher in the controls, the means and standard deviations of wall thickness, epicardial and endocardial volumes for this group were calculated using only 25 values of those describing the temporal changes of the parameters throughout the cardiac cycle. More precisely, we kept the values corresponding to the following frames (**Eq. 3.3**):

$$\text{Frames} = 1^{*}(X/25),\ 2^{*}(X/25),\ 3^{*}(X/25),\ \ldots\ 25^{*}(X/25) \tag{3.3}$$

where X represents the total amount of frames associated with a given CMR scan.

Since our goal was to identify the main features of the data sets, we tabulated the resulting statistics and graphically compared them among the four study groups.

Subsequently, the data were inspected for group differences with the specific aim of determining whether the geometrical parameters and the myocardial stiffness were able to capture the changes induced in LV geometry and function by doxorubicin. This was done using a one-way analysis of

variance (ANOVA) test on global and regional geometrical parameters, and a two-way repeated measures ANOVA on global time-dependent parameters (with time as the repeated factor and group as the non-repeated factor). Additionally, since cumulative doxorubicin dose, female gender, and radiation exposure were shown to be related to a greater risk of developing late cardiotoxicity in childhood acute leukemia survivors (Vachhani et al., 2017), we examined the global geometrical parameters with respect to these risk factors. Lastly, we performed a one-way ANOVA to detect group differences in myocardial stiffness. In all our hypothesis testing, statistical significance was accepted at a probability value of less than 0.05.

In this study, the descriptive statistics were calculated with Microsoft Excel 2018 (Microsoft Corp., Redmond, WA, USA), and the statistical analyses were performed using Minitab Express v1.5 (Minitab Inc., State College, PA, USA), with the exception of two-way ANOVA tests that were computed using Statistica v13.2 (StataSoft Inc., Tulsa, OK, USA).

3.7.2 Correlation between myocardial stiffness and CMR relaxation time

A further analysis was conducted on the myocardial stiffness at rest to evaluate its relationship with the CMR relaxation times in a subgroup of the ALL survivor population (n=39). This analysis was motivated by an earlier study on porcine LV wall tissue which demonstrated that a link exists between the passive stiffness and the CMR parameters of the myocardium (Périé et al., 2013).

To describe the relationship between these variables, we regressed the myocardial stiffness on the transverse relaxation time (T_2) and the partition coefficient of gadolinium (λ) by using a multiple linear regression model (Statistica v13.2). Note that the partition coefficient was calculated from the longitudinal relaxation time before and after the injection of the contrast agent (pre- and post-gadolinium T_1), and T_1 and T_2 values were recorded from quantitative T_1 and T_2 maps.

R-squared was computed to quantify the deviation of the predictions of the regression model from the FE-simulated results (Frey et al., 2002). The outcomes of the correlation analysis were then graphically displayed as scatter plot diagram so as to provide a visual indication of the pattern and strength of the association among the variables.

CHAPTER 4 RESULTS

In this section, we present the results of our effort to evaluate the long-term effects of doxorubicin on myocardial function using a FE model of the LV that integrates accurate in vivo geometry and pressure loading conditions. Intra- and interobserver repeatability of the segmentation results are first described. Next, we report the results of the semi-automated segmentation of the LV at global scale, as well as their comparison between the study groups. Finally, we present the outcomes of the LV mechanical behavior analyses conducted on the MRI-reconstructed models at rest and during peak exercise.

4.1 Results of the repeatability analysis

The degree of agreement between repeated measurements of ejection fraction, myocardial mass, and the other 3D global and regional parameters was established in terms of intraclass correlation coefficient. We recall that this coefficient can range in value from 0 to 1, where values close to 1 indicate that degree of agreement between repeated measurements of the given variable is strong (Weir, 2005). On this ground, inter-observer repeatability was judged to be excellent for the global parameters (ICC values ranged from 0.75 to 1.00) and good for the regional parameters (ICC values ranged from 0.60 to 0.74). Similarly, intra-observer repeatability was excellent for both global and regional geometrical parameters (ICC values ranged from 0.75 to 1.00). This data demonstrates the good-to-excellent repeatability of the estimates obtained with Cardiac Imaging Modeling.

4.2 Results of the sensitivity analysis

Figure 4.1.a displays the relationship between the hyperelastic property C_1 and the diastasis frame for each of the subjects included in the sensitivity analysis. As expected, the predictions of the LV mechanics model were sensitive to the choice of the diastasis: C_1 increases as the diastasis varies from frame 15 to frame 21. An exception to this overall increasing behavior was observed in subject P004, for whom the hyperelastic property increases up to frame 18 and decreases after that.

A closer inspection of **Figure 4.1.a** reveals that the difference between the value of C_1 predicted by the FE model at the real diastasis (see section 3.6) and the value obtained when the previous (or the next) frame was used as diastasis did not exceed the 2.0 kPa. This was observed for all simulated cases. In particular, the smallest variations between C_1 estimates, amounting to 0.22 kPa (frames

17-18) and 0.11 kPa (frames 18-19), were for cases P012 and P004. **Table 4.1** shows the percentage change in the hyperelastic property from the value predicted at the real diastasis.

From **Figure 4.1.a**, we see that some data are missing for subjects P003, P004, and P012 at frame 15. The numerical simulation failed to solve the mechanical problem on these MRI-reconstructed FE models for the inputted pressure and diastasis frame.

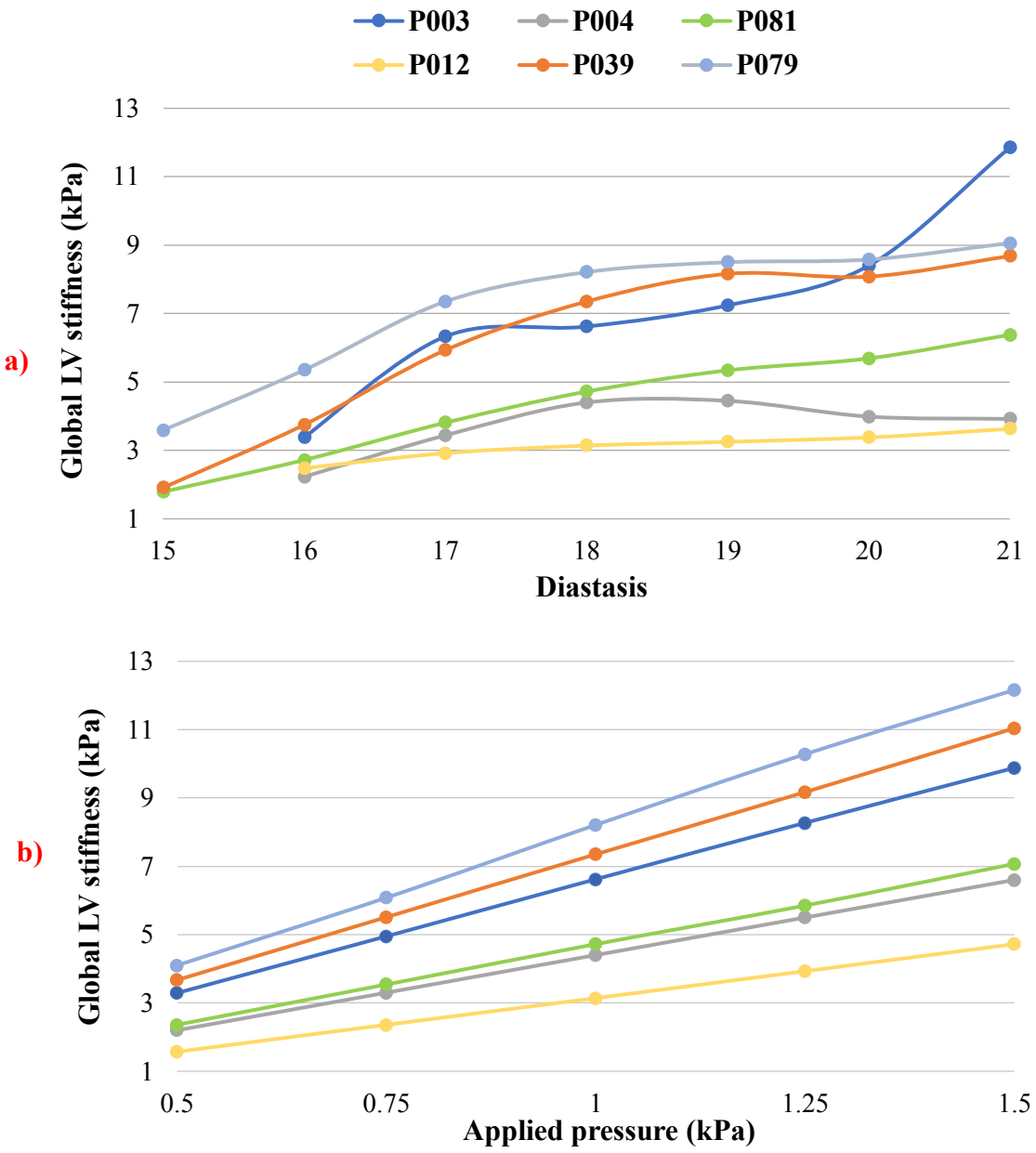

Figure 4.1. Subject-specific FE-predicted results plotted over the range of variation of the diastasis frame number (**a**) and the range of variation of the pressure load (**b**).

The sensitivity of the hyperelastic property to small changes in the pressure load is illustrated in **Figure 4.1.b** for all analyzed LV cases. It is clear from this figure that a nearly linear relationship exists between the hyperelastic property and the pressure applied to the LV mechanics model during the simulations. Note also that the degree of sensitivity was similar across the subjects: the value of C_1 increased by about 25% (~ 2 kPa) with each 2.5 kPa increase in pressure (**Table 4.1**).

Table 4.1. Percentage change in C_1 from the value at the true diastasis frame and those predicted when the previous frame (**left**) or the next frame (**right**) was used as diastasis (*first row*). Percentage change from the C_1 value at 1.0 kPa and those predicted when the pressure was set at 0.75 kPa (**left**) or 1.25 kPa (**right**) (*second row*).

	P003	**P004**	**P012**	**P039**	**P079**	**P081**
Error_left (%)	4.4	21.8	7	19.3	32.9	11.6
Error_right (%)	9.4	1.1	3.5	11	37.4	6.6
Error_left (%)	25.2	25.0	24.8	25.0	25.9	25.0
Error_right (%)	25.2	25.0	25.2	24.8	25.2	23.9

4.3 Global and regional 3D geometrical parameters

The means and standard deviations of end-diastolic volume (EDV), end-systolic volume (ESV), stroke volume (SV), ejection fraction (EF), and left ventricular mass (LVM) are given in **Table 4.2** for each of the four study groups.

Table 4.2. Global geometrical parameters estimated from the subject-specific LV models in CIM. Data are expressed as mean ± standard deviation and presented separately for the SR, HR, HRdex, and HV groups.

	3D measurements of global LV function				
Study group	**EDV** (mL)	**ESV** (mL)	**SV** (mL)	**EF** (%)	**LVM** (g)
SR (n=18)	150.38 ± 33.21	64.51 ± 19.35	85.87 ± 18.32	57.47 ± 6.03	107.05 ± 26.8
HR (n=30)	146.04 ± 33.69	62.12 ± 20.41	83.92 ± 16.1	57.72 ± 5.33	106.03 ± 25.09
HRdex (n=36)	140.14 ± 34.74	57.12 ± 18.5	83.02 ± 17.49	59.82 ± 4.37	104.58 ± 32.2
HV (n=10)	149.97 ± 38.28	65.97 ± 18.65	83.99 ± 20.07	56.31 ± 2.51	112.13 ± 29.49

As can be seen by inspection of this table, the HRdex subjects tended to have a smaller end-diastolic volume and end-systolic volume than those of the other ALL survivors and the healthy volunteers. However, the difference was not statistically significant at the level .05 (one-way ANOVA, $p>0.1$). The HRdex group also showed a smaller mean stroke volume when compared with the other study participant groups, but again this difference lacks statistical significance (ANOVA, $0.05<p<0.1$). No appreciable difference was identified between the four groups on the ejection fraction (one-way ANOVA, $0.05<p<0.1$), although the average value for this cardiac index was somewhat higher in the dexrazoxane-treated group (59.82%) than in the control group (56.31%). Also note that ejection fraction was higher than 50-55%, which is the clinical threshold for abnormal systolic function (Lapointe, 2016), in all groups. Overall, the subjects showed normal ejection fractions with few exceptions in the SR and the HR groups. Specifically, two subjects in the SR group (41.5% and 47.7%) and three subjects in the HR group (range, 45.1 to 48.5%) had an ejection fraction less than 50% (Lapointe, 2016). None of the dexrazoxane-exposed subjects reported an ejection fraction below the clinical threshold for abnormal systolic function.

As regards the myocardial mass, a higher mean value was found in the healthy controls, but again this difference between groups did not achieve statistical significance (one-way ANOVA, $p>0.1$). Therefore, the groups had similar average values for stroke volume, ejection fraction, myocardial mass, end-diastolic and end-systolic volumes that showed no significant difference at the 5% level. Similarly, the comparisons of these indices as a function of gender and radiation exposure did not reveal any statistically significant difference between the SR, HR, HRdex, and HV groups (two-way ANOVA, $p>0.1$).

Further inspection of **Table 4.2** revealed that the standard deviation was very comparable across the study groups for the same cardiac index. The variance was considerable in all estimated indices. In particular, the greatest variance occurred in the end-diastolic volume (range, 33.2 to 38.3 mL), while the ejection fraction was the most stable index since it had the lowest inter-subject standard deviation (2.5 to 6 %).

The analysis of the calculated regional geometrical parameters did not reveal any significant differences between the SR, HR, HRdex, and control groups (one-way ANOVA, $p>0.05$). For this reason, our data are not displayed in this thesis.

4.4 Global time-dependent 3D geometrical parameters

Figure 4.2.a illustrates how the average epicardial volume varies throughout a full cycle of cardiac contraction for the SR, HR, HRdex, and HV groups. Looking at this figure, we first remark that all four curves exhibit the well-known morphological features of the left ventricular volume over time curves. They capture the different phases of the heart cycle, including atrial systole, ejection, and rapid inflow. In particular, we clearly distinguish the rapid inflow (early filling phase of diastole) and the mid-diastolic diastasis (plateau) in all groups and especially in the control group. The same morphological features were also found in the single-subject results.

As detailed in paragraph 3.7.1, group differences on the global time-dependent parameters were investigated by use of a two-way ANOVA with repeated measures. The results of this analysis showed that the epicardial volume differs significantly between the study groups, but only from frame 11 to frame 16 ($p<0.01$). Interestingly, the statistical significance was detected among the HRdex group and the HV or SR groups, and the HV and HR groups. In systole, notably between frames 3 and 8, the curves for the HR and HV groups are so similar as to be almost superimposable.

a)

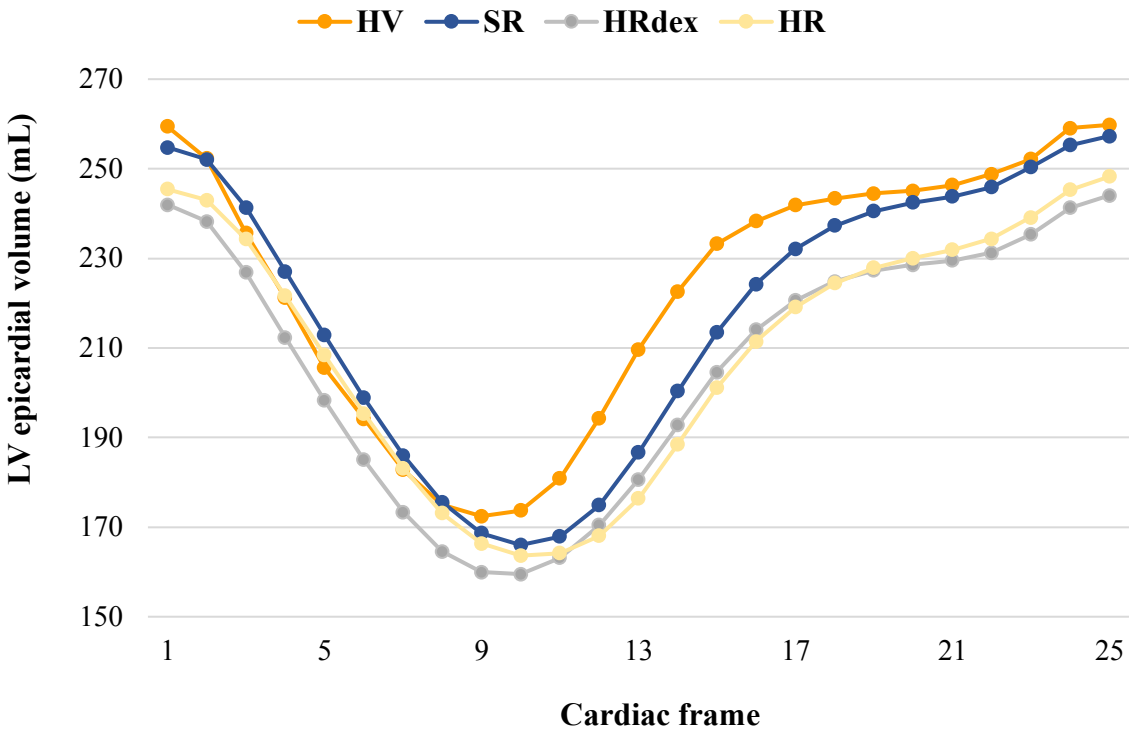
HV
SR
HRdex
HR
LV epicardial volume (mL)
270
250
230
210
190
170
150
1
5
9
13
17
21
25
Cardiac frame

b)

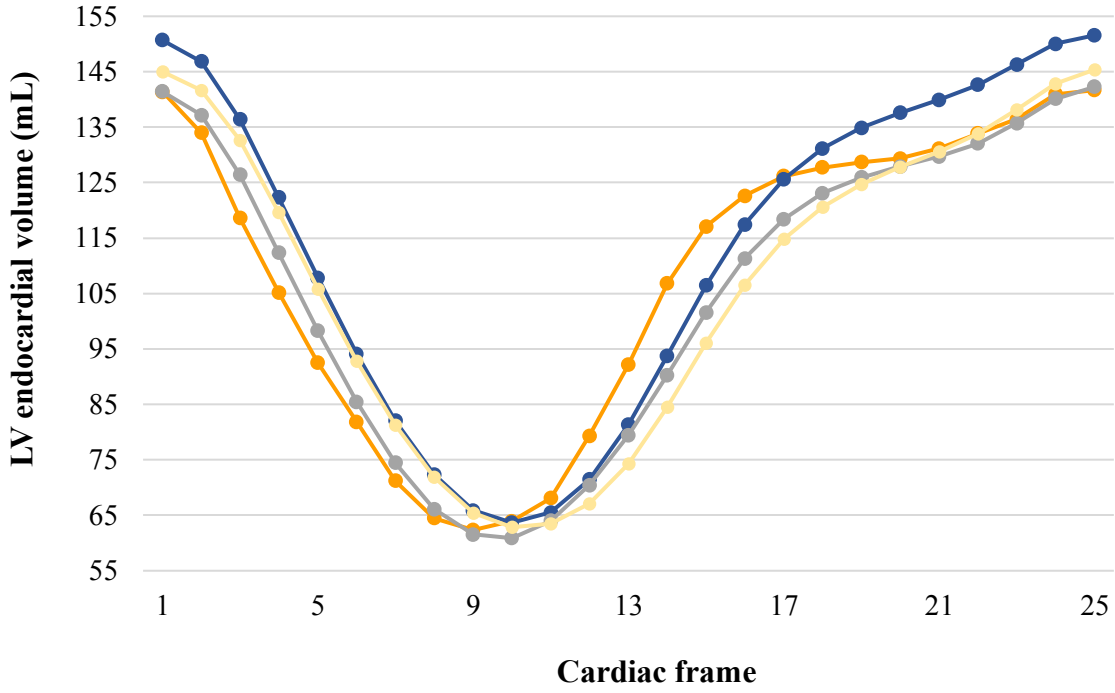
LV endocardial volume (mL)
155
145
135
125
115
105
95
85
75
65
55
1
5
9
13
17
21
25
Cardiac frame

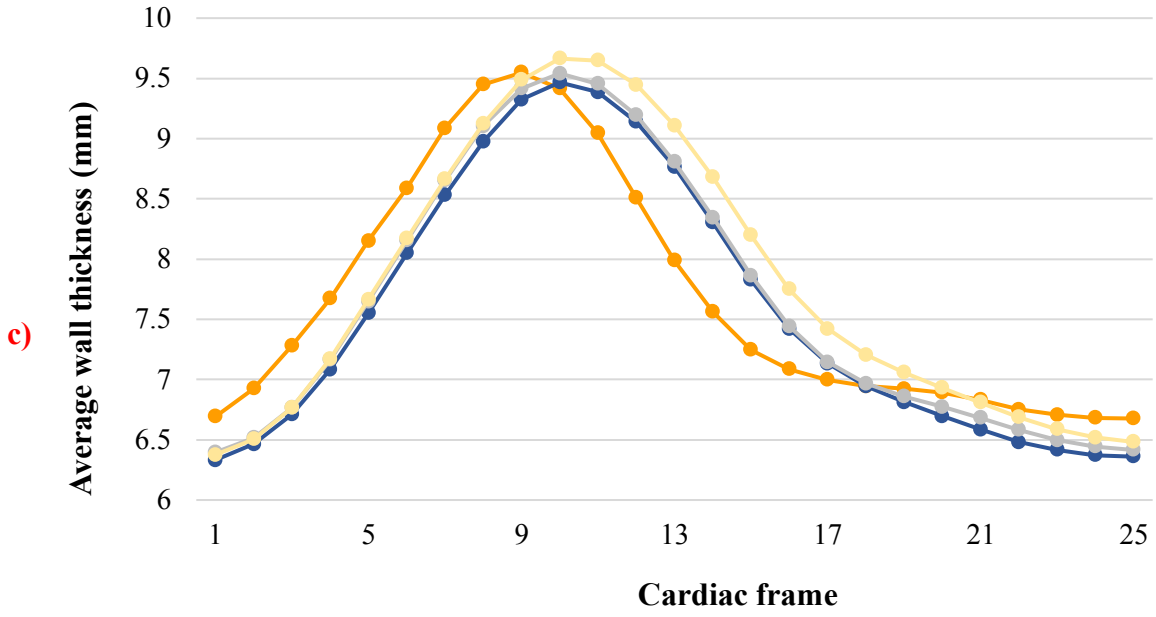

Figure 4.2. Comparisons of LV epicardial volume (**a**), endocardial volume (**b**), and wall thickness (**c**) among the SR, HR, HRdex and HV groups. For the sake of clarity, the corresponding standard deviations are not shown in the graph. The abscissa represents the phases of the heart cycle. Recall that the end-diastole corresponds to the first frame in this cycle, the end-systole is located at frame 9 or 10, and the diastasis lies around frames 16-17. Indeed, the curves for the HV group and those for the survivor group achieve their minimal (maximal) values at different frames in the cardiac cycle (shift of one phase). Also, note the different scales on each graph.

The average endocardial volume plotted against the phase number is showed in **Figure 4.2.b**. The first thing we notice is that the endocardial volume has a lower amplitude along the cardiac cycle compared with the epicardial volume. Such difference in amplitude amount to about 100 mL.
As with the epicardial volume, all four groups exhibit volume-time curves with a similar over-all shape. These curves clearly reflect the different phases of the cycle and are therefore consistent with the volume measurements described in the literature. Here, again, we can easily discriminate the early filling period from the mid-diastolic diastasis in both cancer survivor and control groups. Furthermore, it is interesting to note that the SR and HV groups exhibit higher values over time than the other groups did. More specifically, the SR group presents higher values from frames 1 to 8, while the control group does from frames 9 to 25. Nevertheless, this difference does not achieve

statistical significance at the 5% level ($p<0.1$). In fact, the curves for the SR and HV groups are almost superimposable with that for the HR group at some points of the cardiac cycle.

Figure 4.2.c displays the time-course of changes in average LV wall thickness for the control group and the survivor groups. Again, as noted for the other time-dependent parameters, the shapes of the four curves are very similar and also consistent with literature data (Troung et al., 2008). For example, all curves showed a peak at systole. In this phase the left ventricle contracts and the wall thickness increases.

All of the plots of the volume are comparable. The control and high-risk groups tend to have higher values of wall thickness along the heart cycle, but again this difference lacks statistical significance at the 5% level ($p>0.1$). When looking more closely at the figure, one can notice that the curves for the groups of survivors are almost superimposable at some phases of the cardiac cycle. To be more specific, overlaps were observed among the HR and HRdex groups from frame 1 to frame 8, and among the SR and HRdex groups from frame 12 to frame 18.

It is worthy of attention the fact that the volume and the wall thickness for the HV group achieved the minimal value (end-systole) and the maximal value, respectively, at a different phase in the cardiac cycle (shift of one phase).

4.5 Estimates of myocardial stiffness for standard diastasis pressures

The outcomes of the LV mechanics simulation are reported here in terms of hyperelastic property C_1 and RMS error. The boxplots of **Figure 4.3** display the values of C_1 obtained when a pressure of 0.75 (**a**), 1.0 (**b**), and 1.25 kPa (**c**), respectively, was applied on the endocardial surface of each subject-specific FE LV model. For ease of interpretation, the means and standard deviations of the calculated hyperelastic property are summarized in **Table 4.3** for each study group.

a)

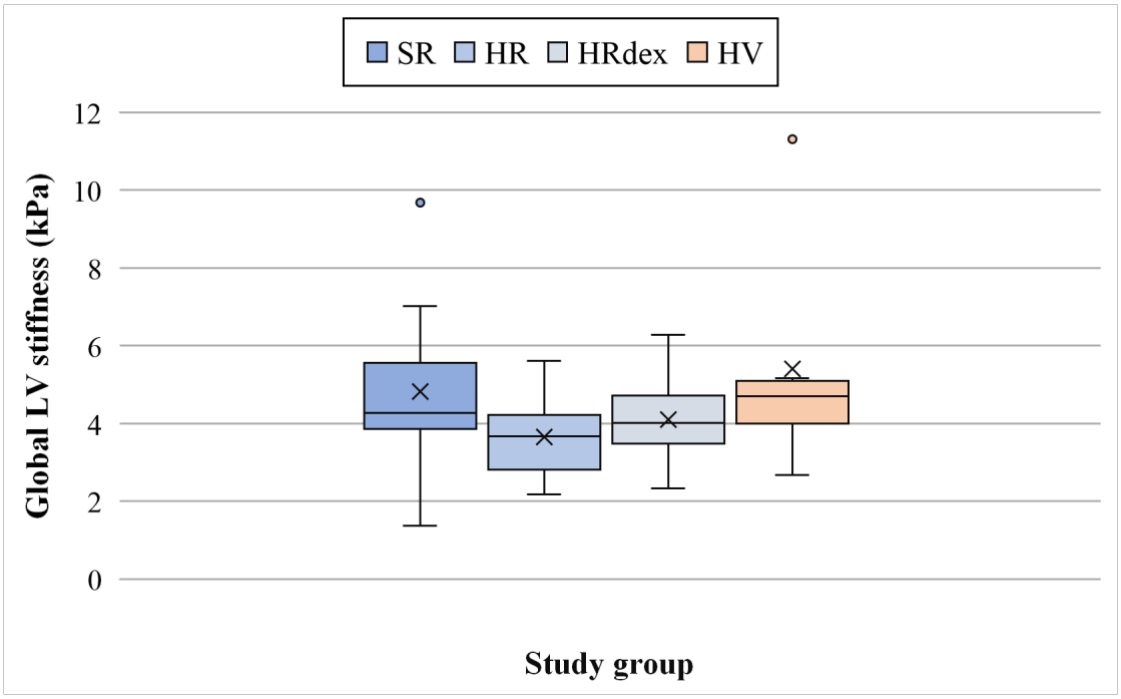

b)

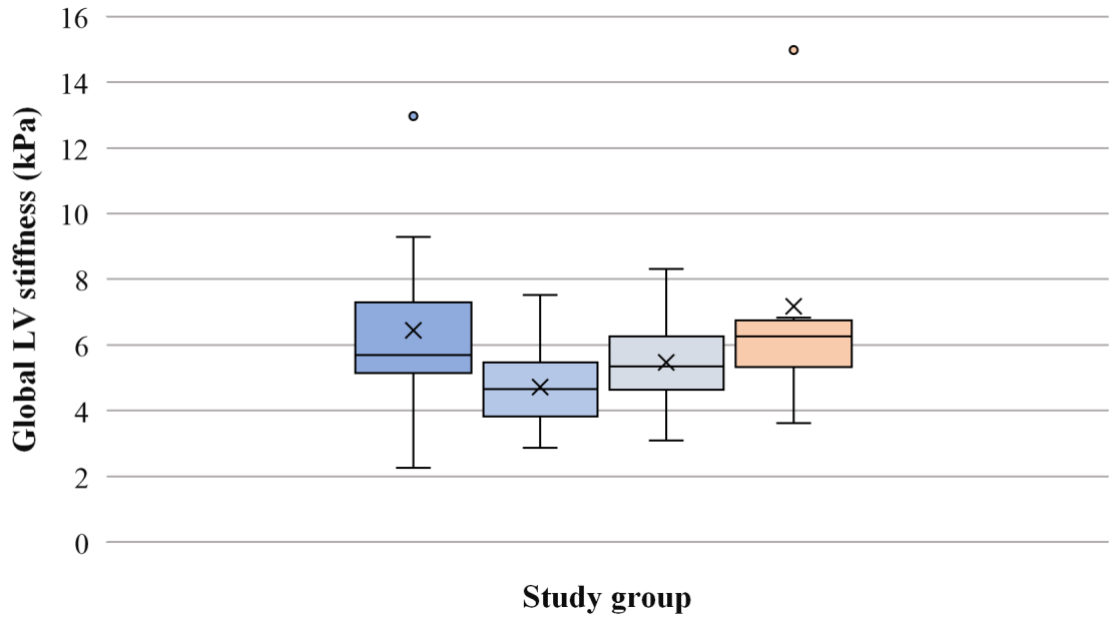

c)

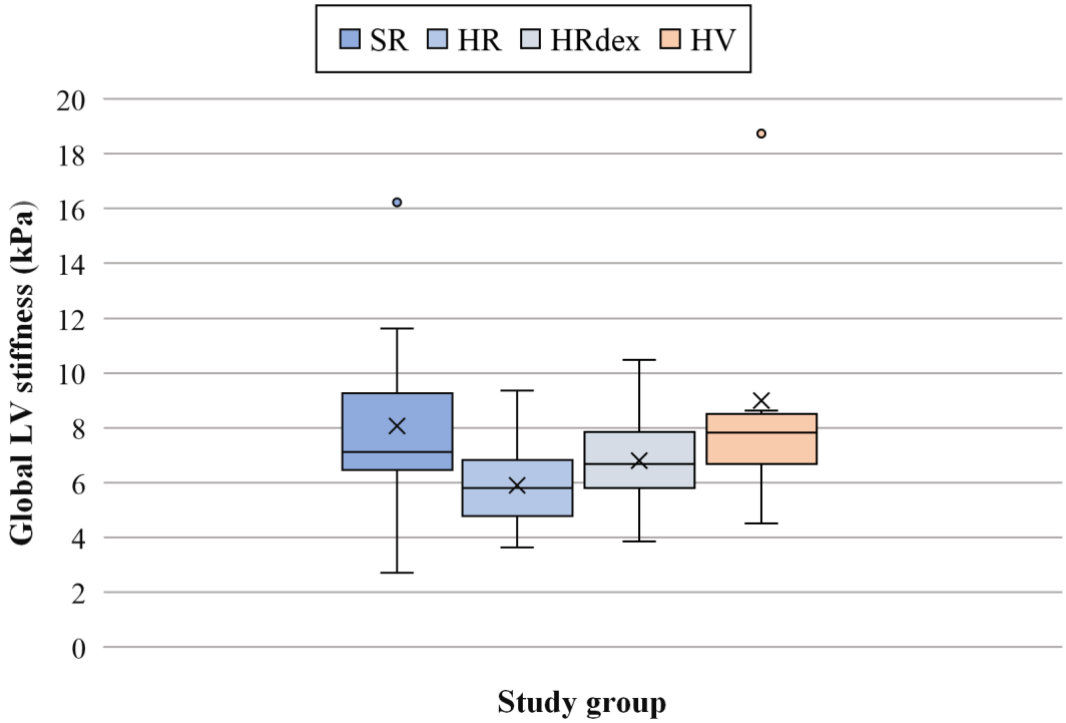

Figure 4.3. Global stiffness of LV myocardium for the HR, SR, HRdex, and HV groups estimated at diastasis under three different pressure boundary constraints: 0.75 (**a**), 1.0 (**b**), and 1.25 kPa (**c**). The boxplots show mean, median, standard deviation, and outliers for each of the four data sets.

Table 4.3. Summary of the average values and standard deviations of the FE-predicted results for each of the study group. This table shows that the estimated hyperelastic property increased as the LV cavity pressure increased.

	Global LV stiffness (kPa)		
Study group	0.75 kPa	1.00 kPa	1.25 kPa
SR (n=12)	4.81 ± 2.1	6.44 ± 2.8	8.06 ± 3.5
HR (n=16)	3.65 ± 1.1	4.71 ± 1.2	5.89 ± 1.5
HRdex (n=20)	4.1 ± 1.2	5.46 ± 1.5	6.8 ± 1.9
HV (n=6)	5.4 ± 3.0	7.18 ± 4.0	8.99 ± 5.0

For each assumed pressure loading constraint, the average value for the hyperelastic property was compared between the four study groups using a one-way ANOVA test. Interestingly, the survivor population had a slightly smaller hyperelastic property than did the control group across the three sets of numerical simulations. In particular, this deviation from the control was most marked in the high-risk subjects ($p=0.035$), who exhibited the smallest C_1 values compared with the other ALL survivors, as illustrated in **Figure 4.3**.

Comparison of the calculated hyperelastic property across the three sets of FE simulations (**Table 4.3**) showed that this biomechanical parameter increased almost linearly with the pressure applied to the left ventricular model. This was in close agreement with the results of the sensitivity analysis (see paragraph 4.2).

Figure 4.4. Plot of the RMS error in the optimal fit for the analyzed LV cases. The blue points represent the average errors of the four groups. Remark that, for the same subject, the RMSE value remains constant as the pressure load varies.

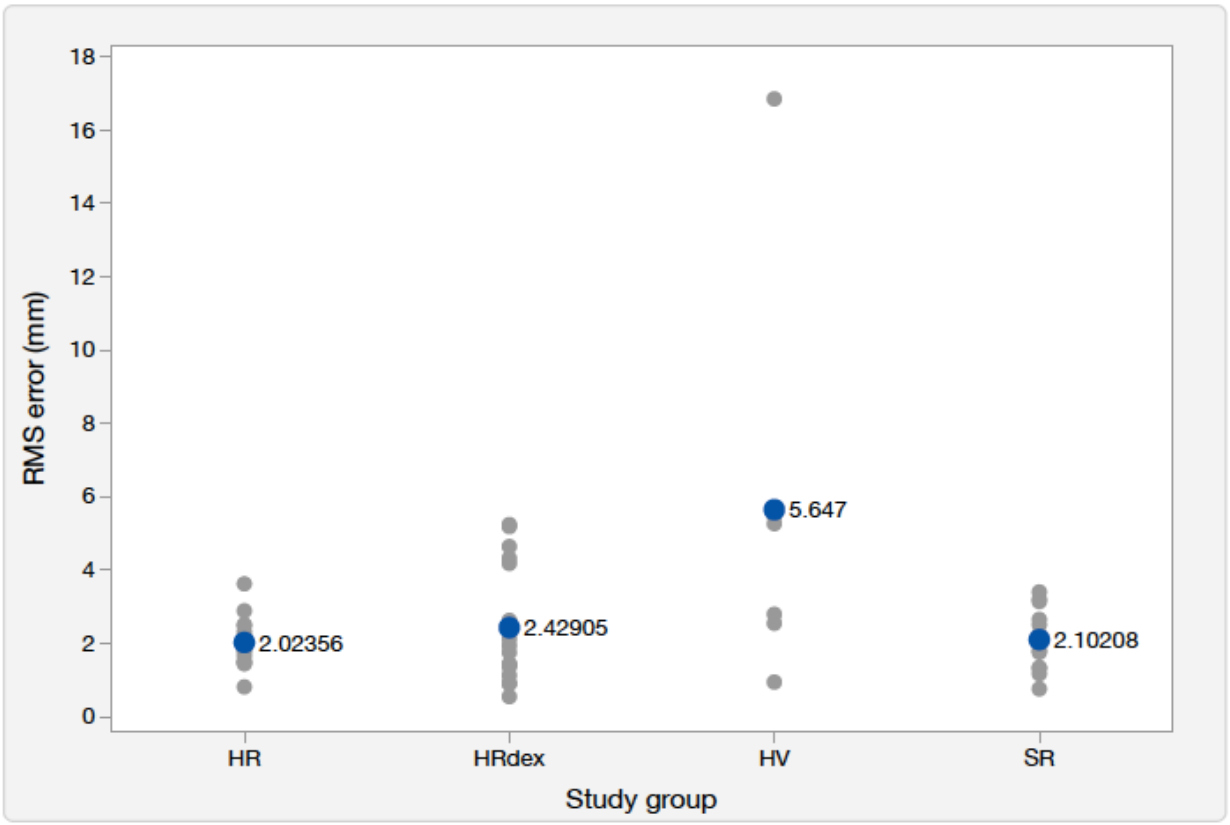

Furthermore, it is worthy of remark that the standard deviation was especially elevated in the SR and HV groups. This was mainly due to the presence of two outliers (the first one belongs to the SR group, the second one to the HV group) that were much higher than the mean values of C_1 for the participant groups.

Figure 4.4 displays the RMS error that has been calculated in the best fit of the FE simulation for each subject. As can be seen, the RMSE estimates ranged from 0.95 to 16.8 mm for the HV group, from 0.75 to 3.4 mm for the SR group, from 0.81 to 3.62 mm for the HR group, and from 0.55 to 5.24 mm for the HRdex group. We remark that the RMSE values were especially marked in some simulations (the error should be zero). The analysis of these data also revealed that the numerical simulations had larger RMSE values for the healthy volunteers than did for the leukemia survivors (one-way ANOVA, $p=0.005$). The errors for the SR group (mean, 2.10 mm) and the HR group (2.02 mm) were in a similar range. The reason for this observation is discussed in the next chapter. Also notable is the fact that, for the same subject, varying the pressure load had no effect on the RMSE value. This has been linked to the definition of RMS error in this study: the deviation of the CMR-predicted points from those predicted by the model. This deviation does not change with the pressure boundary condition.

4.6 Estimates of in vivo myocardial stiffness

For each subject, the boxplots of **Figure 4.5** (**a**)-(**b**) show the stiffness estimates obtained when the intra-ventricular pressure at rest and peak exercise were incorporated in the FE analysis framework. Means and standard deviations for the three groups of participants are reported in **Table 4.4**.

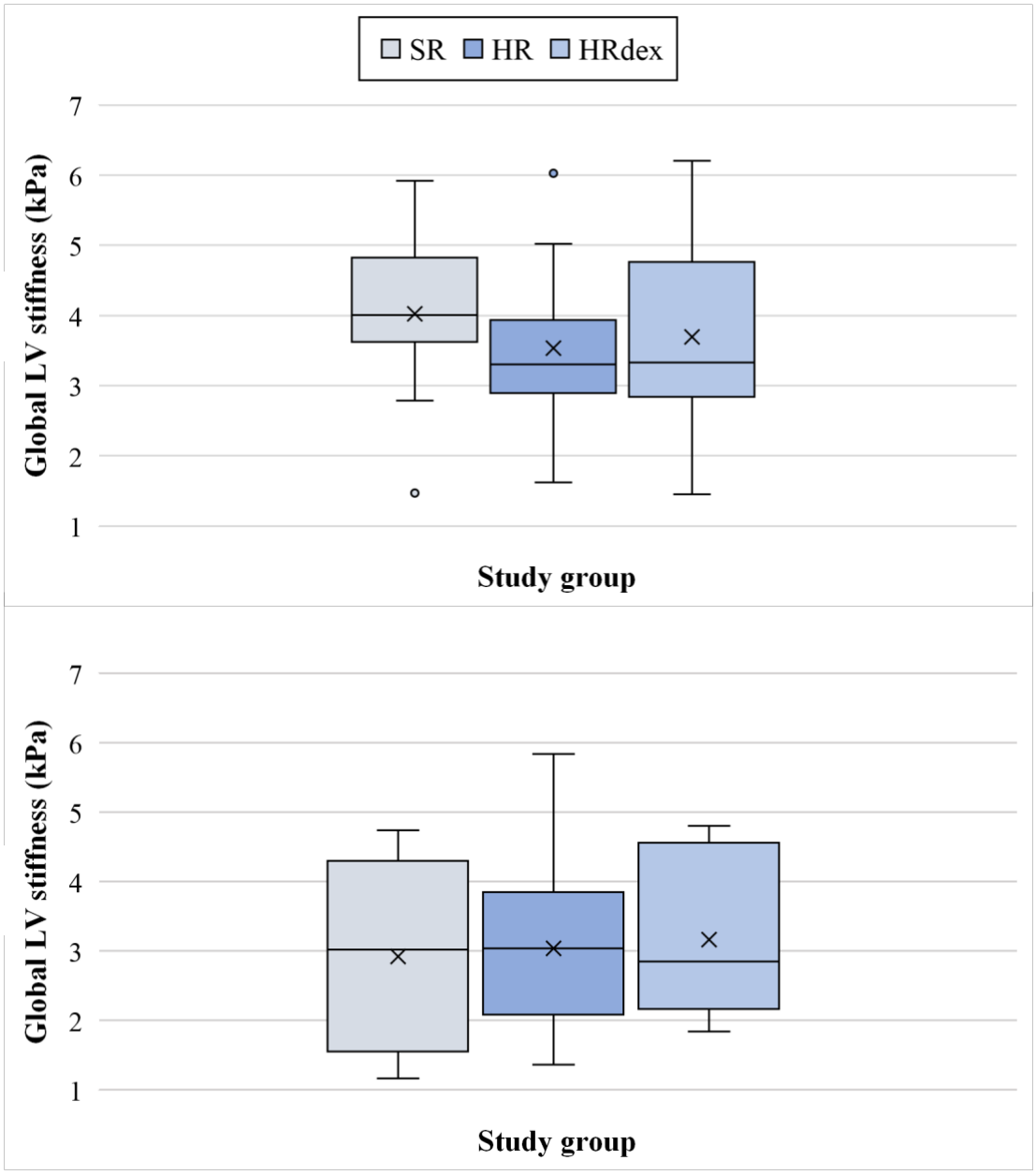

Figure 4.4. Global stiffness of LV myocardium measured at rest (**a**) and peak exercise (**b**) for the HR, SR, and HRdex groups. Outliers, mean, median, and standard deviation values are illustrated for each data set.

Table 4.4. summarized the average values and standard deviation for the LV stiffness at rest and during exercise in the three groups of ALL survivors.

	Global LV stiffness (kPa)	
Study group	**REST**	**PEAK EXERCISE**
SR (n=10)	4.03 ± 1.3	3.10 ± 1.3
HR (n=15)	3.53 ± 1.1	3.04 ± 1.3
HRdex (n=14)	3.69 ± 1.3	3.16 ± 1.1

As this table illustrates, the average value for the LV stiffness at rest was 4.0 kPa for the SR group, 3.5 kPa for the HR group, and 3.7 kPa for the HRdex group. In line with the results obtained previously for the standard diastasis pressures, the high-risk group exhibited a smaller hyperelastic property than did the other groups of leukemia survivors. However, this difference did not reach the statistical significance at the level 0.05 (one-way ANOVA, $p>0.1$). We also observe that the standard deviation of the estimated hyperelastic property, amounting to about 1.2 kPa, was very comparable among the three study groups. This was despite the presence of two outliers: the first one, belonging to the SR group, was smaller than the correspondent group mean, and the second one, belonging to the HR group, was greater than the group mean.

At peak exercise, the average values for the LV stiffness were 3.1, 3.0, and 3.2 kPa for the standard-risk, high-risk, and dexrazoxane-exposed groups, respectively. Similar to before, the HR group had a slightly smaller hyperelastic property when compared against the SR and HRdex groups, but the difference was not statistically significant (one-way ANOVA, $p>0.1$). Here, again, we note that the standard deviation of the hyperelastic property (~1.2 kPa) was very similar across the three groups. For the entire group of ALL survivors, the mean and standard deviation of the LV stiffness were measured to be 3.1 ± 0.2 kPa at rest, and 3.64 ± 0.2 kPa during exercise. Comparing the results of the two sets of numerical simulations revealed that the overall stiffness at rest was similar to the one obtained at peak exercise (ANOVA, $p>0.1$) even though the heart was under a greater pressure during exercise. There was no difference between the stiffness at rest and peak exercise within each group of survivors or the population of survivors (ANOVA, $p>0.1$). In addition, no appreciable difference was identified in the overall stiffness among the three combined groups.

4.7 Results of the correlation analysis

Figure 4.8 illustrates the correlation between the hyperelastic property C_1 at rest and the partition coefficient λ of gadolinium in 39 acute lymphoblastic leukemia survivors.

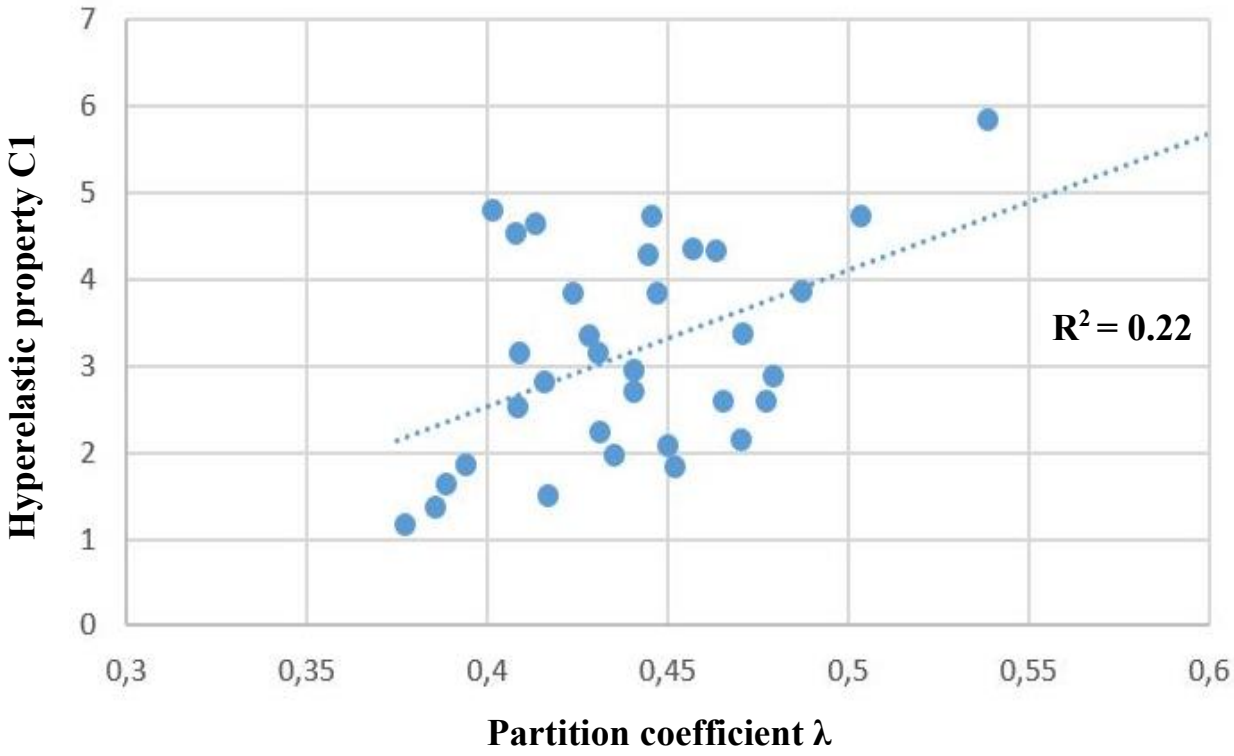

Figure 4.5. Plot of C_1 versus partition coefficient λ of gadolinium. The blue dashed line represents the predictions of the multiple linear regression model, while the circles indicate the results of the FE simulations for each of the 39 subjects.

As indicated by the coefficient of determination (R^2=0.22), only 20% of the hyperelastic property values could be predicted from a linear combination of the transverse relaxation time T_2 and the partition coefficient of gadolinium (C_1 = -6,3 + 0,008 * T_2 + 14,3 * λ). In the figure, we see that some points fall fairly close to the regression line while the majority are far from it. Accordingly, the hyperelastic property showed a modest tendency to correlate with the partition coefficient. This notwithstanding, the reported correlation was significant (p=0.016). The relationship between the pair of variables was also positive: the FE-predicted results tended to increase together with the partition coefficient.

In this multiple linear regression, only the partition coefficient exhibited a significant contribution to the hyperelastic property. The transverse relaxation time did not provide a significant correlation with the hyperelastic property ($p=0.4$) and, for this reason, the correspondent scatter plot was not reported in this thesis.

CHAPTER 5 GENERAL DISCUSSION

5.1 Comment

The present study was designed to assess the LV chamber remodeling induced by low-to-moderate doses of doxorubicin in a group of leukemia survivors 13 years after the last course of treatment. Ventricular geometry and function in the survivors were first evaluated by analyzing the global and regional geometrical parameters calculated from the subject-specific models of the left ventricle. Such analysis did not reveal any significant differences in ejection fraction, mass, and the other indices of cardiac performance among the four groups of participants ($p>0.01$).

These results are in agreement with some previous studies of the long-term effects of modest doses of doxorubicin therapy on echocardiographic measurements of adult survivors of childhood cancer. More specifically, supporting data comes from the work of Li et al. (2017). Despite evidence of subclinical myocardial injury, they observed no difference in the echocardiographic assessment of LV ejection fraction and myocardial mass between healthy controls and long-term survivors of childhood leukemias (median, 14 years from diagnosis) treated with moderate dose chemotherapy (227±100 mg/m). Similarly, Vandecruys et al. (2012) reported no changes in LV ejection fraction or mass estimates (at greater than 10 years after therapy) when analyzing a group of 33 pediatric ALL survivors assigned to receive cumulative doxorubicin doses less than 240 mg/m (from 180 to 240 mg/m). Although subclinical cardiac abnormalities were documented in one third of the cohort, no evidence of myocardial injury could be measured with LV mass and ejection fraction. Given this information, it is perhaps not surprising that our results are not consonant with ejection fraction or mass as a surrogate for doxorubicin-induced abnormalities in LV function and structure. The data reflects the fact that the subjects participating in the study had been treated with relatively low cumulative doses of antileukemic agent. As detailed in chapter 3, the patients with high-risk ALL received a median cumulative doxorubicin dose of 296.4 mg/m^2, while those with standard-risk ALL received a median dose of 60.2 mg/m^2. In agreement with previous studies, these modest dosages predisposed them to a lower risk of delayed cardiotoxic effects (Zile et al., 2004; Lipshultz et al., 2012; Harake et al., 2012). The cancer survivors presumably developed low-level myocardial injury and LV remodeling, whose extent was not sufficiently large to exceed the sensitivity threshold of ejection fraction, mass, or the other 3D geometrical parameters (Jurcut et al., 2008). It is therefore clear that these parameters were not sensitive enough to detect the subclinical

abnormalities in LV function and structure associated with exposure to doxorubicin in this setting. Supporting this line of reasoning, the work by Jain (2000) suggests that the relationship between cumulative dose and impairment in ejection fraction is exponential.

As far as concern the time-dependent geometrical parameters, both endocardial volume and wall thickness failed to demonstrate statistical differences between healthy controls and leukemia survivors ($p>0.05$). The only significant difference was detected in the epicardial between end-systole and diastasis among the HRdex and HV or SR groups, and among the HV and HR groups ($p<0.01$). This observation suggests that early diastole was more affected by doxorubicin-mediated cardiotoxicity than systole or late diastole. Our result is consistent with findings such as those by Dorup and associates (2004), who referred that diastolic abnormalities precede changes in systolic function in long-term survivors of ALL.

Also notable is the fact that the epicardial and endocardial volumes in the control group exhibited a less synchronous contraction pattern than those in the cancer survivor groups. These curves were less aligned and achieve their minimal value (end-systole) at a different phase in the cardiac cycle (one phase shift). The reason for the above is partly related to the procedure which we have used to calculate the average values of the time-varying volumes for the control group. We remind that such calculation was performed using only 25 values among those describing the evolution of the volumes over the cardiac cycle.

As an additional step to investigate the functional changes of the LV due to cardiotoxicity, we analyze the stiffness of passive myocardium. This parameter has shown capable of discriminating cancer survivors from healthy volunteers. The HR group demonstrated a smaller stiffness than the control or the other survivor groups did across the three sets of numerical simulations, suggesting that structural changes occurred within the muscle tissue. This data in particular indicates that the HR subjects had a myocardium more prone to dilatation if increased intra-ventricular pressure is applied compared with the other participants. Increased myocardial stiffness is in accordance with the well-known late cardiotoxic effects for high doses of doxorubicin in survivors of adult ALL. A considerable portion of survivors showed signs and symptoms consistent with dilated cardiomyopathy, a cardiac disease state characterized by dilation of the LV chamber and loss of myocardial contractility (Giantris, Abdurrahman, Hinkle, et Asselin, 1998). This condition has also been described in survivors of childhood ALL. In this case, however, investigators have referred that dilated cardiomyopathy tends to evolve over time and progressively

develop the characteristics of the restrictive cardiomyopathy (Lipshultz et al 2005; Gianni et al., 2008; Lipshultz et al., 2013).

In order to provide a more realistic prediction of in vivo myocardial stiffness, personalized ventricular pressures at rest and peak exercise were incorporated in the FE analysis framework and used to simulate the ventricular mechanics. The analysis of the resulting values for the hyperelastic property did not reveal any association among the magnitude of stiffness and the ALL risk category for relapse. In other words, we did not find reduced or increased tissue stiffness in the standard-risk group when compared with the high-risk group. Also, our data did not indicate any benefit of dexrazoxane in terms of protection from doxorubicin-induced cardiotoxicity.

The lack of statistical significance for myocardial stiffness can be primarily explained by the fact that the computational framework simulated and solved the LV mechanics only for the diastasis phase rather than for the entire cycle of cardiac contraction. As explained in chapter 2, the pressure developed in the ventricular chamber changes throughout the cardiac cycle assuming its minimum value precisely at diastasis. In systole, when the LV pressure raises, the ventricle contracts, resists stretching by pressure and discharges blood into the aortic arch, determining an increase in tissue stiffness. On the contrary, during diastole, the ventricular pressure drops, the blood enters the ventricle and stretches the cardiac muscle fibers leading to a decrease in stiffness (Wang et al., 2013; Wassenaar et al., 2016). This argument was proven by findings such as those by Wassenaar et al. (2016), who reported a higher LV myocardial stiffness in healthy subjects during end-systole as compared with end-diastole. In line with this are also the results of the sensitivity analysis, which show that myocardial stiffness increases as the ventricular pressure increases. On this basis, we speculated that the difference in the extent of muscle injury between the survivor groups was too subtle to be captured in the diastolic myocardial stiffness. We believe that the inclusion of higher intra-ventricular pressures in the mechanical simulation would heighten the hyperelastic property and consequently magnify the difference in stiffness among the three groups.

It is also pertinent to note that the lack of measurements for the healthy volunteers did not help in highlighting the differences in stiffness across the study groups. In fact, due to the unavailability of personalized hemodynamics data for these subjects, we were unable to make direct comparisons between cancer survivors and controls with regard to the hyperelastic property.

Moreover, we considered the possibility that errors coming from different sources have influenced the stiffness estimates, with potential consequences for the comparison between groups. However,

such errors would need to be extreme to alter the result of the comparison substantially. The sources of errors are discussed later in the chapter.

In the absence of baseline data for in vivo myocardial stiffness, we qualitatively compared our estimates of C_1 at rest with those predicted by Wang et al. (2013) by applying the mathematical modeling framework, which we have tested here, to the study of the mechanisms underlying the heart failure (**Table 5.1**). We recall that a more detailed description of this work can be found in section 2.5.1.

Table 5.1. Comparison of in vivo myocardial stiffness for the three groups analyzed by Wang et al. and the three groups of childhood ALL survivors assessed in the current investigation. Data are presented as means with standard deviation.

Investigations	**Study group**	**C1** (kPa)
Wang et al. (2013)	Normal	1.8 ± 0.6
	Hyperthrophy	6.0 ± 1.3
	NI-HF	5.9 ± 1.7
Current study	Standard-risk	**4.0 ± 1.3**
	High-risk	**3.5 ± 1.1**
	DEX-exposed	**3.7 ± 1.3**

As can be appreciated in **Table 5.1**, current data appears to be in reasonable agreement with the experience of Wang and colleagues. This qualitative comparison showed that the mean values for C_1 in the three groups of ALL survivors (around 3.7 kPa) lie between those for the normal subjects and the individuals with non-ischemic heart failure (NI-FE) or hypertrophy. The results of our FE simulations provided, thus, a plausible representation of in vivo values for LV myocardial stiffness. In particular, we note that the average values of C_1 in the present study are slightly higher than the one obtained by Wang et al. for the healthy subjects. Support for this observation comes from the work of Li and colleagues (2017). By analyzing the late alterations in LV diastolic wall strain in a similar population of childhood leukemias survivors, these researchers documented an increased myocardial stiffness in the survivors when compared against the referent controls (see paragraph

2.4.1). It should be mentioned, however, that the estimates by Li et al. may not entirely capture the global LV stiffness because of the procedure by which they were determined.

This data alone seems to suggest that the administration of modest doses of doxorubicin has the effect of increasing the LV myocardial stiffness in long-term survivors of ALL. However, in the absence of a more valid comparison, it would be purely speculative to support such a conclusion. Indeed, although Wang at al. applied the same computational framework as we did, the participants in this study were significantly older (range, 45 to 86 years) than the cancer survivors (Fonseca et al., 2011). In other words, the two populations were not age-matched. Moreover, the pressure loading constraints were chosen based on experimental measurements reported in the literature and, consequently, were not patient-specific. Such differences hinder the comparisons among the two works.

Clearly, further investigation is required to confirm the findings of the current study and to draw a firm conclusion about the relationship between leukemia risk status and myocardial stiffness in this or similar cohorts of ALL survivors.

5.2 Limitations of the study

The present work has a few limitations that deserve consideration.

- The FE models of the healthy hearts were reconstructed on a relatively small number of CMR slices of fair image quality. As detailed in chapter 3, the control subjects were imaged following a different CMR acquisition protocol than the ALL survivors, resulting in datasets with a higher number of phases and a lower number of slices per phase. The inclusion of such relatively small number of slices turned out to negatively affect both the accuracy of the 3D reconstruction and the performance of the ventricular mechanics model, as shown by the RMS errors estimated in the best fit of the numerical simulations. The RMS errors were largest in the healthy volunteers compared with the leukemia survivors.

- In this study, the stiffness of the ventricular myocardium was initially calculated by assuming physiologically realistic diastasis pressures of 0.75, 1, and 1.25 kPa as boundary conditions for all subjects. It thus follows that our stiffness estimates only reflected the geometrical effects of myocardial remodeling induced by doxorubicin toxicity on the passive LV mechanics. In other words, these estimates did not account for the effects of changes in LV loading conditions

associated with geometrical changes of the LV. Support for this argument comes from the work of Wang et al. (2013).

- The real intra-ventricular pressure was not available for the study participants since its direct measurement is invasive and, thus, not recommended in clinically healthy young adults. Under these circumstances, we relied upon the CircAdapt model of the heart to quantify the LV cavity pressure non-invasively. The simulated pressures at rest and peak exercise were temporally synchronized with the CMR images and then incorporated into the FE analysis framework in order to calculate the hyperelastic property. Despite the accuracy of the evaluation procedure, the hemodynamic data obtained in such a way were only an estimate of the real LV pressure. It is, therefore, plausible that this approximation has introduced errors in the estimation of C_1, preventing us from demonstrating significant differences between the SR and HR survivors. Another source of error that may have influenced our findings is the temporal synchronization. Because of the way in which the pressure was derived, there can be no guarantee that the chosen match between MRI and hemodynamic data was perfect. This is especially true for the values of hyperelastic property at peak exercise.

  The study was also limited by the fact that the FE models used for simulating the LV mechanics during peak exercise were constructed on MR images capturing the heart wall motion in resting conditions. Indeed, during a CMR examination, the subjects are required to stay still (Machata, Willschke, Kabon, et Kettner, 2008). While offering some insights into the myocardial changes brought about by cardiotoxicity, this simplification may have led to misrepresentation of C_1 at peak exercise.

- The evaluation of global LV stiffness was conducted within a small sample of healthy subjects and childhood leukemia survivors. Specifically, the control group comprised 10 volunteers, but only a few of them were considered for the mechanical analysis. Among the cancer survivors, we could analyze only 48 of the 84 subjects enrolled in the study: 12 of them belonged to the SR group, 16 to the HR group, and 20 to the HRdex group. Thirty-nine ALL survivors were considered for assessing the stiffness at rest and peak exercise: 10 of them belonged to the SR group, 15 to the HR group, and 14 to the HRdex group. Larger samples might be more suitable for detection of between-group differences that are expected to be subtle. We, therefore, suspect that the sizes of the four groups have affected our statistical power to demonstrate significant differences in myocardial stiffness.

CHAPTER 6 CONCLUSION AND RECOMMENDATIONS

The following pages briefly recapitulate the key results of the present work, while articulating their implications for the detection of late cardiotoxicity in childhood ALL survivors. To conclude, this last section explores enhancements and future directions for research related to this topic.

6.1 Highlights

In this study, we applied the FE modeling framework implemented by the Bioengineering Institute at the University of Auckland to gain new insights into the LV chamber remodeling that occurred in long-term survivors of childhood ALL after exposure to moderate doxorubicin doses. The main results of this evaluation and their contributions to the existing literature can be shortly summarized as follows:

- The global and regional 3D geometrical parameters (e.g., ejection fraction, myocardial mass, and wall thickness) were not sufficiently sensitive to capture the subtle asymptomatic changes occurred in LV structure and function due to late doxorubicin cardiotoxicity. Nonetheless, we found preliminary evidence that early diastole was more affected by doxorubicin exposure than systole or late diastole. It is, therefore, clear that our first research hypothesis was not verified: these parameters cannot be used to assess subclinical cardiotoxicity in the selected population of ALL survivors.
- The passive myocardial stiffness appeared to be more sensitive than the ejection fraction or the other 3D geometrical parameters for differentiating cancer survivors from healthy subjects. We observed a significantly lower tissue stiffness in the high-risk group compared with the control, suggesting a myocardium more prone to dilatation if increased ventricular pressure is applied. However, this biomechanical parameter failed to demonstrate a significant difference between the three groups of cancer survivors, even after incorporation of subject-specific LV pressure data in the FE model. Although the use of myocardial stiffness during systole may be more appropriate for this investigation, our results corroborate the hypothesis that passive stiffness reflects subtle myocardial changes triggered by the late cardiotoxicity of doxorubicin.

6.2 Concluding remarks and future developments

The present work responds to the call for more research on late-occurring cardiotoxicity of modern chemotherapy regimens in young survivors of pediatric leukemia. In particular, this computational study extends current knowledge in this area by providing a quantitative description of ventricular geometry and function in a group of ALL survivors returning for follow-up 13 years after the completion of therapy with doxorubicin. The collected data gives information on the cardiac status of these subjects and may prove useful for clinicians and researchers interested in improving the prevention of myocardial injury to enhance the quality of long-term survival among ALL patients. Despite the lack of strong cardiotoxic evidence, the contribution provided to the existing literature was deemed original. To the best of our knowledge, there have been very few studies aiming to quantify subclinical cardiotoxicity in terms of myocardial stiffness in long-term survivors of ALL. Furthermore, our study was the first to evaluate this cardiotoxicity through the mechanical behavior analysis of the left ventricle on CMR images. In fact, while the previous works assessed the late alterations in muscle stiffness based on echocardiographically-derived parameters, we simulated the ventricular mechanics and estimated the in vivo stiffness using a FE computational framework.

In light of the above considerations, it would be interesting to apply the same methodology, which we have proposed here, to further investigate the relationship between stiffness changes and ALL risk status in this or a similar cohort of survivors. To do so, some methodological refinements and additions in the FE analysis are necessary.

A first step would be to include the FE simulation of the ventricular mechanics during systole and early diastole into the current study. As discussed in chapter 5, we theorize that the imposition of higher intra-ventricular pressures (as those applied to the heart over systole and early diastole) on the FE LV models would increase the hyperelastic properties and magnify differences among the three groups of cancer survivors. This enhancement would permit to capture the changes in tissue stiffness better across the groups and, thereby, explore the relationship between these changes and ALL risk status. In the context of this study, the simulation of LV deformation during cardiac cycle can be done by incorporating the myocardial contractility in the behavior law of the model and by applying appropriate pressure loading constraints. The pressure loading can be obtained using the CircAdapt lumped parameter model. Indeed, under proper conditions, the model can simulate the ventricular pressure throughout a complete cycle of cardiac contraction (Kuijpers et al., 2012).

Much of this work is currently underway in another master project on a larger population of ALL survivors.

Moreover, in the future, it could be of interest to evaluate the active mechanical properties of the LV myocardium in terms of maximal contractile stress in this or a similar cohort. Such analysis is expected to be done by applying the same non-invasive FE modeling framework employed for the estimation and assessment of myocardial stiffness. It will be sufficient to make some changes in the input parameters of the framework.

Another aspect that needs to be improved is the procedure for evaluating the LV cavity pressure from incremental exercise testing and hemodynamic modeling. By enhancing the accuracy of this procedure, one could obtain more realistic pressure loading constraints.

Once this solution has been implemented, it would be desirable to perform an incremental exercise test on the healthy subjects and, subsequently, integrate the resulting personalized data on pressure into the computational framework. It would permit a more realistic prediction of the in vivo LV stiffness for the controls and, also, direct comparisons with the cancer survivors. To improve the statistical power of this analysis, we recommend increasing the size of the control population.

Lastly, for a more accurate determination of the subject-specific ventricular geometry, it might be convenient to improve the temporal resolution of the CMR images in both leukemia survivors and healthy volunteers. We also believe that increasing the temporal resolution to 35 - 40 cardiac phases would help detect the subtle cardiac damage that we were unable to capture with a resolution of 25 phases.

BIBLIOGRAPHY

Adams, M. J., & Lipshultz, S. E. (2005). Pathophysiology of anthracycline-and radiation-associated cardiomyopathies: Implications for screening and prevention. *Pediatric blood & cancer*, *44*(7), 600-606.

Aissiou, M. (2016). *Early detection of doxorubicin-induced cardiotoxicity using combined biomechanical modeling and multi-parametric cardiovascular MRI*. (Doctoral dissertation, École Polytechnique de Montréal, Montréal, QC).

Ali, M. K., Ewer, M. S., Gibbs, H. R., Swafford, J., & Graff, K. L. (1994). Late doxorubicin-associated cardiotoxicity in children. *Cancer*, *74*(1), 182-188.

Bansal, N., Amdani, S., Lipshultz, E. R., & Lipshultz, S. E. (2017). Chemotherapy-induced cardiotoxicity in children. *Expert opinion on drug metabolism & toxicology*, *13*(8), 817-832.

Bassareo, P. P., Monte, I., Romano, C., Deidda, M., Piras, A., Cugusi, L., Coppola, C., Galletta, F., & Mercuro, G. (2016). Cardiotoxicity from anthracycline and cardioprotection in paediatric cancer patients. *Journal of Cardiovascular Medicine*, *17*(1), S55-S63.

Belson, M., Kingsley, B., & Holmes, A. (2006). Risk factors for acute leukemia in children: a review. *Environmental health perspectives*, *115*(1), 138-145.

Bensamoun, S. F., Ringleb, S. I., Littrell, L., Chen, Q., Brennan, M., Ehman, R. L., & An, K. N. (2006). Determination of thigh muscle stiffness using magnetic resonance elastography. *Journal of Magnetic Resonance Imaging: An Official Journal of the International Society for Magnetic Resonance in Medicine*, *23*(2), 242-247.

Bhojwani, D., Yang, J. J., & Pui, C. H. (2015). Biology of childhood acute lymphoblastic leukemia. *Pediatric Clinics*, *62*(1), 47-60.

Bryant, J., Picot, J., Levitt, G., Sullivan, I., Baxter, L., & Clegg, A. (2007). Cardioprotection against the toxic effects of anthracyclines given to children with cancer: a systematic review. *Health Technology Assessment (Winchester, England)*, *11*(27), iii-ix.

Burden, D. A., & Osheroff, N. (1998). Mechanism of action of eukaryotic topoisomerase II and drugs targeted to the enzyme. *Biochimica et Biophysica Acta (BBA)-Gene Structure and Expression*, *1400*(1-3), 139-154.

Cerqueira, M. D., Weissman, N. J., Dilsizian, V., Jacobs, A. K., Kaul, S., Laskey, W. K., Pennell, D. J., Rumberger, J. A., Ryan, T., & Verani, M. S. American Heart Association Writing Group on Myocardial Segmentation, and Registration for Cardiac Imaging. (2002). Standardized myocardial segmentation and nomenclature for tomographic imaging of the heart: a statement for healthcare professionals from the Cardiac Imaging Committee of the Council on Clinical Cardiology of the American Heart Association. *Circulation*, *105*(4), 5.

Champlin, R., & Gale, R. P. (1989). Acute lymphoblastic leukemia: Recent advances in biology and therapy. *Blood*, *73*(8), 2051-2066.

Chang, D. (2012). *A wiggers diagram, showing the cardiac cycle events occurring the left ventricle*. March 23, 2019, from https://commons.wikimedia.org/wiki/File:Wiggers_Diagram.svg

Chang, V. Y., & Wang, J. J. (2018). Pharmacogenetics of Chemotherapy-Induced Cardiotoxicity. *Current oncology reports*, *20*(7), 52. doi:10.1007/s11912-018-0696-8.

Collins, J. J., & De Luca, C. J. (1993). Open-loop and closed-loop control of posture: a random-walk analysis of center-of-pressure trajectories. *Experimental brain research*, *95*(2), 308-318.

Costa, K. D., Holmes, J. W., & McCulloch, A. D. (2001). Modelling cardiac mechanical properties in three dimensions. *Philosophical Transactions of the Royal Society of London A: Mathematical, Physical and Engineering Sciences*, *359*(1783), 1233-1250.

Coviello, J. S. (2018). Cardiovascular and Cancer Risk: The Role of Cardio-oncology. *Journal of the advanced practitioner in oncology*, *9*(2), 160.

Da Silveira, J. S., Scansen, B. A., Wassenaar, P. A., Raterman, B., Eleswarpu, C., Jin, N., White, R. D., Bonagure, J. D., & Kolipaka, A. (2016). Quantification of myocardial stiffness using magnetic resonance elastography in right ventricular hypertrophy: initial feasibility in dogs. *Magnetic resonance imaging*, *34*(1), 26-34.

DeAngelo, D. J., Stevenson, K. E., Dahlberg, S. E., Silverman, L. B., Couban, S., Supko, J. G., Amrein, P. C., Ballen, K. K., Seftel, M. D., Turner, A. R., Leber, B., Howson-Jan, K., Kelly, K., Cohen, S., Matthews, J. H., Savoie, L., Wadleigh, M., Sirulnik, L. A., Galinsky, I., Neuberg, D. S.,

Sallan, S. E., & Stone, R. M. (2015). Long-term outcome of a pediatric-inspired regimen used for adults aged 18-50 years with newly diagnosed acute lymphoblastic leukemia. *Leukemia*, *29*(3), 526–534.

Delvin, E., Alos, N., Rauch, F., Marcil, V., Morel, S., Boisvert, Lecours, M., Laverdière, C., Sinnett, D., Krajinovic, M., Dubois, J., Drouin, S., Lefebvre, G., Samoilenko, M., Nyalendo, C., Cavalier, E., & Levy, E. (2018). Vitamin D nutritional status and bone turnover markers in childhood acute lymphoblastic leukemia survivors: A PETALE study. *Clinical Nutrition*.

Dodos, F., Halbsguth, T., Erdmann, E., & Hoppe, U. C. (2008). Usefulness of myocardial performance index and biochemical markers for early detection of anthracycline-induced cardiotoxicity in adults. *Clinical Research in Cardiology*, *97*(5), 318-326.

Dokos, S., Smaill, B. H., Young, A. A., & LeGrice, I. J. (2002). Shear properties of passive ventricular myocardium. *American Journal of Physiology-Heart and Circulatory Physiology*, *283*(6), H2650-H2659.

Dong, J., & Chen, H. (2018). Cardiotoxicity of anticancer therapeutics. *Frontiers in Cardiovascular Medicine*, *5*, 9.

Dorup, I., Levitt, G., Sullivan, I., & Sorensen, K. (2004). Prospective longitudinal assessment of late anthracycline cardiotoxicity after childhood cancer: the role of diastolic function. *Heart*, *90*(10), 1214-1216.

Enderlein, G. (1988). Fleiss, JL: The Design and Analysis of Clinical Experiments. Wiley, New York–Chichester–Brislane–Toronto–Singapore 1986, 432. *Biometrical Journal*, *30*(3), 304-304.

Fallah-Rad, N., Walker, J. R., Wassef, A., Lytwyn, M., Bohonis, S., Fang, T., Tian, G., Kirkpatrick, I. D. C., Singal, P. K., Krahn, M., Grenier, D., & Jassal, D. S. (2011). The utility of cardiac biomarkers, tissue velocity and strain imaging, and cardiac magnetic resonance imaging in predicting early left ventricular dysfunction in patients with human epidermal growth factor receptor II–positive breast cancer treated with adjuvant trastuzumab therapy. *Journal of the American College of Cardiology*, *57*(22), 2263-2270.

Fleiss, J. L. (1986). Analysis of data from multiclinic trials. *Controlled clinical trials*, *7*(4), 267-275.

Fonseca, C. G., Backhaus, M., Bluemke, D. A., Britten, R. D., Chung, J. D., Cowan, B. R., Dinov, D., Finn, J. P., Hunter, P. J., Kadish, A. H. Lee, D. C., Lima, Medrano-Gracia, P., Shivkumar, K., Suinesiaputra, A., Tao, W., & Young, A. A. (2011). The Cardiac Atlas Project—an imaging database for computational modeling and statistical atlases of the heart. *Bioinformatics*, *27*(16), 2288-2295.

Friedman, M. A., Bozdech, M. J., Billingham, M. E., & Rider, A. K. (1978). Doxorubicin cardiotoxicity: serial endomyocardial biopsies and systolic time intervals. *Jama*, *240*(15), 1603-1606.

Frey, H. C., & Patil, S. R. (2002). Identification and review of sensitivity analysis methods. *Risk analysis*, *22*(3), 553-578.

Gianni, L., Herman, E. H., Lipshultz, S. E., Minotti, G., Sarvazyan, N., & Sawyer, D. B. (2008). Anthracycline cardiotoxicity: from bench to bedside. *Journal of clinical oncology: official journal of the American Society of Clinical Oncology*, *26*(22), 3777.

Giantris, A., Abdurrahman, L., Hinkle, A., Asselin, B., & Lipshultz, S. E. (1998). Anthracycline-induced cardiotoxicity in children and young adults. *Critical reviews in oncology/hematology*, *27*(1), 53-68.

Guillemont, A. F. (2016). *Caractérisation du comportement mécanique du tissu cardiaque par modélisation éléments finis et IRM*. (Rapport de stage, École Polytechnique de Montréal, Montréal, QC).

Guccione, J. M., McCulloch, A. D., & Waldman, L. K. (1991). Passive material properties of intact ventricular myocardium determined from a cylindrical model. *Journal of biomechanical engineering*, *113*(1), 42-55.

Guccione, J. M., Salahieh, A., Moonly, S. M., Kortsmit, J., Wallace, A. W., & Ratcliffe, M. B. (2003). Myosplint decreases wall stress without depressing function in the failing heart: a finite element model study. *The Annals of thoracic surgery*, *76*(4), 1171-1180.

Gupta, K. B., Ratcliffe, M. B., Fallert, M. A., Edmunds, L. H., & Bogen, D. K. (1994). Changes in passive mechanical stiffness of myocardial tissue with aneurysm formation. *Circulation*, *89*(5), 2315-2326.

Hande, K. R. (1998). Clinical applications of anticancer drugs targeted to topoisomerase II. *Biochimica et Biophysica Acta (BBA)-Gene Structure and Expression*, *1400*(1-3), 173-184.

Harake, D., Franco, V. I., Henkel, J. M., Miller, T. L., & Lipshultz, S. E. (2012). Cardiotoxicity in childhood cancer survivors: strategies for prevention and management. *Future cardiology*, *8*(4), 647-670.

Hashimoto, I., Ichida, F., Miura, M., Okabe, T., Kanegane, H., Uese, K. I., Hamamichi, Y., Misaki, T., Koizumi, S., & Miyawaki, T. (1999). Automatic border detection identifies subclinical anthracycline cardiotoxicity in children with malignancy. *Circulation*, *99*(18), 2367-2370.

Hasinoff, B. B., & Herman, E. H. (2007). Dexrazoxane: how it works in cardiac and tumor cells. Is it a prodrug or is it a drug?. *Cardiovascular toxicology*, *7*(2), 140-144.

Healy, J., Richer, C., Bourgey, M., Kritikou, E. A., & Sinnett, D. (2010). Replication analysis confirms the association of ARID5B with childhood B-cell acute lymphoblastic leukemia. *Haematologica*, haematol-2010.

Hequet, O., Le, Q. H., Moullet, I., Pauli, E., Salles, G., Espinouse, D., Dumontet, C., Thieblemont, C., Arnaud, P., Antal, D., Bouafia, F., & Coiffier, B. (2004). Subclinical late cardiomyopathy after doxorubicin therapy for lymphoma in adults. *Journal of Clinical Oncology*, *22*(10), 1864-1871.

Holger, S. (2006). *Passive myocardial mechanics: constitutive law and material parameter estimation.* (Doctoral dissertation, University of Auckland, Auckland, New Zealand).

Hsu, S. J., Bouchard, R. R., Dumont, D. M., Wolf, P. D., & Trahey, G. E. (2007). In vivo assessment of myocardial stiffness with acoustic radiation force impulse imaging. *Ultrasound in medicine & biology*, *33*(11), 1706-19.

Hudson, M. M., Link, M. P., & Simone, J. V. (2014). Milestones in the curability of pediatric cancers. *Journal of clinical Oncology*, *32*(23), 2391.

Hudson, M. M., Rai, S. N., Nunez, C., Merchant, T. E., Marina, N. M., Zalamea, N., Cox, C., Phipps, S., Pompeu, R., & Rosenthal, D. (2007). Noninvasive evaluation of late anthracycline cardiac toxicity in childhood cancer survivors. *Journal of clinical oncology*, *25*(24), 3635-3643.

Hunger, S. P., & Mullighan, C. G. (2015). Acute lymphoblastic leukemia in children. *New England Journal of Medicine*, *373*(16), 1541-1552.

Jain, D. (2000). Cardiotoxicity of doxorubicin and other anthracycline derivatives. *Journal of Nuclear Cardiology*, *7*(1), 53.

Jain, D., Russell, R. R., Schwartz, R. G., Panjrath, G. S., & Aronow, W. (2017). Cardiac complications of cancer therapy: pathophysiology, identification, prevention, treatment, and future directions. *Current cardiology reports*, *19*(5), 36.

Johnson-Arbor, K., & Dubey, R. (2018). Doxorubicin. In *StatPearls [Internet]*. StatPearls Publishing.

Jurcut, R., Wildiers, H., Ganame, J., D'hooge, J., Paridaens, R., & Voigt, J. U. (2008). Detection and monitoring of cardiotoxicity—what does modern cardiology offer?. *Supportive Care in Cancer*, *16*(5), 437-445.

Kadner, K., Dobner, S., Franz, T., Bezuidenhout, D., Sirry, M. S., Zilla, P., & Davies, N. H. (2012). The beneficial effects of deferred delivery on the efficiency of hydrogel therapy post myocardial infarction. *Biomaterials*, *33*(7), 2060-2066.

Kichula, E. T., Wang, H., Dorsey, S. M., Szczesny, S. E., Elliott, D. M., Burdick, J. A., & Wenk, J. F. (2014). Experimental and computational investigation of altered mechanical properties in myocardium after hydrogel injection. *Annals of biomedical engineering*, *42*(7), 1546-1556.

Khouri, M. G., Klein, M. R., Velazquez, E. J., & Jones, L. W. (2015). Current and emerging modalities for detection of cardiotoxicity in cardio-oncology. *Future cardiology*, *11*(4), 471-484.

Kolipaka, A., Araoz, P. A., McGee, K. P., Manduca, A., & Ehman, R. L. (2010). Magnetic resonance elastography as a method for the assessment of effective myocardial stiffness throughout the cardiac cycle. *Magnetic resonance in medicine*, *64*(3), 862-870.

Kolipaka, A., McGee, K. P., Araoz, P. A., Glaser, K. J., Manduca, A., Romano, A. J., & Ehman, R. L. (2009). MR elastography as a method for the assessment of myocardial stiffness: comparison with an established pressure–volume model in a left ventricular model of the heart. *Magnetic Resonance in Medicine: An Official Journal of the International Society for Magnetic Resonance in Medicine*, *62*(1), 135-140.

Kuijpers, N. H., Dassen, W., van Dam, P. M., van Dam, E. M., Hermeling, E., Lumens, J., Arts, T., & Delhaas, T. (2012). CircAdapt: A user-friendly learning environment for (patho) physiology of heart and circulation. In *2012 Computing in Cardiology* (pp. 969-972). IEEE.

Lam, H. I. (2012). *Mathematical tools for ventricular analysis using Cardiac MRI*. (Doctoral dissertation, University of Auckland, Auckland, New Zealand).

Lang, R. M., Badano, L. P., Mor-Avi, V., Afilalo, J., Armstrong, A., Ernande, L., Flachskampf, F. A., Foster, E., Goldstein, S. A., Kuznetsova, T., Lancellotti, P., Muraru, D., Picard, M. H., Rietzschel, E. R., Rudski, L., Spencer, K. T., Tsang, W., & Voigt, J. U. (2015). Recommendations for cardiac chamber quantification by echocardiography in adults: an update from the American Society of Echocardiography and the European Association of Cardiovascular Imaging. *European Heart Journal-Cardiovascular Imaging*, *16*(3), 233-271.

Lapointe, M-O. (2016). *Évaluation du propriétés mécaniques du tissu cardiaque par échocardiographie*. (Master's thesis, École Polytechnique de Montréal, Montréal, QC).

Lee, L. C., Wall, S. T., Klepach, D., Ge, L., Zhang, Z., Lee, R. J., Hinsone, A., Gorman, J. H., Gormanf, R. C., & Guccione, J. M. (2013). Algisyl-LVR™ with coronary artery bypass grafting reduces left ventricular wall stress and improves function in the failing human heart. *International journal of cardiology*, *168*(3), 2022-2028.

Lee, L. C., Wenk, J. F., Zhong, L., Klepach, D., Zhang, Z., Ge, L., Ratcliffe, M. B., Zohdi, T. I., Hsu, E., Navia, J. L., Kassab, G. S., & Guccione, J. M. (2013). Analysis of patient-specific surgical ventricular restoration: importance of an ellipsoidal left ventricular geometry for diastolic and systolic function. *Journal of applied physiology*, *115*(1), 136-144.

Levis, B. E., Binkley, P. F., & Shapiro, C. L. (2017). Cardiotoxic effects of anthracycline-based therapy: what is the evidence and what are the potential harms?. *The Lancet Oncology*, *18*(8), e445-e456.

Li, V. W. Y., Cheuk, D. K. L., Cheng, F. W. T., Yang, J. Y. K., Yau, J. P. W., Ho, K. K. H., Li, C. K., Li, R. C. H., Yuen, H.L., Ling, A. S. C., Chan, G. C. F., & Cheung, Y. F. (2017). Myocardial stiffness as assessed by diastolic wall strain in adult survivors of childhood leukaemias with preserved left ventricular ejection fraction. *European Heart Journal-Cardiovascular Imaging*, *18*(4), 451-458.

Lin, X., Cowan, B. R., & Young, A. A. (2006). Automated detection of left ventricle in 4D MR images: experience from a large study. In *International Conference on Medical Image Computing and Computer-Assisted Intervention* (pp. 728-735). Springer, Berlin, Heidelberg.

Lipshultz, S. E., Cochran, T. R., Franco, V. I., & Miller, T. L. (2013). Treatment-related cardiotoxicity in survivors of childhood cancer. *Nature reviews Clinical oncology*, *10*(12), 697.

Lipshultz, S. E., Lipsitz, S. R., Mone, S. M., Goorin, A. M., Sallan, S. E., Sanders, S. P., Orav, E. J., Gelber, R. D., & Colan, S. D. (1995). Female sex and higher drug dose as risk factors for late cardiotoxic effects of doxorubicin therapy for childhood cancer. *New England Journal of Medicine*, *332*(26), 1738-1744.

Lipshultz, S. E., Lipsitz, S. R., Sallan, S. E., Dalton, V. M., Mone, S. M., Gelber, R. D., & Colan, S. D. (2005). Chronic progressive cardiac dysfunction years after doxorubicin therapy for childhood acute lymphoblastic leukemia. *Journal of clinical oncology*, *23*(12), 2629-2636.

Lipshultz, S. E., Miller, T. L., Lipsitz, S. R., Neuberg, D. S., Dahlberg, S. E., Colan, S. D., Silverman, L. B., Henkel, J. M., Franco, V. I., Cushman, L. L., Asselin, B. L., Clavell, L. A., Athale, U., Michon, B., Laverdière, C., Schorin, M. A., Larsen, E., Usmani, N., Sallan, S. E., Dana-Farber Cancer Institute Acute Lymphoblastic Leukemia Consortium (2012). Continuous Versus Bolus Infusion of Doxorubicin in Children With ALL: Long-term Cardiac Outcomes. *Pediatrics*, *130*(6), 1003-11.

Lipshultz, S. E., Miller, T. L., Scully, R. E., Lipsitz, S. R., Rifai, N., Silverman, L. B., Colan, S. D., Neuberg, D. S., Dahlberg, S. E., Henkel, J. M., Asselin, B. L., Athale, U. H., Clavell, L. A., Laverdière, C., Michon, B., Schorin, M. A., & Sallan, S. E. (2012). Changes in cardiac biomarkers during doxorubicin treatment of pediatric patients with high-risk acute lymphoblastic leukemia: associations with long-term echocardiographic outcomes. *Journal of clinical oncology: official journal of the American Society of Clinical Oncology*, *30*(10), 1042-9.

Loganathan, R., Bilgen, M., Al-Hafez, B., & Smirnova, I. V. (2006). Characterization of alterations in diabetic myocardial tissue using high resolution MRI. *The international journal of cardiovascular imaging*, *22*(1), 81-90.

Lumens, J., & Delhaas, T. (2012). Cardiovascular modeling in pulmonary arterial hypertension: focus on mechanisms and treatment of right heart failure using the CircAdapt model. *The American journal of cardiology*, *110*(6), S39-S48.

Lumens, J., Delhaas, T., Kirn, B., & Arts, T. (2009). Three-wall segment (TriSeg) model describing mechanics and hemodynamics of ventricular interaction. *Annals of biomedical engineering*, *37*(11), 2234-2255.

Lunning, M. A., Kutty, S., Rome, E. T., Li, L., Padiyath, A., Loberiza, F., & Porter, T. R. (2015). Cardiac magnetic resonance imaging for the assessment of the myocardium after doxorubicin-based chemotherapy. *American journal of clinical oncology*, *38*(4), 377-381.

Lynch, B. J., Guinee Jr, D. G., & Holden, J. A. (1997). Human DNA topoisomerase II-alpha: a new marker of cell proliferation in invasive breast cancer. *Human pathology*, *28*(10), 1180-1188.

Lyu, Y. L., Kerrigan, J. E., Lin, C. P., Azarova, A. M., Tsai, Y. C., Ban, Y., & Liu, L. F. (2007). Topoisomerase IIβ–mediated DNA double-strand breaks: implications in doxorubicin cardiotoxicity and prevention by dexrazoxane. *Cancer research*, *67*(18), 8839-8846.

Machata, A. M., Willschke, H., Kabon, B., Kettner, S. C., & Marhofer, P. (2008). Propofol-based sedation regimen for infants and children undergoing ambulatory magnetic resonance imaging. *British journal of anaesthesia*, *101*(2), 239-243.

Marcoux, S., Drouin, S., Laverdière, C., Alos, N., Andelfinger, G. U., Bertout, L., Curnier, D., Friedrich, M. G., Kritikou, E.A., Lefebvre, G., Levy, E., Lippé, S., Marcil, V., Raboisson, M. J., Rauch, F., Robaey, P., Samoylenko, M., Séguin, C., Sultan, S., Krajinovic, M., Sinnett, D., & Levy, E. (2017). The PETALE study: Late adverse effects and biomarkers in childhood acute lymphoblastic leukemia survivors. *Pediatric blood & cancer*, *64*(6), e26361.

Mazumder, R., Schroeder, S., Mo, X., Clymer, B. D., White, R. D., & Kolipaka, A. (2016). In vivo quantification of myocardial stiffness in hypertensive porcine hearts using MR elastography. *Journal of magnetic resonance imaging: JMRI*, *45*(3), 813-820.

McGibbon, C. A. (2003). Inter-rater and intra-rater reliability of subchondral bone and cartilage thickness measurement from MRI. *Magnetic resonance imaging*, *21*(7), 707-714.

McGowan, J. V., Chung, R., Maulik, A., Piotrowska, I., Walker, J. M., & Yellon, D. M. (2017). Anthracycline chemotherapy and cardiotoxicity. *Cardiovascular drugs and therapy*, *31*(1), 63-75.

Meiners, B., Shenoy, C., & Zordoky, B. N. (2018). Clinical and preclinical evidence of sex-related differences in anthracycline-induced cardiotoxicity. *Biology of sex differences*, *9*(1), 38.

Miller, R., Kolipaka, A., Nash, M. P., & Young, A. A. (2017, June). Identification of Transversely Isotropic Properties from Magnetic Resonance Elastography Using the Optimised Virtual Fields Method. In *International Conference on Functional Imaging and Modeling of the Heart* (pp. 421-431). Springer, Cham.

Mirsky, I. (1984). Assessment of diastolic function: suggested methods and future considerations. *Circulation*, *69*(4), 836-841.

Mojsejenko, D., McGarvey, J. R., Dorsey, S. M., Gorman, J. H., Burdick, J. A., Pilla, J. J., Gorman, R. C., & Wenk, J. F. (2014). Estimating passive mechanical properties in a myocardial infarction using MRI and finite element simulations. *Biomechanics and modeling in mechanobiology*, *14*(3), 633-47.

Nash, M. (1998). *Mechanics and material properties of the heart using an anatomically accurate mathematical model*. (Doctoral dissertation, University of Auckland, Auckland, New Zealand).

Nishimura, R. A., Housmans, P. R., Hatle, L. K., & Tajik, A. J. (1989). Assessment of diastolic function of the heart: background and current applications of Doppler echocardiography. Part I. Physiologic and pathophysiologic features. In *Mayo Clinic Proceedings* (Vol. 64, No. 1, pp. 71-81). Elsevier.

Nonogi, H., Hess, O. M., Ritter, M., & Krayenbuehl, H. P. (1988). Diastolic properties of the normal left ventricle during supine exercise. *Heart*, *60*(1), 30-38.

Ohtani, T., Mohammed, S. F., Yamamoto, K., Dunlay, S. M., Weston, S. A., Sakata, Y., Rodeheffer, R. J., Roger, V. L., & Redfield, M. M. (2012). Diastolic stiffness as assessed by diastolic wall strain is associated with adverse remodelling and poor outcomes in heart failure with preserved ejection fraction. *European heart journal*, *33*(14), 1742-1749.

Onciu, M. (2009). Acute lymphoblastic leukemia. *Hematologyloncology clinics of North America*, *23*(4), 655-674.

Peng, P., Lekadir, K., Gooya, A., Shao, L., Petersen, S. E., & Frangi, A. F. (2016). A review of heart chamber segmentation for structural and functional analysis using cardiac magnetic resonance imaging. *Magnetic Resonance Materials in Physics, Biology and Medicine*, *29*(2), 155-195.

Petitjean, C., & Dacher, J. N. (2011). A review of segmentation methods in short axis cardiac MR images. *Medical image analysis*, *15*(2), 169-184.

Périé, D., Dahdah, N., Foudis, A., & Curnier, D. (2013). Multi-parametric MRI as an indirect evaluation tool of the mechanical properties of in-vitro cardiac tissues. *BMC cardiovascular disorders*, *13*(1), 24.

Pui, C. H. (2011). *Acute lymphoblastic leukemia* (pp. 23-26). Springer Berlin Heidelberg.

Rahman, A. M., Yusuf, S. W., & Ewer, M. S. (2007). Anthracycline-induced cardiotoxicity and the cardiac-sparing effect of liposomal formulation. *International journal of nanomedicine*, *2*(4), 567.

Raj, S., Franco, V. I., & Lipshultz, S. E. (2014). Anthracycline-induced cardiotoxicity: a review of pathophysiology, diagnosis, and treatment. *Current treatment options in cardiovascular medicine*, *16*(6), 315.

Rea, D., Coppola, C., Barbieri, A., Monti, M. G., Misso, G., Palma, G., Bimonte, S., Zarone, M. R., Luciano, A., Liccardo, D., Maiolino, P., Cittadini, A., Ciliberto, G., Maurea, N., & Arra, C. (2016). Strain analysis in the assessment of a mouse model of cardiotoxicity due to chemotherapy: sample for preclinical research. *in vivo*, *30*(3), 279-290.

Sabbah, H. N., & Goldstein, S. (1993). Ventricular remodelling: consequences and therapy. *European heart journal*, *14*(suppl_C), 24-29.

Sack, K. L., Davies, N. H., Guccione, J. M., & Franz, T. (2016). Personalised computational cardiology: Patient-specific modelling in cardiac mechanics and biomaterial injection therapies for myocardial infarction. *Heart failure reviews*, *21*(6), 815-826.

Schunke, K. J., Coyle, L., Merrill, G. F., & Denhardt, D. T. (2013). Acetaminophen attenuates doxorubicin-induced cardiac fibrosis via osteopontin and GATA4 regulation: reduction of oxidant levels. *Journal of cellular physiology*, *228*(10), 2006-14.

Sepe, D. M., Ginsberg, J. P., & Balis, F. M. (2010). Dexrazoxane as a cardioprotectant in children receiving anthracyclines. *The oncologist*, *15*(11), 1220-1226.

Sermesant, M., Delingette, H., & Ayache, N. (2006). An electromechanical model of the heart for image analysis and simulation. *IEEE transactions on medical imaging*, *25*(5), 612-625.

Sharalaya, Z., & Collier, P. (2018). Prevention of Cardiotoxicities With Traditional and Novel Chemotherapeutic Agents. *Current heart failure reports*, *15*(4), 260-269.

Silverman, L. B. (2014). Balancing cure and long-term risks in acute lymphoblastic leukemia. *ASH Education Program Book*, *2014*(1), 190-197.

Sirry, M. S., Butler, J. R., Patnaik, S. S., Brazile, B., Bertucci, R., Claude, A., McLaughlin, R., Davies, N. H., Liao, J., & Franz, T. (2016). Characterisation of the mechanical properties of infarcted myocardium in the rat under biaxial tension and uniaxial compression. *journal of the mechanical behavior of biomedical materials*, *63*, 252-264.

Smith, L. A., Cornelius, V. R., Plummer, C. J., Levitt, G., Verrill, M., Canney, P., & Jones, A. (2010). Cardiotoxicity of anthracycline agents for the treatment of cancer: systematic review and meta-analysis of randomised controlled trials. *BMC cancer*, *10*(1), 337.

Sommer, G., Schriefl, A. J., Andrä, M., Sacherer, M., Viertler, C., Wolinski, H., & Holzapfel, G. A. (2015). Biomechanical properties and microstructure of human ventricular myocardium. *Acta biomaterialia*, *24*, 172-192.

Sorensen, K., Levitt, G. A., Bull, C., Dorup, I., & Sullivan, I. D. (2003). Late anthracycline cardiotoxicity after childhood cancer: a prospective longitudinal study. *Cancer: Interdisciplinary International Journal of the American Cancer Society*, *97*(8), 1991-1998.

Stava, C. J., Jimenez, C., & Vassilopoulou-Sellin, R. (2007). Endocrine sequelae of cancer and cancer treatments. *Journal of Cancer Survivorship*, *1*(4), 261-274.

Swain, S. M., Whaley, F. S., & Ewer, M. S. (2003). Congestive heart failure in patients treated with doxorubicin: a retrospective analysis of three trials. *Cancer: Interdisciplinary International Journal of the American Cancer Society*, *97*(11), 2869-2879.

Swift, L. P., Rephaeli, A., Nudelman, A., Phillips, D. R., & Cutts, S. M. (2006). Doxorubicin-DNA adducts induce a non-topoisomerase II–mediated form of cell death. *Cancer research*, *66*(9), 4863-4871.

Tham, E. B., Haykowsky, M. J., Chow, K., Spavor, M., Kaneko, S., Khoo, N. S., Pagano, J. J., Mackie, A. S., & Thompson, R. B. (2013). Diffuse myocardial fibrosis by T 1-mapping in children with subclinical anthracycline cardiotoxicity: relationship to exercise capacity, cumulative dose and remodeling. *Journal of Cardiovascular Magnetic Resonance*, *15*(1), 48.

Terwilliger, T., & Abdul-Hay, M. (2017). Acute lymphoblastic leukemia: a comprehensive review and 2017 update. *Blood cancer journal*, *7*(6), e577.

Truong, Q. A., Singh, J. P., Cannon, C. P., Sarwar, A., Nasir, K., Auricchio, A., Faletra,F. F., Sorgente, A., Conca, C., Moccetti, T., Handschumacher, M., Brady, T. J., & Hoffmann, U. (2008). Quantitative analysis of intraventricular dyssynchrony using wall thickness by multidetector computed tomography. *JACC: Cardiovascular Imaging*, *1*(6), 772-781.

Vachhani, P., Shin, S., Baron, J., Thompson, J. E., Wetzler, M., Griffiths, E. A., Ontiveros, E. P., Spangenthal, E. J., & Wang, E. S. (2017). Dexrazoxane for cardioprotection in older adults with acute myeloid leukemia. *Leukemia research reports*, *7*, 36-39.

Vandecruys, E., Mondelaers, V., De Wolf, D., Benoit, Y., & Suys, B. (2012). Late cardiotoxicity after low dose of anthracycline therapy for acute lymphoblastic leukemia in childhood. *Journal of Cancer Survivorship*, *6*(1), 95-101.

Vejpongsa, P., & Yeh, E. T. (2014). Prevention of anthracycline-induced cardiotoxicity: challenges and opportunities. *Journal of the American College of Cardiology*, *64*(9), 938-945.

Vetter, F. J., & McCulloch, A. D. (2000). Three-dimensional stress and strain in passive rabbit left ventricle: a model study. *annals of biomedical engineering*, *28*(7), 781-792.

Volpe, J. K., & Makaryus, A. N. (2019). Anatomy, Thorax, Heart and Pericardial Cavity. In *StatPearls [Internet]*. StatPearls Publishing.

Vrooman, L. M., & Silverman, L. B. (2009). Childhood acute lymphoblastic leukemia: update on prognostic factors. *Current opinion in pediatrics*, *21*(1), 1-8.

Wang, V. Y., Lam, H. I., Ennis, D. B., Cowan, B. R., Young, A. A., & Nash, M. P. (2009). Modelling passive diastolic mechanics with quantitative MRI of cardiac structure and function. *Medical image analysis*, *13*(5), 773-784.

Wang, V. Y., Nielsen, P. M. F., & Nash, M. P. (2015). Image-based predictive modeling of heart mechanics. *Annual review of biomedical engineering*, *17*, 351-383.

Wang, V. Y., Young, A. A., Cowan, B. R., & Nash, M. P. (2013). Changes in in vivo myocardial tissue properties due to heart failure. In *International Conference on Functional Imaging and Modeling of the Heart* (pp. 216-223). Springer, Berlin, Heidelberg.

Wassenaar, P. A., Eleswarpu, C. N., Schroeder, S. A., Mo, X., Raterman, B. D., White, R. D., & Kolipaka, A. (2016). Measuring age-dependent myocardial stiffness across the cardiac cycle using MR elastography: a reproducibility study. *Magnetic resonance in medicine*, *75*(4), 1586-1593.

Weir, J. P. (2005). Quantifying test-retest reliability using the intraclass correlation coefficient and the SEM. *The Journal of Strength & Conditioning Research*, *19*(1), 231-240.

Weiss, J. A., & Gardiner, J. C. (2001). Computational modeling of ligament mechanics. *Critical Reviews™ in Biomedical Engineering*, *29*(3).

Wenk, J. F., Eslami, P., Zhang, Z., Xu, C., Kuhl, E., Gorman III, J. H., Robb, J. D., Ratcliffe, M. B., Gorman, R. C., & Guccione, J. M. (2011). A novel method for quantifying the in-vivo mechanical effect of material injected into a myocardial infarction. *The Annals of thoracic surgery*, *92*(3), 935-941.

Wouters, K. A., Kremer, L. C., Miller, T. L., Herman, E. H., & Lipshultz, S. E. (2005). Protecting against anthracycline-induced myocardial damage: a review of the most promising strategies. *British journal of haematology*, *131*(5), 561-578.

Yang, F., Teves, S. S., Kemp, C. J., & Henikoff, S. (2014). Doxorubicin, DNA torsion, and chromatin dynamics. *Biochimica et Biophysica Acta (BBA)-Reviews on Cancer*, *1845*(1), 84-89.

Yeoh, E. J., Ross, M. E., Shurtleff, S. A., Williams, W. K., Patel, D., Mahfouz, R., Behm, F. G., Raimondi, S. C., Relling, M. V., Patel, A., Cheng, C., Campana, D., Wilkins, D., Zhou, X., Li, J., Liu, H., Pui, C., Evans, W. E., Naeve, C., Wong, L., & Downing J. R. (2002). Classification, subtype discovery, and prediction of outcome in pediatric acute lymphoblastic leukemia by gene expression profiling. *Cancer cell*, *1*(2), 133-143.

Young, A. A., Cowan, B. R., Schoenberg, S. O., & Wintersperger, B. J. (2008). Feasibility of single breath-hold left ventricular function with 3 Tesla TSENSE acquisition and 3D modeling analysis. *Journal of Cardiovascular Magnetic Resonance*, *10*(1), 24.

Young, A. A., Cowan, B. R., Thrupp, S. F., Hedley, W. J., & Dell'Italia, L. J. (2000). Left ventricular mass and volume: fast calculation with guide-point modeling on MR images. *Radiology*, *216*(2), 597-602.

Xi, J., Lamata, P., Shi, W., Niederer, S., Land, S., Rueckert, D., Duckett, D. G., Shetty, A. K., Rinaldi, C. A., Razavi, R., & Smith, N. (2011, May). An automatic data assimilation framework

for patient-specific myocardial mechanical parameter estimation. In *International Conference on Functional Imaging and Modeling of the Heart* (pp. 392-400). Springer, Berlin, Heidelberg.

Zile, M. R., Baicu, C. F., & Gaasch, W. H. (2004). Diastolic heart failure—abnormalities in active relaxation and passive stiffness of the left ventricle. *New England Journal of Medicine*, *350*(19), 1953-1959.

Zhou, S., Starkov, A., Froberg, M. K., Leino, R. L., & Wallace, K. B. (2001). Cumulative and irreversible cardiac mitochondrial dysfunction induced by doxorubicin. *Cancer Research*, *61*(2), 771-777.

ZooFari. (2010). *Heart diagram. Blue components indicate de-oxygenated blood pathways and red components indicate oxygenated blood pathways*. March 23, 2019, from https://commons.wikimedia.org/wiki/File:Heart_diagram-en.svg